

## Abstract

### Uncovering a Critical Role for Calmodulin in Calcium-Dependent Regulation of the Nociceptor TRPA1

Justin H. Sanders

2024

Transient receptor potential (TRP) channels are sensory receptors expressed throughout the peripheral nervous system that help shape how we respond to our environment. TRPA1 has been identified as a key component in the transition from acute to chronic pain and inflammation making it a prime target for development of novel analgesics. Calcium has been shown to regulate TRPA1 by rapidly potentiating channel activity followed by rapid desensitization. While the effects of calcium on TRPA1 activity have been well-described, the mechanisms governing these calcium effects have been difficult to elucidate. Work described within this thesis details the discovery of a novel calmodulin (CaM) binding site (CaMBS) that is required for rapid desensitization of TRPA1. The CaMBS is located within the distal, disordered C-terminus and is evolutionarily conserved across vertebrate TRPA1 orthologs. Mutagenesis of the CaMBS results in total loss of CaM binding under basal cellular conditions and leads to channel hyperactivity through a dramatic slowing of calcium-mediated desensitization. CaM operates as an auxiliary subunit of TRPA1 that is necessary for proper channel function and regulation. This represents a step forward in understanding calcium regulation of TRPA1 activity and necessitates a closer look at previously proposed sites of calcium-mediated regulation. A calcium binding site was identified between two transmembrane helices of TRPA1 (S2-S3 CBS) and proposed to

regulate both potentiation and desensitization, and a different CaM binding domain (CaMBD) was also proposed to regulate both potentiation and desensitization. This thesis work suggests a model of TRPA1 calcium regulation where the CaMBS is the main driver of calcium-mediated desensitization, the CaMBD is an ancillary site with smaller effects on desensitization, and the S2-S3 CBS primarily serves functions in structural role.

Uncovering a Critical Role for Calmodulin in Calcium-Dependent Regulation of the  
Nociceptor TRPA1

A Dissertation  
Presented to the Faculty of the Graduate School  
of  
Yale University  
In Candidacy for the Degree of  
Doctor of Philosophy

By  
Justin H. Sanders

Dissertation Director: Candice E. Paulsen

May 2024

©2024 by Justin H. Sanders

All Rights Reserved

## Contents

<b>Chapter 1: Introduction.....</b>	<b>1</b>
<b>I: Overview of TRPA1 Function.....</b>	<b>1</b>
<b>II: Contribution of TRPA1 to Chronic Pain, inflammation, and disease.....</b>	<b>5</b>
<b>III: Complex Calcium Regulation of TRPA1.....</b>	<b>12</b>
<b>IV: TRPA1 Structural Insights.....</b>	<b>16</b>
<b>References.....</b>	<b>22</b>
<b>Chapter 2: Calmodulin binding is required for Ca<sup>2+</sup> mediated TRPA1 desensitization.....</b>	<b>27</b>
<b>1. Introduction.....</b>	<b>29</b>
<b>2. Results.....</b>	<b>32</b>
2.1 Calmodulin colocalizes with TRPA1 in cells and regulates its activity.....	32
2.2 The TRPA1 distal C-terminus contains a critical Calmodulin binding element.....	33
2.3 The TRPA1 distal C-terminus has a high affinity for Calmodulin.....	35
2.4 The TRPA1 Calmodulin binding site is highly conserved.....	37
2.5 Loss of Calmodulin binding is associated with hyperactive TRPA1 channels.....	38
2.6 CaM binding to the TRPA1 Calmodulin binding site is critical for channel desensitization.....	40
2.7 The CaM C-lobe is sufficient to regulate TRPA1 activity.....	43
2.8 High extracellular Ca <sup>2+</sup> partially rescues desensitization resistant TRPA1.....	44
<b>3. Discussion.....</b>	<b>45</b>
<b>4. Methods.....</b>	<b>50</b>
<b>References.....</b>	<b>62</b>
<b>Figures.....</b>	<b>66</b>
<b>Chapter 3: Contribution of S2-S3 CBS and CaMBD to TRPA1 Ca<sup>2+</sup> Regulation.....</b>	<b>89</b>
<b>1. Introduction.....</b>	<b>89</b>
<b>2. Results.....</b>	<b>91</b>
2.1 Ablating the S2-S3 CBS destabilizes TRPA1.....	91
2.2 The TRP-like Helix enhances Calmodulin binding of the CaMBD.....	93

2.3 The TRP-CaMBD influences Calmodulin binding of full-length TRPA1 .....	95
2.4 Calmodulin binding at the CaMBD slightly enhances Ca <sup>2+</sup> -mediated desensitization.....	96
<b>3. Discussion.....</b>	<b>96</b>
<b>4. Methods.....</b>	<b>98</b>
<b>References.....</b>	<b>104</b>
<b>Figures.....</b>	<b>106</b>
<b>Chapter 4: Conclusions and Future Directions.....</b>	<b>112</b>
<b>References.....</b>	<b>118</b>

## **Chapter 1: Introduction**

Over billions of years of evolution, organisms from every kingdom of life have developed systems to detect and respond to deleterious conditions in their environments. In animals this system is referred to as nociception and involves the detection of noxious stimuli by the peripheral nervous system (PNS) which is communicated to the central nervous system (CNS) that evokes an avoidance response to best remove the animal from the noxious stimulus<sup>1</sup>. Nociception that elicits an emotional response to the suffering caused by the noxious stimulus is known as pain which is a nearly universal human experience which we devote substantial resources to treat and avoid<sup>2</sup>.

The PNS is able to detect such a vast array of environmental changes due to its heterogenous population of neurons expressing dozens of ion channel receptors capable of responding to specific painful stimuli such as high temperature, low temperature, mechanical stress, acidic pH, and chemical irritants (**Fig. 1**)<sup>1,3</sup>. The early years of molecular pain research sought to identify what ion channel was activated by a given painful stimulus which contributed greatly to our understanding of acute pain. However, understanding the transition from acute to chronic pain and inflammation, which has profoundly negative effects on quality of life and fueled the opioid addiction epidemic, requires characterizing the underlying pathways that are involved in regulating channel activity and maintaining a state of hypersensitivity<sup>4,5</sup>.

### **I: Overview of TRPA1 function**

Transient receptor potential cation channel subfamily A member 1, commonly referred to as TRPA1, is an ion channel receptor found in vertebrates as well as

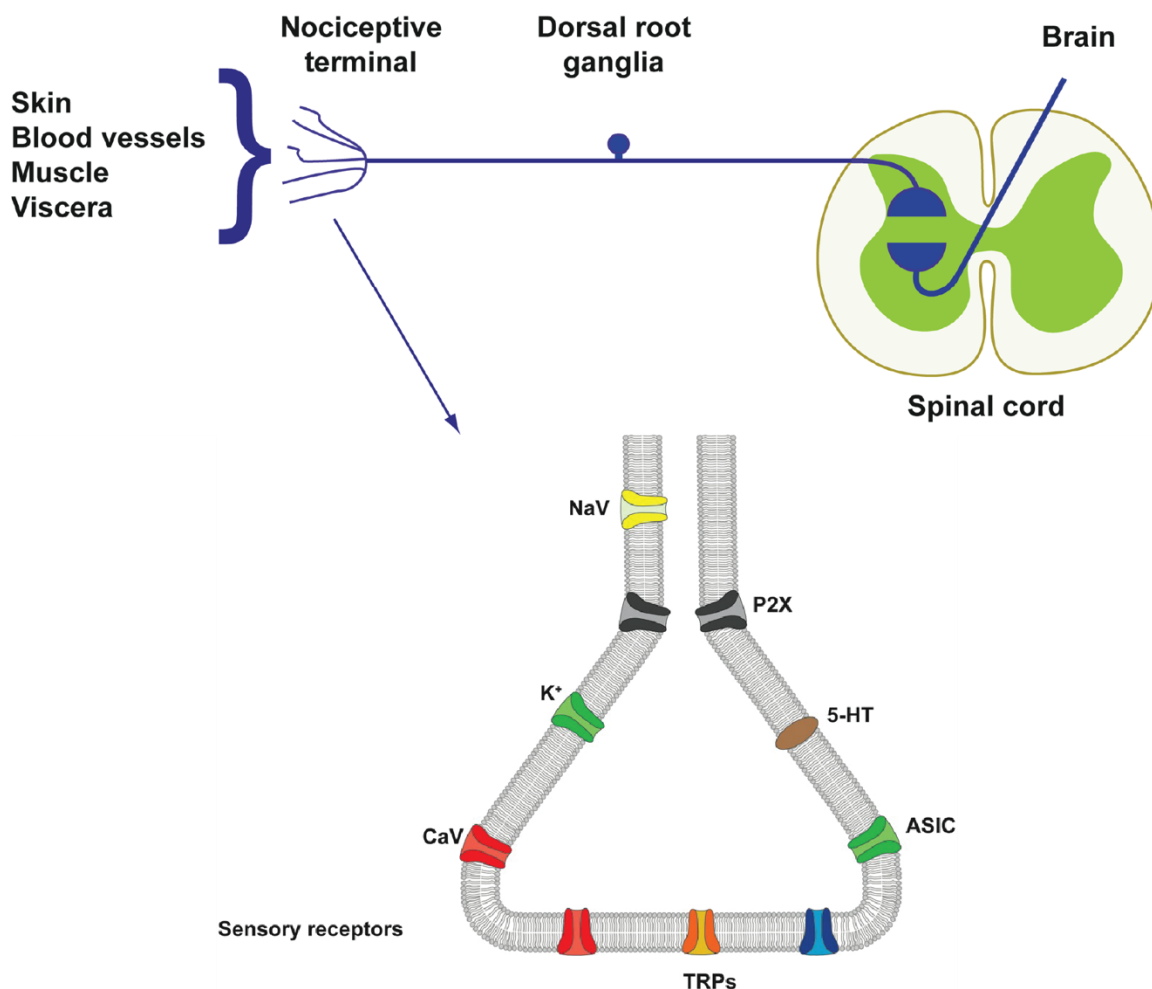


**Figure 1.** Diversity of sensory receptors within the peripheral nervous system underlies our ability to sense changes in the environment and respond accordingly.

invertebrates<sup>1,3,6,7</sup>. TRPA1 mainly functions as a thermosensor in invertebrates and distant vertebrates that promotes avoidance responses to high heat or allows infrared detection<sup>6,8</sup>. However, in mammals TRPA1 has evolved to be a chemosensor that generates avoidance responses to chemical irritants that are strong electrophiles that covalently modify intracellular reactive cysteines on TRPA1 with little bias against shape or size of the molecule making TRPA1 sensitive to a broad array of compounds<sup>7,9-12</sup> (**Fig. 2**). This allows

TRPA1 to act as a cellular alarm system alerting the CNS to the presence of compounds that can covalently modify amino acid side chains, particularly cysteines, and wreak havoc on redox sensitive pathways<sup>9-20</sup>. Several endogenous ligands of TRPA1 have also been identified suggesting TRPA1 plays a role outside of a cellular alarm system for environmental irritants<sup>9,21-30</sup>.

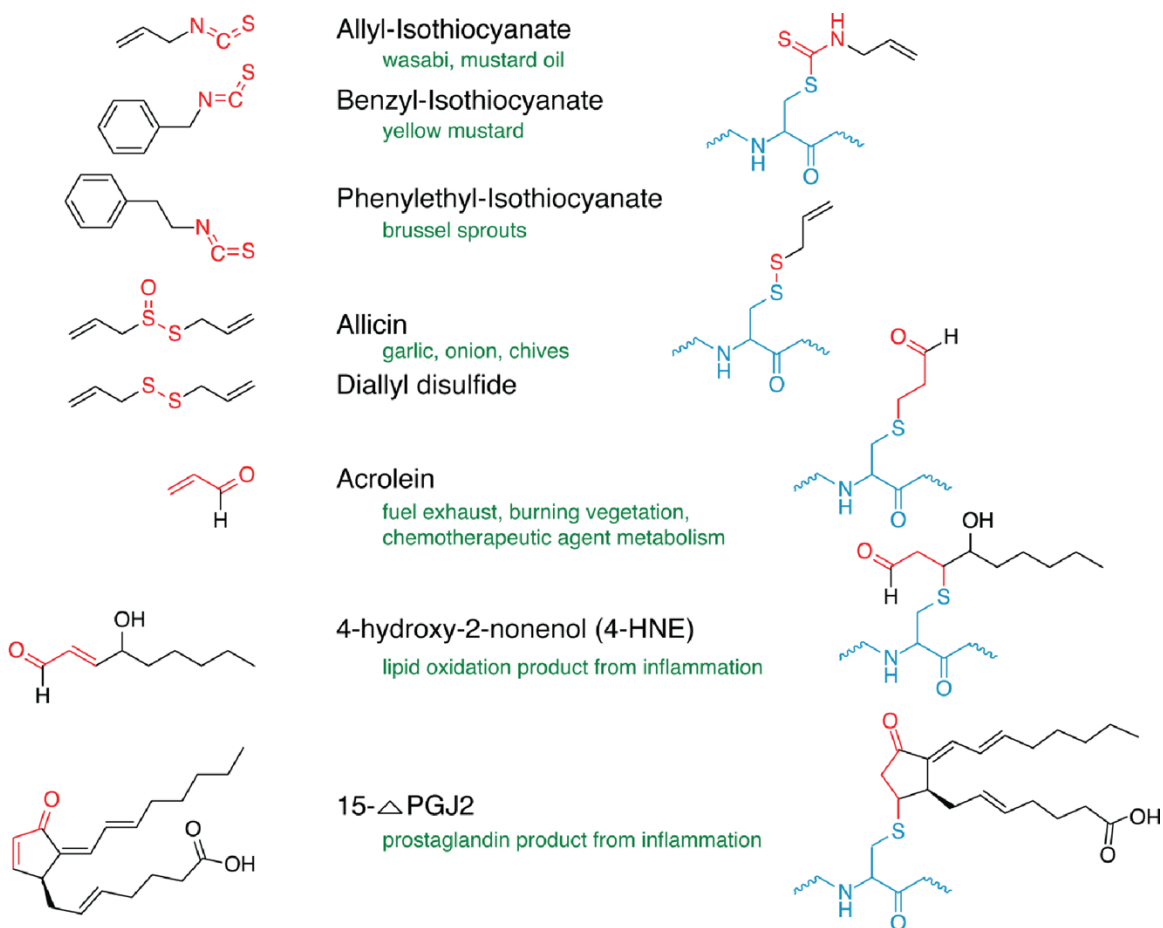


**Figure 2.** Mammalian TRPA1 is activated by a broad array of electrophilic compounds. The left-hand column depicts the electrophilic compound alone, and the right-hand column depicts the thiol adduct formed with TRPA1 cysteine sidechains.

Most of the endogenous activators of TRPA1 are only present under conditions of local inflammation that occur at sites of injury or during infection. Immune cells that are recruited to damaged tissues release reactive oxygen species (ROS) which can react with lipids in the plasma membrane creating lipid peroxides<sup>31</sup>. Two lipid peroxides produced by immune cell ROS release that are known to activate TRPA1 through covalent modification of cysteines are 4-hydroxynonenal (4-HNE) and 4-oxononenal (4-ONE)<sup>29,30</sup>. Injection of 4-HNE into rodent hind paws is able to elicit nocifensive responses but not in rodents lacking TRPA1 suggesting 4-HNE can trigger acute pain through TRPA1 activity<sup>29</sup>. This allows TRPA1 to enhance acute pain to tissue damaged caused by a broad variety of noxious stimuli while TRPA1 itself can only respond directly to electrophilic compounds. Oxidative stress is also a hallmark of respiratory diseases which causes endogenously formed lipid peroxides to accumulate in the upper airway<sup>31,32</sup>. 4-ONE was shown to be a particularly potent activator of TRPA1 in bronchopulmonary neurons leading to increased cough sensitivity<sup>30</sup>. ROS can also react with circulating nitric oxide creating reactive nitrogen species (RNS), and these RNS react with lipids in a similar manner as ROS creating electrophilic nitrated lipids which have been shown to specifically activate TRPA1<sup>27,33</sup>.

In addition to the bevy of endogenous electrophilic ligands created by ROS, inflammatory conditions modulate TRPA1 activity through activation of GPCRs and downstream signaling pathways<sup>9,14,23,25,28,34-37</sup>. Bradykinin is a small peptide released by immune cells in response to tissue damage and is involved in initiating inflammatory signaling cascades<sup>38,39</sup>. Bradykinin has been shown to activate TRPA1 through Phospholipase C (PLC) activity<sup>9</sup>. PLC is activated by liberated Gαq subunits and cleaves

phosphatidylinositol 4,5-bisphosphate (PIP<sub>2</sub>) between the inositol head group and the glycerol backbone generating inositol 1,4,5-triphosphate (IP<sub>3</sub>) and diacylglycerol (DAG) each of which are second messengers that have been shown to modulate TRPA1 activity<sup>40-42</sup>. Accumulating DAG can be converted to arachidonic acid, which is the precursor molecule for prostaglandins, and these lipid autacoids play critical roles in both promoting and resolving inflammation<sup>34,36</sup>. A subset of prostaglandins are electrophilic and can selectively activate TRPA1 *in vitro*, and 15-deoxy-Delta(12,14)-prostaglandin J(2) (15d-PGJ<sub>2</sub>) can activate cultured mouse trigeminal neurons in a TRPA1 dependent manner<sup>23,25,28</sup>. Cutaneous administration of 15d-PGJ<sub>2</sub> also triggers acute nociceptive responses in mice suggesting it has the potential to amplify pain under inflammatory conditions<sup>23</sup>. The IP<sub>3</sub> receptor is an endoplasmic reticulum (ER) resident protein that functions as a ligand-gated calcium (Ca<sup>2+</sup>) channel that opens after binding IP<sub>3</sub><sup>43</sup>. As the ER is the main reservoir of intracellular Ca<sup>2+</sup>, IP<sub>3</sub> receptor activation results in an increase in cytosolic Ca<sup>2+</sup> concentrations. Increases in intracellular Ca<sup>2+</sup> concentrations have been shown to play a key role in TRPA1 regulation which will be detailed in a later section.

## **II: Contribution of TRPA1 to chronic pain, inflammation, and disease**

In addition to being activated by several mediators of inflammation to enhance acute pain, TRPA1 itself is able to initiate inflammatory signaling cascades. TRPA1 is expressed in peptidergic C-fibers which are a subset of nociceptive afferent neurons that contain the neuropeptides substance P (SP) and calcitonin gene-related peptide (CGRP) which play critical roles in neurogenic inflammation and neuronal sensitization<sup>22,35,44-49</sup>. SP and CGRP are small peptides stored in large, dense-core vesicles that are released via Ca<sup>2+</sup>-mediated

exocytosis<sup>50</sup>. Specific activation of TRPA1 has been demonstrated to trigger neuropeptide release through its ability to pass  $\text{Ca}^{2+}$  ions into the cytosol<sup>13,22,25,29,51-54</sup>. CGRP is an incredibly powerful vasodilator that can increase local blood flow at femtomolar concentrations and maintain erythema for up to 6 hours at picomolar concentrations<sup>55</sup>. SP is a weak vasodilator compared to CGRP, but it is able to promote leukocyte extravasation by altering vascular permeability and upregulating the expression of endothelial-leukocyte adhesion molecules<sup>35,49,56</sup>. Together, these neuropeptides are able to efficiently generate local inflammation through increased blood flow and promotion of leukocyte chemotaxis.

TRPA1's ability to initiate neurogenic inflammation places it at a key regulatory control point in a positive feedback loop for pain and inflammation<sup>22,57</sup> (**Fig. 3**). TRPA1 activity is able to depolarize neurons to the threshold potential generating an action potential leading to pain while the  $\text{Ca}^{2+}$  it brings into the neuron triggers exocytosis of SP and CGRP. These neuropeptides promote immune cell recruitment to the surrounding tissues where they release an inflammatory soup which contains several compounds that are able to activate TRPA1 thus sustaining the cycle. This TRPA1-mediated positive feedback loop is striking in how universal its activation can be given that it only requires leukocyte extravasation to inflamed tissues which occurs for almost all instances of tissue damage. Indeed, TRPA1 has been shown to be required for persistent thermal and mechanical hypersensitivity under inflammatory conditions using TRPA1 null knockout mice or pharmacological blockade.

Aberrant activity of TRPA1 has been linked to a plethora of diseases affecting several organ systems. TRPA1 has become increasingly linked to the development of asthma<sup>22,51,58-60</sup>. Using the ovalbumin asthma mouse model, TRPA1 has been shown to play a key role in asthma pathogenesis<sup>51</sup>. Airways of TRPA1 null mice were found to have limited

leukocyte infiltration, lower levels of cytokines, less mucus production, reduced neuropeptide release, and almost no hyperreactivity compared to wild type mice. The phenotype of TRPA1 null mice could also be reproduced in wild type mice by

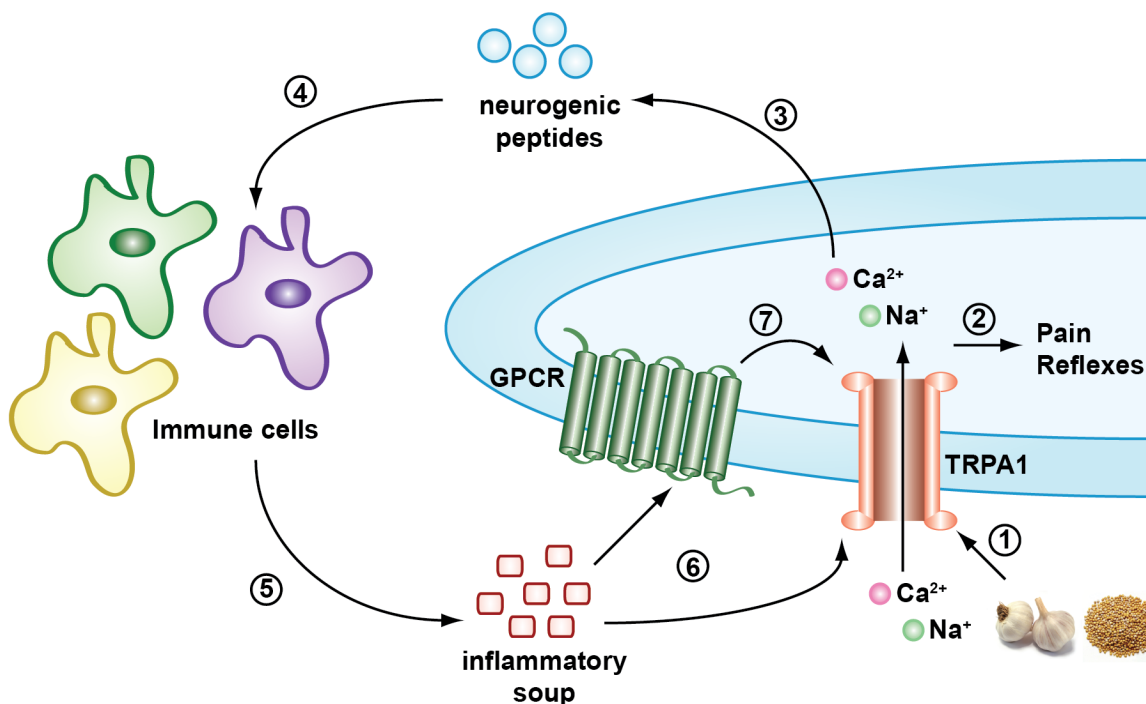


**Figure 3.** TRPA1 sits atop a neurogenic inflammation loop<sup>22</sup> (adapted from Bautista et al. 2013). TRPA1 can be activated by environmental irritants or by endogenous compounds generated by the inflammatory soup released from immune cells. Activation of TRPA1 leads to pain signaling as well as the calcium-dependent release of neuropeptides. These neuropeptides cause vasodilation and promote immune cell recruitment to the site of injury. The immune cells then release the inflammatory soup completing the TRPA1 activation loop.

administering a selective TRPA1 antagonist during ovalbumin challenge. Single nucleotide polymorphisms of TRPA1 have also been associated with the development of childhood asthma<sup>59</sup>. Both acute and chronic colitis (inflammation of the large intestine) in mouse

models of inflammatory bowel diseases is mediated by TRPA1 activity particularly through the release of SP<sup>52,61,62</sup>. Referred pain from visceral inflammation of the colon is also regulated by TRPA1<sup>63</sup>. In humans mRNA levels of TRPA1 were found to be upregulated in colonic tissues samples obtained via biopsy from patients suffering from inflammatory bowel diseases<sup>61</sup>. Activation of TRPA1 in mouse trigeminal neurons and subsequent release of CGRP is believed to contribute to the development of migraines through increased meningeal blood flow<sup>17,47,54</sup>. TRPA1 has also been implicated in inflammatory conditions affecting the skin and cardiovascular system further solidifying its role as a key regulator of inflammation<sup>64-67</sup>.

In addition to inflammatory disorders, TRPA1 has been shown to contribute to the development of chronic pain. Diabetic neuropathy (DN) affects approximately 10% of diabetes patients and has symptoms ranging from numbness and tingling to debilitating pain<sup>68</sup>. Rodent models of DN show upregulation of TRPA1 expression in extracted peripheral neurons doubling the percentage of neurons sensitive to the TRPA1 selective agonist allyl isothiocyanate (AITC)<sup>69</sup>. Behavioral studies show neuropathic mice have increased painful responses to AITC and display both mechanical and thermal (cold and hot) hypersensitivity<sup>69,70</sup>. Methylglyoxal (MG) is an electrophilic compound produced during glucose metabolism and accumulates at higher concentrations in diabetic patients<sup>71</sup>. MG is able to directly modify TRPA1 and injections of MG induce painful responses in wild-type mice but not TRPA1 null mice<sup>21,72,73</sup>. Inhibition of TRPA1 in diabetic mouse models with an antagonist was able to prevent neuronal damage that is a hallmark of DN<sup>70</sup>. A genetic analysis of 392 patients suffering from painful neuropathies or nociplastic pain revealed that rare variants of TRPA1 were highly enriched compared to healthy controls<sup>74</sup>.

Patients with rare TRPA1 variants had been diagnosed with either fibromyalgia, widespread chronic pain, or painful neuropathy with a majority of the TRPA1 variants being missense mutations in regions expected to be critical to channel function and regulation.

TRPA1 has definitively been shown to contribute to acute pain, chronic pain, and inflammation in humans through the discovery and characterization of two inherited pain disorders<sup>75,76</sup>. Familial Episodic Pain Syndrome (FEPS) was identified in related individuals in Colombia sharing a single missense mutation in TRPA1 (N855S) with symptoms appearing in infancy<sup>75</sup>. Pain episodes typically consist of debilitating upper body pain that lasts for approximately 1.5 hours followed by exhaustion and a deep sleep. The main triggers for painful episodes are fasting and fatigue with a host of contributing factors such as illness, cold temperatures, and physical exertion. Painful episodes often require the presence of several factors to be triggered, and an episode is not guaranteed to occur when the triggers are present. It is quite striking that all of the triggers for these TRPA1-induced painful episodes occur under specific physiological conditions that affect cellular signaling pathways across the entire body supporting the model of TRPA1 as a polymodal signal integrator.

Perhaps the most important insight from studying FEPS patients is the direct contribution of TRPA1 to hypersensitivity and inflammation in humans that can be explained by electrophysiology data obtained *in vitro*. Application of AITC to the volar forearm of FEPS patients does not evoke a stronger acute pain response compared to healthy volunteers. However, the inflammatory response and secondary hyperalgesia is more severe in FEPS patients. Skin flare in FEPS patients had a higher mean area compared

to the control group and half of the FEPS patients developed very large flairs ( $> 8 \text{ cm}^2$ ) which was not seen in the control group. The area of punctate hyperalgesia was significantly larger in FEPS patients at both 10 minutes and 60 minutes and the area of brush-evoked allodynia was also larger but non-significant. Whole cell patch clamp electrophysiology studies of HEK293 cells expressing N855S revealed the mutation results in drastically larger inward currents near resting membrane potentials (-100 mV to -70 mV) compared to wild type channels. This was true for both the exogenous agonist cinnamaldehyde and the endogenous agonist 4-HNE suggesting this enhanced activity would also occur *in vivo* under inflammatory conditions. There were relatively small to no changes in the EC50 and voltage dependency of N855S showing that changes in activity are likely due to changes in channel gating. TRPA1 selective antagonists are able to inhibit N855S to a similar degree as wild type channels suggesting the overall channel architecture is preserved.

The other inherited TRPA1 disease was discovered in a father-son pair that were initially diagnosed with cramp-fasciculation (CFS) syndrome due to chronic, debilitating cramps and muscle twitching from muscle hyperexcitability<sup>76</sup>. However, they also presented with symptoms atypical for CFS including generalized chronic pain and pruritis, cold hyperalgesia including more intense cramps triggered by cold temperatures, migraine with visual aura, heart palpitations, paroxysmal resting tachycardia, asthma as well as chronic cough that worsens in cold temperatures, and various symptoms of GI distress. Whole exome sequencing of the father-son pair as well as healthy family members revealed only one candidate variant that was present in both the father-son pair and absent from the healthy family members: a TRPA1 mutation in one allele resulting in a nonsense mutation

in the pore loop (R919\*). This rare disease was renamed to cramp-fasciculation, reflux, asthma/anxiety, migraine, paresthesias/pain, and tachycardia/tremor (CRAMPT) syndrome to better reflect the symptoms associated with the variant. As discussed in previous sections, TRPA1 has been linked to many of the symptoms experienced by patients with CRAMPT. Our lab characterized the effects of this mutation on TRPA1 activity and found that patient heterozygosity was essential for developing the disease<sup>77</sup>. Homomeric R919\* channels are inactive likely due to severely perturbed channel architecture as well as inability to traffic to the plasma membrane. However, heteromeric channels comprised of wild type and R919\* subunits are able to traffic to the plasma membrane and are hyperactive compared to wild type homomeric channels. Two electrode voltage-clamp (TEVC) of *Xenopus laevis* oocytes expressing wild-type and R919\* TRPA1 shows hyperactivity arises from a nearly 5-fold enhancement in agonist sensitivity as well as changes to the pore architecture that likely increase its diameter. While the pore architecture of R919\* heteromeric channels is likely perturbed, selective TRPA1 antagonists are able to inhibit heteromeric channel activity suggesting overall channel architecture is minimally perturbed.

FEPS and CRAMPT definitively show that TRPA1 activity in humans contributes to pain and inflammation across several organ systems consistent with data collected from animal models and *in vitro*. TRPA1 is not merely a cellular alarm system for environmental threats but acts as a key signal integrator allowing for bidirectional communication between the immune system and peripheral nervous system to maintain neuronal hypersensitivity and inflammation making it a prime target for the development of novel analgesics<sup>16,17,20,22,24,30,41,46,51,53,54,57-59,61-63,70,78-84</sup>. Being positioned in such a critical

regulatory juncture for pain and inflammation as well as being permeable to such a critical second messenger in  $\text{Ca}^{2+}$  would suggest *in vivo* mechanisms exist to control TRPA1 activity and prevent the development of chronic pain and inflammation and spurious activation of  $\text{Ca}^{2+}$  signaling cascades. Indeed,  $\text{Ca}^{2+}$  has been shown to be critical for proper channel regulation.

### III: Complex calcium regulation of TRPA1

TRPA1 exhibits complex  $\text{Ca}^{2+}$  regulation where changes in extracellular and intracellular  $\text{Ca}^{2+}$  concentrations both positively and negatively regulate TRPA1 activity<sup>77,85-90</sup>. The muscarinic acetylcholine receptor (mAChR) is a GPCR that can be used as a model system for  $\text{G}\alpha_q/\text{PLC}$  signaling *in vitro* which ultimately results in robust increases in cytosolic  $\text{Ca}^{2+}$  through the IP3 receptor in the ER<sup>91,92</sup>. In the absence of a known TRPA1 agonist, stimulation of mAChR with carbachol was found to activate TRPA1<sup>7</sup>. This effect could also be produced using thapsigargin which increases cytosolic  $\text{Ca}^{2+}$  by inhibiting  $\text{Ca}^{2+}$  pumps in the ER suggesting  $\text{Ca}^{2+}$  was responsible for activating TRPA1 rather than a separate pathway activated by PLC<sup>7</sup>. Perfusion of  $\text{Ca}^{2+}$  onto excised inside-out patches containing TRPA1 was also able to generate TRPA1 currents supporting the hypothesis that TRPA1 is directly activated by  $\text{Ca}^{2+}$  ions<sup>87,88</sup>.

In whole-cell and outside-out electrophysiology experiments electrophilic agonists can generate stable TRPA1 currents in the absence of extracellular  $\text{Ca}^{2+}$  for upwards of 10 minutes<sup>11</sup>. However, upon the addition of physiologically relevant concentrations of extracellular  $\text{Ca}^{2+}$  (2 mM), TRPA1 currents are rapidly potentiated followed by desensitization<sup>7,77,86,90</sup>. A TRPA1 pore mutant with dramatically reduced  $\text{Ca}^{2+}$  permeability

has essentially no  $\text{Ca}^{2+}$ -induced potentiation and slowed desensitization rates demonstrating that extracellular  $\text{Ca}^{2+}$  must permeate through TRPA1 to initiate potentiation and desensitization rather than binding an extracellular site on TRPA1<sup>86</sup>. Potentiation and desensitization and have also been shown to be separate events regulated by different mechanisms rather than a single, concerted mechanism<sup>86,89,90</sup>. Photo uncaging of intracellular DMNP-chelated  $\text{Ca}^{2+}$  was able to trigger sustained potentiation of active TRPA1 channels, but the addition of 2 mM extracellular  $\text{Ca}^{2+}$  was required to trigger desensitization<sup>86</sup>. This was confirmed by exposing inside-out patches of TRPA1 to low amounts of  $\text{Ca}^{2+}$  for sustained potentiation and higher amounts of  $\text{Ca}^{2+}$  for potentiation followed by desensitization. This can also be observed in whole-cell configurations by manipulating the extracellular concentrations of  $\text{Ca}^{2+}$ . Intriguingly, desensitization can also be slowed by truncating the last 20 residues of the TRPA1 C-terminus while potentiation remains unaffected suggesting the TRPA1 C-terminus is essential for initiating  $\text{Ca}^{2+}$ -dependent desensitization<sup>93</sup>.

The effects of  $\text{Ca}^{2+}$  on TRPA1 activity have been extensively documented, particularly by work done in the Liman lab<sup>86</sup>, but the mechanisms governing these effects have remained a point of controversy in the field. While several TRP channels are regulated by the universal  $\text{Ca}^{2+}$  sensor calmodulin (CaM), initial investigations into TRPA1  $\text{Ca}^{2+}$  regulation suggested that CaM had no effect on TRPA1<sup>94-98</sup>. For many ion channels regulated by CaM, binding of CaM occurs under basal conditions in cells as well as in the absence of  $\text{Ca}^{2+}$  *in vitro*<sup>99-101</sup>. This pre-association allows the channel to rapidly respond to changes in cytosolic  $\text{Ca}^{2+}$  through CaM rather than direct coordination of  $\text{Ca}^{2+}$  to the channel. The  $\text{Ca}^{2+}$ -independent binding can be exploited through the use of a CaM

construct that cannot bind  $\text{Ca}^{2+}$  ( $\text{CaM}_{1234}$ ) and acts as a dominant negative mutant through competitive inhibition of CaM. Co-expression of TRPA1 and  $\text{CaM}_{1234}$  had no discernible effect on TRPA1 activity demonstrating that CaM cannot bind TRPA1 in a  $\text{Ca}^{2+}$ -independent manner and strongly suggesting that CaM does not pre-associate with TRPA1<sup>86-89</sup>. However, it is possible that CaM only requires a low concentration of  $\text{Ca}^{2+}$  to bind TRPA1 which might be present under basal cellular conditions. To test this possibility, inside-out patches of cells expressing TRPA1 were exposed to the  $\text{Ca}^{2+}$  chelator EGTA to remove all remaining  $\text{Ca}^{2+}$  which would disrupt any potential  $\text{Ca}^{2+}$ -dependent CaM binding followed by buffer exchanges to remove free CaM. Under these conditions TRPA1 activity was still modulated by the addition of  $\text{Ca}^{2+}$  to the inside-out patches suggesting TRPA1 coordinates  $\text{Ca}^{2+}$  ions to regulate activity.

Several  $\text{Ca}^{2+}$  binding sites have been proposed for TRPA1 with conflicting and inconclusive evidence for their role in regulating TRPA1. A putative EF-hand was identified in the N-terminus of TRPA1 within the ankyrin repeat domain (ARD) and was suggested to control direct gating of TRPA1 by  $\text{Ca}^{2+}$  ions<sup>87,88,102</sup>. However, other groups have failed to replicate these results through their own mutagenesis studies casting doubt on the EF-hand model of  $\text{Ca}^{2+}$  regulation<sup>12,86</sup>. There is also no direct evidence that  $\text{Ca}^{2+}$  binds this region of TRPA1. A second putative  $\text{Ca}^{2+}$  binding site was identified in the distal C-terminus within the last 50 residues of the primary sequence<sup>93</sup>. This proposed C-terminal  $\text{Ca}^{2+}$  binding site is comprised of an acidic cluster of residues that has homology with the  $\text{Ca}^{2+}$  activation bowl in big conductance potassium (BK) channels. Mutagenesis of some of the acidic cluster residues resulted in impaired potentiation and overall lower activity compared to wild type channels. Molecular dynamic simulations of the acidic cluster

region suggested it has the potential to bind  $\text{Ca}^{2+}$ , but there is no direct evidence confirming  $\text{Ca}^{2+}$  binding in this region. The only confirmed  $\text{Ca}^{2+}$  binding site (CBS) on TRPA1 lies in the loop connecting the S2 and S3 transmembrane helices which was discovered via a cryo-EM structure and is conserved within the TRPM family<sup>90</sup>. A single point mutation of a  $\text{Ca}^{2+}$  coordinating residue (E788S) in the CBS results in loss of potentiation and sensitivity to carbachol, and a triple point mutation (E788S, Q791S, N805S) also leads to a loss in desensitization. However, the purification strategy used to obtain the structure of the CBS suggests this site may not have the ability to act as a  $\text{Ca}^{2+}$  sensor. This will be covered in detail in the next section on insights from TRPA1 structures.

While early work on TRPA1  $\text{Ca}^{2+}$  regulation suggested CaM was not involved, more recent research from the Zhang lab provides evidence that CaM is involved in both  $\text{Ca}^{2+}$  dependent potentiation and desensitization for mouse TRPA1 (mTRPA1)<sup>89</sup>. They demonstrated that CaM binds mTRPA1 in a  $\text{Ca}^{2+}$ -dependent manner, but only requires 0.1  $\mu\text{M}$   $\text{Ca}^{2+}$  for robust binding which would allow the interaction to occur under basal cellular conditions and possibly behave as an auxiliary subunit. Whole-cell electrophysiology studies of HEK293 cells overexpressing TRPA1 and CaM or CaM<sub>1234</sub> show that CaM is required for potentiation at low extracellular  $\text{Ca}^{2+}$  concentrations and desensitization at higher extracellular  $\text{Ca}^{2+}$  concentrations. Further experiments demonstrated these effects could be replicated using CaM<sub>12</sub> which ablates  $\text{Ca}^{2+}$  binding in the low  $\text{Ca}^{2+}$  affinity N-lobe while CaM<sub>34</sub> has no effect on TRPA1 similar to CaM<sub>1234</sub>. Regulation of TRPA1 through CaM only requires  $\text{Ca}^{2+}$  sensitivity in the C-lobe of CaM. This highly suggests binding of TRPA1 occurs through the C-lobe of CaM. Using a GST-tagged intracellular C-terminus of mTRPA1 with progressively larger truncations, they identified a CaM binding domain

(CaMBD) just past the TRP-like helix in the primary sequence corresponding to residues W996-P1010 (W993-P1007 in humans). When co-expressed with TRPA1 this peptide was able to block the regulatory effect of CaM on TRPA1 activity by sequestering CaM. Mutagenesis of residues within the CaMBD reduced the ability of CaM to bind TRPA1 and affected potentiation and desensitization. While this work shows that CaM is likely involved in TRPA1 Ca<sup>2+</sup> regulation, there are concerns for the role of the proposed CaMBD in this process. Point mutations within the CaMBD that reduce CaM binding also lead to a 5-to-10-fold reduction in activity in the *absence* of extracellular Ca<sup>2+</sup>. It is possible that mutagenesis of the CaMBD causes channel instability leading to lower activity rather than through loss of CaM binding. This work also does not address why exposure to EGTA in inside-out patches has no apparent effect on TRPA1 Ca<sup>2+</sup> regulation.

#### **IV: TRPA1 Structural Insights**

The collection of several high-resolution cryo-EM structures provided the greatest insights into the mechanisms of electrophile activation and channel gating. However, the mechanism of Ca<sup>2+</sup> regulation has remained elusive.

It was known that reactive cysteines were required for electrophile sensitivity, but cryo-EM structures revealed the mechanism that allows such promiscuity in ligand binding and how this information is transmitted to the ion conduction pathway<sup>90,103</sup>. The reactive cysteines are in an intracellular, solvent exposed pocket formed by a helix-loop-helix structure that sits just beneath the TRP-like helix dubbed the linker domain which contacts the pre-S1 helix as well as the S4-S5 linker forming an allosteric nexus that can readily communicate with the pore<sup>90,103,104</sup>. Covalent modification of these cysteines triggers the

nearby activation loop to transition from the “down” conformation to the “up” conformation which allows K671 to interact with carbonyl backbones at the C-terminus of the TRP-like helix. It is proposed this interaction enhances the dipole moment of the TRP-like helix leading to an expansion of the channel through movement of the S6 helix and stabilizing the open conformation. Mutagenesis studies confirmed that K671 is a critical component of electrophilic gating.

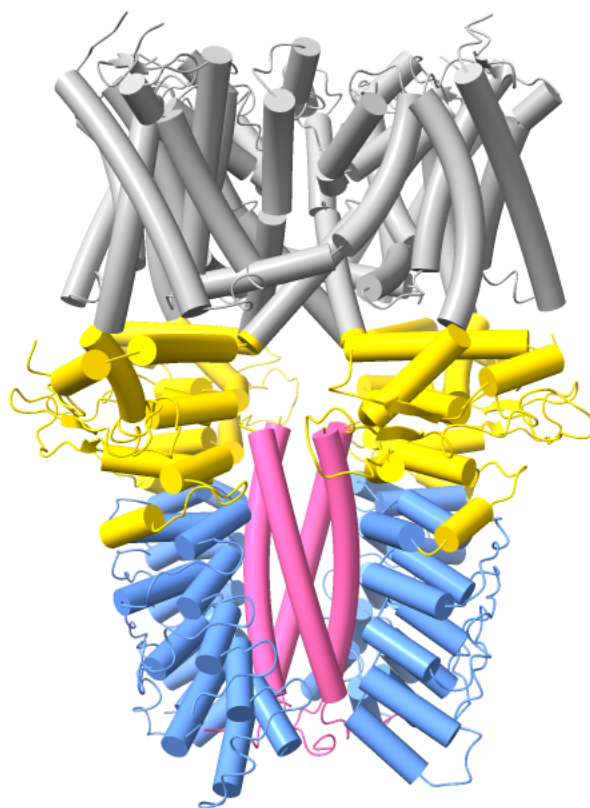


**Figure 4.** Overall channel architecture of TRPA1. Ankyrin repeats 12-16 are depicted as blue tubes, the linker domain and allosteric nexus are depicted as yellow tubes, the coiled coil is depicted as pink tubes, and the transmembrane domain is depicted as gray tubes. The spring-like structure of the ankyrin repeats and the coiled coil sitting just beneath the

allosteric nexus suggests long-range allosteric communication between the ARD, coiled-coil, and the pore are possible.

While the cryo-EM structures of TRPA1 do not fully explain  $\text{Ca}^{2+}$  regulation, they do provide a basis for how channel gating can be regulated through allosteric effects communicated through the intracellular domains. Ankyrin repeats 12-16 are the first residues within the primary sequence to be structurally resolved, and the repeats adopt a linear solenoid structure with little to no curvature similar to the rungs of a ladder. The ankyrin repeats from each of the four protomers form a cage around a central coiled-coil comprised of 4 helices with 1 helix provided from the intracellular C-terminus of each protomer. The extensive contacts between the coiled-coil and the structured ARDs forms a spring-like structure that appears to be primed to move as a single domain rather than four independent domains. Ankyrin repeat 16 is also positioned just below and contacts the linker domain that houses the electrophilic cysteines involved in channel gating. The allosteric nexus is also just above the linker domain which provides a potential mechanism for long-range allosteric regulation of the pore through the ARD and coiled coil.

Of the four proposed  $\text{Ca}^{2+}$  regulation sites on TRPA1, three of the putative sites are visible in the high-resolution maps while the last 41 residues of the C-terminus which includes the acidic cluster are disordered. The residues of the putative EF-hand domain form a helix-loop-helix structure but in a manner inconsistent with a typical EF-hand. This could still possibly coordinate a  $\text{Ca}^{2+}$ , but no solved structures have a bound  $\text{Ca}^{2+}$  in that position. The available structures of TRPA1 provide an appealing model to potentially explain why the S2-S3 CBS and the CaMBD both contribute to  $\text{Ca}^{2+}$  potentiation and

desensitization. Individually,  $\text{Ca}^{2+}$  binding at the S2-S3 CBS could induce changes within the S1-S4 helical bundle that could readily be communicated to the pore lining helices. The CaMBD is immediately adjacent to the TRP-like domain and the linker domain, so any conformational change in CaM upon  $\text{Ca}^{2+}$  influx could easily be communicated to the allosteric nexus as well. In addition, the S1-S4 helical bundle including the S2-S3 CBS and the CaMBD are packed against each other in the structure. It is possible that these regions influence each other upon  $\text{Ca}^{2+}$  influx and work in concert to provide that complex  $\text{Ca}^{2+}$  regulation displayed by TRPA1. However, there are important caveats for this model. During the purification of the channels used to generate S2-S3  $\text{Ca}^{2+}$  bound structures, the buffers did not contain any supplemented  $\text{Ca}^{2+}$  ions<sup>90</sup>. This indicates the CBS likely has a high affinity for  $\text{Ca}^{2+}$  and is saturated at basal  $\text{Ca}^{2+}$  concentrations. If this is the case, it cannot function as a  $\text{Ca}^{2+}$  sensor and likely plays a role in structural stability. The CaMBD also does not resemble a typical CaM binding motif even amongst non-canonical binding sites<sup>105-107</sup>. A CaM binding site is almost always a single helix that binds the hydrophobic grooves in both the N and C-lobe of CaM or two helices that bind each lobe separately. However, the CaMBD is comprised of a short two-turn helix and a  $\beta$ -strand connected by a short loop. Of the three residues in the CaMBD found to be most important to  $\text{Ca}^{2+}$  regulation and CaM binding, only W993 was in the helix while V1005 and P1007 were located in the  $\beta$ -strand<sup>89</sup>. In addition, both V1005 and P1007 face away from the cytosol and are packed against the pre-S1 helix making them unavailable to bind CaM. This suggests the effects of V1005 and P1007 on channel activity and CaM binding are due to broader structural changes and channel instability rather than reduced ability to bind CaM.

The distal C-terminus (AA 1079-1119) which houses most of the acidic cluster has remained unresolved across TRPA1 structures and is likely disordered. However, we can reasonably infer it is in position to allosterically regulate channel activity. The structured region of the distal C-terminus typically terminates just beneath the coiled-coil and between Ankyrin repeat 12 of adjacent protomers. Upon  $\text{Ca}^{2+}$  influx, the acidic cluster might coordinate  $\text{Ca}^{2+}$  and undergo a disorder-to-order transition<sup>93</sup>. Given its close proximity to the ARD and the coiled-coil this structural change would influence the spring-like intracellular domain to potentially regulate potentiation. The disordered C-terminus beyond the acidic cluster has been shown to have two other effects on TRPA1 activity which is surprising given its size compared to the full channel. Truncation of the final 26 residues (TRPA1 $_{\Delta 1094-1119}$ ) produces channels that cannot generate currents when expressed in cells which is likely due to a trafficking defect. However, adding back only six residues (TRPA1 $_{\Delta 1100-1119}$ ) produces channels that can generate currents but with dramatically slower desensitization as opposed to reduced potentiation. It is difficult to rationalize how two regulatory regions within the last 41 residues of the distal and disordered C-terminus can seemingly modulate  $\text{Ca}^{2+}$ -dependent potentiation and desensitization independently of each other given their distance from the pore. Additionally, there has been no putative mechanism put forth to explain how the final 20 residues of TRPA1 could be regulating desensitization.

### **Concluding Remarks**

TRPA1 has emerged as a prime target for the development of novel therapeutics to treat chronic pain and inflammation. Ligand gating of TRPA1 through covalent modification of intracellular cysteines with little regard for shape and size of the reactive electrophile

allows TRPA1 to be activated by a wide array of electrophilic molecules. The immune system has taken advantage of this by releasing ROS at sites of injury creating electrophilic lipids that activate TRPA1 enhancing acute pain by depolarizing neurons to the threshold potential. In turn, TRPA1 activity leads to  $\text{Ca}^{2+}$  influx and the release of neurogenic peptides that recruit more immune cells and promote inflammation. This allows TRPA1 to act as a key signal integrator allowing for bidirectional communication between the immune system and peripheral nervous system to maintain neuronal hypersensitivity and inflammation. Understanding the mechanisms that regulate TRPA1 activity will be critical for developing novel therapeutics.

The first line of defense for regulating TRPA1 activity is  $\text{Ca}^{2+}$ -dependent desensitization.  $\text{Ca}^{2+}$  that permeates through the pore of TRPA1 is able to rapidly desensitize the channel. While this phenomenon has been well documented, the mechanism governing this process has remained controversial within the field. There are several putative sites of  $\text{Ca}^{2+}$  regulation and conflicting evidence regarding  $\text{Ca}^{2+}$  coordination and CaM binding in TRPA1. Uncovering the mechanism of TRPA1  $\text{Ca}^{2+}$  regulation would provide a new avenue for rational drug design to treat pain and inflammation.

## References

1. Julius, D. & Basbaum, A.I. Molecular mechanisms of nociception. *Nature* **413**, 203-210 (2001).
2. Gaskin, D.J. & Richard, P. The Economic Costs of Pain in the United States. *Journal of Pain* **13**, 715-724 (2012).
3. Julius, D. TRP channels and pain. *Annu Rev Cell Dev Biol* **29**, 355-84 (2013).
4. Mattson, C.L. et al. Trends and Geographic Patterns in Drug and Synthetic Opioid Overdose Deaths - United States, 2013-2019. *Mmwr-Morbidity and Mortality Weekly Report* **70**, 202-207 (2021).
5. Sehgal, N., Manchikanti, L. & Smith, H.S. Prescription Opioid Abuse in Chronic Pain: A Review of Opioid Abuse Predictors and Strategies to Curb Opioid Abuse. *Pain Physician* **15**, Es67-Es92 (2012).
6. Chen, J. et al. Species differences and molecular determinant of TRPA1 cold sensitivity. *Nature Communications* **4**(2013).
7. Jordt, S.E. et al. Mustard oils and cannabinoids excite sensory nerve fibres through the TRP channel ANKTM1. *Nature* **427**, 260-265 (2004).
8. Cordero-Morales, J.F., Gracheva, E.O. & Julius, D. Cytoplasmic ankyrin repeats of transient receptor potential A1 (TRPA1) dictate sensitivity to thermal and chemical stimuli. *Proceedings of the National Academy of Sciences of the United States of America* **108**, E1184-E1191 (2011).
9. Bandell, M. et al. Noxious cold ion channel TRPA1 is activated by pungent compounds and bradykinin. *Neuron* **41**, 849-857 (2004).
10. Hinman, A., Chuang, H.H., Bautista, D.M. & Julius, D. TRP channel activation by reversible covalent modification. *Proceedings of the National Academy of Sciences of the United States of America* **103**, 19564-19568 (2006).
11. Macpherson, L.J. et al. Noxious compounds activate TRPA1 ion channels through covalent modification of cysteines. *Nature* **445**, 541-545 (2007).
12. Nilius, B., Prenen, J. & Owsianik, G. Irritating channels: the case of TRPA1. *J Physiol* **589**, 1543-9 (2011).
13. André, E. et al. Cigarette smoke-induced neurogenic inflammation is mediated by  $\alpha,\beta$ -unsaturated aldehydes and the TRPA1 receptor in rodents. *Journal of Clinical Investigation* **118**, 2574-2582 (2008).
14. Bautista, D.M. et al. TRPA1 mediates the inflammatory actions of environmental irritants and proalgesic agents. *Cell* **124**, 1269-1282 (2006).
15. Cavanaugh, E.J., Simkin, D. & Kim, D. Activation of transient receptor potential A1 channels by mustard oil, tetrahydrocannabinol and Ca reveals different functional channel states. *Neuroscience* **154**, 1467-1476 (2008).
16. King, J.V.L. et al. A Cell-Penetrating Scorpion Toxin Enables Mode-Specific Modulation of TRPA1 and Pain. *Cell* **178**, 1362-+ (2019).
17. Kunkler, P.E., Ballard, C.J., Oxford, G.S. & Hurley, J.H. TRPA1 receptors mediate environmental irritant-induced meningeal vasodilatation. *Pain* **152**, 38-44 (2011).
18. Kwan, K.Y. et al. TRPA1 contributes to cold, mechanical, and chemical Nociception but is not essential for hair-cell transduction. *Neuron* **50**, 277-289 (2006).
19. Meents, J.E., Ciotu, C.I. & Fischer, M.J.M. TRPA1: a molecular view. *J Neurophysiol* **121**, 427-443 (2019).
20. Meseguer, V. et al. TRPA1 channels mediate acute neurogenic inflammation and pain produced by bacterial endotoxins. *Nature Communications* **5**(2014).
21. Andersson, D.A. et al. Methylglyoxal Evokes Pain by Stimulating TRPA1. *Plos One* **8**(2013).

22. Bautista, D.M., Pellegrino, M. & Tsunozaki, M. TRPA1: A Gatekeeper for Inflammation. *Annual Review of Physiology*, Vol 75 **75**, 181-200 (2013).
23. Cruz-Orengo, L. et al. Cutaneous nociception evoked by 15-delta PGJ2 via activation of ion channel TRPA1. *Mol Pain* **4**, 30 (2008).
24. Lennertz, R.C., Kossyрева, E.A., Smith, A.K. & Stucky, C.L. TRPA1 Mediates Mechanical Sensitization in Nociceptors during Inflammation. *Plos One* **7**(2012).
25. Materazzi, S. et al. Cox-dependent fatty acid metabolites cause pain through activation of the irritant receptor TRPA1. *Proceedings of the National Academy of Sciences of the United States of America* **105**, 12045-12050 (2008).
26. Sisignano, M. et al. 5,6-EET Is Released upon Neuronal Activity and Induces Mechanical Pain Hypersensitivity via TRPA1 on Central Afferent Terminals. *Journal of Neuroscience* **32**, 6364-6372 (2012).
27. Taylor-Clark, T.E., Ghatta, S., Bettner, W. & Udem, B.J. Nitrooleic Acid, an Endogenous Product of Nitrative Stress, Activates Nociceptive Sensory Nerves via the Direct Activation of TRPA1. *Molecular Pharmacology* **75**, 820-829 (2009).
28. Taylor-Clark, T.E. et al. Prostaglandin-induced activation of nociceptive neurons via direct interaction with transient receptor potential A1 (TRPA1). *Mol Pharmacol* **73**, 274-81 (2008).
29. Trevisani, M. et al. 4-Hydroxynonenal, an endogenous aldehyde, causes pain and neurogenic inflammation through activation of the irritant receptor TRPA1. *Proceedings of the National Academy of Sciences of the United States of America* **104**, 13519-13524 (2007).
30. Taylor-Clark, T.E. et al. Relative contributions of TRPA1 and TRPV1 channels in the activation of vagal bronchopulmonary C-fibres by the endogenous autacoid 4-oxononenal. *Journal of Physiology-London* **586**, 3447-3459 (2008).
31. Mittal, M., Siddiqui, M.R., Tran, K., Reddy, S.P. & Malik, A.B. Reactive Oxygen Species in Inflammation and Tissue Injury. *Antioxidants & Redox Signaling* **20**, 1126-1167 (2014).
32. Holguin, F. Oxidative stress in airway diseases. *Ann Am Thorac Soc* **10 Suppl**, S150-7 (2013).
33. Kalyanaraman, B. Nitrated lipids: A class of cell-signaling molecules. *Proceedings of the National Academy of Sciences of the United States of America* **101**, 11527-11528 (2004).
34. Ricciotti, E. & FitzGerald, G.A. Prostaglandins and Inflammation. *Arteriosclerosis Thrombosis and Vascular Biology* **31**, 986-1000 (2011).
35. Richardson, J.D. & Vasko, M.R. Cellular mechanisms of neurogenic inflammation. *Journal of Pharmacology and Experimental Therapeutics* **302**, 839-845 (2002).
36. Stella, N. Cell biology. Anatomy of prostaglandin signals. *Science* **334**, 768-9 (2011).
37. Sun, L. & Ye, R.D. Role of G protein-coupled receptors in inflammation. *Acta Pharmacol Sin* **33**, 342-50 (2012).
38. Dray, A. & Perkins, M. Bradykinin and Inflammatory Pain. *Trends in Neurosciences* **16**, 99-104 (1993).
39. Kidd, B.L. & Urban, L.A. Mechanisms of inflammatory pain. *British Journal of Anaesthesia* **87**, 3-11 (2001).
40. Kadamur, G. & Ross, E.M. Mammalian Phospholipase C. *Annual Review of Physiology*, Vol 75 **75**, 127-154 (2013).
41. Dai, Y. et al. Sensitization of TRPA1 by PAR2 contributes to the sensation of inflammatory pain. *Journal of Clinical Investigation* **117**, 1979-1987 (2007).
42. Wang, S. et al. Phospholipase C and protein kinase A mediate bradykinin sensitization of TRPA1: a molecular mechanism of inflammatory pain. *Brain* **131**, 1241-1251 (2008).
43. Mikoshiba, K. IP3 receptor Calcium channel: from discovery to new signaling concepts. *Journal of Neurochemistry* **102**, 1426-1446 (2007).

44. Hjerling-Leffler, J., AlQatari, M., Ernfors, P. & Koltzenburg, M. Emergence of functional sensory subtypes as defined by transient receptor potential channel expression. *Journal of Neuroscience* **27**, 2435-2443 (2007).
45. Kim, Y.S. et al. Expression of Transient Receptor Potential Ankyrin 1 (TRPA1) in the Rat Trigeminal Sensory Afferents and Spinal Dorsal Horn. *Journal of Comparative Neurology* **518**, 687-698 (2010).
46. Chiu, I.M., von Hehn, C.A. & Woolf, C.J. Neurogenic inflammation and the peripheral nervous system in host defense and immunopathology. *Nature Neuroscience* **15**, 1063-1067 (2012).
47. Iyengar, S., Ossipov, M.H. & Johnson, K.W. The role of calcitonin gene-related peptide in peripheral and central pain mechanisms including migraine. *Pain* **158**, 543-559 (2017).
48. Matsuda, M., Huh, Y. & Ji, R.R. Roles of inflammation, neurogenic inflammation, and neuroinflammation in pain. *Journal of Anesthesia* **33**, 131-139 (2019).
49. O'Connor, T.M. et al. The role of substance P in inflammatory disease. *Journal of Cellular Physiology* **201**, 167-180 (2004).
50. Russo, A.F. Overview of Neuropeptides: Awakening the Senses? *Headache* **57**, 37-46 (2017).
51. Caceres, A.I. et al. A sensory neuronal ion channel essential for airway inflammation and hyperreactivity in asthma. *Proceedings of the National Academy of Sciences of the United States of America* **106**, 9099-9104 (2009).
52. Engel, M.A. et al. TRPA1 and Substance P Mediate Colitis in Mice. *Gastroenterology* **141**, 1346-1358 (2011).
53. Gouin, O. et al. TRPV1 and TRPA1 in cutaneous neurogenic and chronic inflammation: pro-inflammatory response induced by their activation and their sensitization. *Protein Cell* **8**, 644-661 (2017).
54. Nassini, R., Materazzi, S., Benemei, S. & Geppetti, P. The TRPA1 Channel in Inflammatory and Neuropathic Pain and Migraine. *Reviews of Physiology, Biochemistry and Pharmacology, Vol 167* **167**, 1-43 (2014).
55. Russell, F.A., King, R., Smillie, S.J., Kodji, X. & Brain, S.D. Calcitonin Gene-Related Peptide: Physiology and Pathophysiology. *Physiological Reviews* **94**, 1099-1142 (2014).
56. Harrison, S. & Geppetti, P. Substance P. *International Journal of Biochemistry & Cell Biology* **33**, 555-576 (2001).
57. Landini, L. et al. TRPA1 Role in Inflammatory Disorders: What Is Known So Far? *International Journal of Molecular Sciences* **23**(2022).
58. Balestrini, A. et al. A TRPA1 inhibitor suppresses neurogenic inflammation and airway contraction for asthma treatment. *Journal of Experimental Medicine* **218**(2021).
59. Gallo, V. et al. gene polymorphisms and childhood asthma. *Pediatric Allergy and Immunology* **28**, 191-198 (2017).
60. Grace, M.S., Baxter, M., Dubuis, E., Birrell, M.A. & Belvisi, M.G. Transient receptor potential (TRP) channels in the airway: role in airway disease. *Br J Pharmacol* **171**, 2593-607 (2014).
61. Cseko, K., Beckers, B., Keszthelyi, D. & Helyes, Z. Role of TRPV1 and TRPA1 Ion Channels in Inflammatory Bowel Diseases: Potential Therapeutic Targets? *Pharmaceuticals* **12**(2019).
62. Holzer, P. TRP Channels in the Digestive System. *Current Pharmaceutical Biotechnology* **12**, 24-34 (2011).
63. Jain, P. et al. Transient receptor potential ankyrin 1 contributes to somatic pain hypersensitivity in experimental colitis. *Scientific Reports* **10**(2020).
64. Maglie, R. et al. The Role of TRPA1 in Skin Physiology and Pathology. *International Journal of Molecular Sciences* **22**(2021).

65. Wilson, S.R. et al. The Ion Channel TRPA1 Is Required for Chronic Itch. *Journal of Neuroscience* **33**, 9283-9294 (2013).
66. Zhang, X.M. Targeting TRP ion channels for itch relief. *Naunyn-Schmiedeberg's Archives of Pharmacology* **388**, 389-399 (2015).
67. Liu, B.Y. et al. TRPA1 controls inflammation and pruritogen responses in allergic contact dermatitis. *Faseb Journal* **27**, 3549-3563 (2013).
68. Said, G. Diabetic neuropathy - a review. *Nature Clinical Practice Neurology* **3**, 331-340 (2007).
69. Koivisto, A. et al. Inhibiting TRPA1 ion channel reduces loss of cutaneous nerve fiber function in diabetic animals: sustained activation of the TRPA1 channel contributes to the pathogenesis of peripheral diabetic neuropathy. *Pharmacol Res* **65**, 149-58 (2012).
70. Wei, H., Hämäläinen, M.M., Saarnilehto, M., Koivisto, A. & Pertovaara, A. Attenuation of Mechanical Hypersensitivity by an Antagonist of the TRPA1 Ion Channel in Diabetic Animals. *Anesthesiology* **111**, 147-154 (2009).
71. Maessen, D.E.M., Stehouwer, C.D.A. & Schalkwijk, C.G. The role of methylglyoxal and the glyoxalase system in diabetes and other age-related diseases. *Clinical Science* **128**, 839-861 (2015).
72. Huang, Q., Chen, Y., Gong, N.A. & Wang, Y.X. Methylglyoxal mediates streptozotocin-induced diabetic neuropathic pain via activation of the peripheral TRPA1 and Nav1.8 channels. *Metabolism-Clinical and Experimental* **65**, 463-474 (2016).
73. Ohkawara, S., Tanaka-Kagawa, T., Furukawa, Y. & Jinno, H. Methylglyoxal activates the human transient receptor potential ankyrin 1 channel. *Journal of Toxicological Sciences* **37**, 831-835 (2012).
74. Marchi, M. et al. TRPA1 rare variants in chronic neuropathic and nociplastic pain patients. *Pain* **164**, 2048-2059 (2023).
75. Kremeyer, B. et al. A Gain-of-Function Mutation in TRPA1 Causes Familial Episodic Pain Syndrome. *Neuron* **66**, 671-680 (2010).
76. Nirenberg, M.J., Chaouni, R., Biller, T.M., Gilbert, R.M. & Paisán-Ruiz, C. A novel variant is associated with carbamazepine-responsive cramp-fasciculation syndrome. *Clinical Genetics* **93**, 164-168 (2018).
77. Bali, A. et al. Molecular mechanism of hyperactivation conferred by a truncation of TRPA1. *Nature Communications* **14**(2023).
78. Asgar, J. et al. The Role of Trpa1 in Muscle Pain and Mechanical Hypersensitivity under Inflammatory Conditions in Rats. *Neuroscience* **310**, 206-215 (2015).
79. Fernandes, E.S., Fernandes, M.A. & Keeble, J.E. The functions of TRPA1 and TRPV1: moving away from sensory nerves. *British Journal of Pharmacology* **166**, 510-521 (2012).
80. Lapointe, T.K. & Altier, C. The role of TRPA1 in visceral inflammation and pain. *Channels* **5**, 525-529 (2011).
81. Liu, B. & Jordt, S.E. TRPA1 Controls Inflammation and Pruritogen Responses in Allergic Contact Dermatitis. *Journal of General Physiology* **144**, 10a-10a (2014).
82. Petrus, M. et al. A role of TRPA1 in mechanical hyperalgesia is revealed by pharmacological inhibition. *Molecular Pain* **3**(2007).
83. Talavera, K. et al. Mammalian Transient Receptor Potential Trpa1 Channels: From Structure to Disease. *Physiological Reviews* **100**, 725-803 (2020).
84. Wang, Z. et al. The TRPA1 Channel in the Cardiovascular System: Promising Features and Challenges. *Frontiers in Pharmacology* **10**(2019).
85. Nagata, K., Duggan, A., Kumar, G. & García-Añoveros, J. Nociceptor and hair cell transducer properties of TRPA1, a channel for pain and hearing. *Journal of Neuroscience* **25**, 4052-4061 (2005).

86. Wang, Y.Y., Chang, R.B., Waters, H.N., Mckemy, D.D. & Liman, E.R. The Nociceptor Ion Channel TRPA1 Is Potentiated and Inactivated by Permeating Calcium Ions. *Journal of Biological Chemistry* **283**, 32691-32703 (2008).
87. Zurborg, S., Yurgionas, B., Jira, J.A., Caspani, O. & Heppenstall, P.A. Direct activation of the ion channel TRPA1 by Ca. *Nature Neuroscience* **10**, 277-279 (2007).
88. Doerner, J.F., Gisselmann, G., Hatt, H. & Wetzel, C.H. Transient receptor potential channel a1 is directly gated by calcium ions. *Journal of Biological Chemistry* **282**, 13180-13189 (2007).
89. Hasan, R., Leeson-Payne, A.T.S., Jaggar, J.H. & Zhang, X.M. Calmodulin is responsible for Ca<sup>2+</sup>-dependent regulation of TRPA1 Channels. *Scientific Reports* **7**(2017).
90. Zhao, J., Lin King, J.V., Paulsen, C.E., Cheng, Y. & Julius, D. Irritant-evoked activation and calcium modulation of the TRPA1 receptor. *Nature* **585**, 141-145 (2020).
91. Nathanson, N.M. Molecular-Properties of the Muscarinic Acetylcholine-Receptor. *Annual Review of Neuroscience* **10**, 195-236 (1987).
92. van Koppen, C.J. & Kaiser, B. Regulation of muscarinic acetylcholine receptor signaling. *Pharmacology & Therapeutics* **98**, 197-220 (2003).
93. Sura, L. et al. C-terminal Acidic Cluster Is Involved in Ca<sup>2+</sup>-induced Regulation of Human Transient Receptor Potential Ankyrin 1 Channel. *Journal of Biological Chemistry* **287**, 18067-18077 (2012).
94. Pedersen, S.F., Owsianik, G. & Nilius, B. TRP channels: An overview. *Cell Calcium* **38**, 233-252 (2005).
95. Zhu, M.X. Multiple roles of calmodulin and other Ca<sup>2+</sup>-binding proteins in the functional regulation of TRP channels. *Pflugers Archiv-European Journal of Physiology* **451**, 105-115 (2005).
96. Hughes, T.E.T. et al. Structural insights on TRPV5 gating by endogenous modulators. *Nature Communications* **9**(2018).
97. Dang, S.Y. et al. Structural insight into TRPV5 channel function and modulation. *Proceedings of the National Academy of Sciences of the United States of America* **116**, 8869-8878 (2019).
98. Singh, A.K., McGoldrick, L.L., Twomey, E.C. & Sobolevsky, A.I. Mechanism of calmodulin inactivation of the calcium-selective TRP channel TRPV6. *Science Advances* **4**(2018).
99. Peterson, B.Z., DeMaria, C.D. & Yue, D.T. Calmodulin is the Ca<sup>2+</sup> sensor for Ca<sup>2+</sup>-dependent inactivation of l-type calcium channels. *Neuron* **22**, 549-558 (1999).
100. Saimi, Y. & Kung, C. Calmodulin as an ion channel subunit. *Annual Review of Physiology* **64**, 289-311 (2002).
101. Schumacher, M.A., Rivard, A.F., Bächinger, H.P. & Adelman, J.P. Structure of the gating domain of a Calcium activated K-channel complexed with Calcium/calmodulin. *Nature* **410**, 1120-1124 (2001).
102. Zayats, V. et al. Regulation of the transient receptor potential channel TRPA1 by its N-terminal ankyrin repeat domain. *Journal of Molecular Modeling* **19**, 4689-4700 (2013).
103. Suo, Y. et al. Structural Insights into Electrophile Irritant Sensing by the Human TRPA1 Channel. *Neuron* **105**, 882-+ (2020).
104. Paulsen, C.E., Armache, J.P., Gao, Y., Cheng, Y. & Julius, D. Structure of the TRPA1 ion channel suggests regulatory mechanisms. *Nature* **525**, 552 (2015).
105. Tidow, H. & Nissen, P. Structural diversity of calmodulin binding to its target sites. *Febs Journal* **280**, 5551-5565 (2013).
106. Rhoads, A.R. & Friedberg, F. Sequence motifs for calmodulin recognition. *Faseb Journal* **11**, 331-340 (1997).
107. Yap, K.L. et al. Calmodulin target database. *J Struct Funct Genomics* **1**, 8-14 (2000).

## **Chapter 2: Calmodulin binding is required for Ca<sup>2+</sup> mediated TRPA1 desensitization**

Justin H. Sanders<sup>1</sup>, Glory A. Adekanye<sup>1</sup>, Avnika Bali<sup>1</sup>, Yuekang Zhang<sup>1</sup>, and Candice E. Paulsen<sup>1\*</sup>

<sup>1</sup>Department of Molecular Biophysics and Biochemistry, Yale University, New Haven, Connecticut, USA.

The following work was submitted to Nature Structural & Molecular Biology and is currently under peer review

### **Abstract**

Ca<sup>2+</sup> (Ca<sup>2+</sup>) ions affect nearly all aspects of biology. Excessive Ca<sup>2+</sup> entry is cytotoxic and Ca<sup>2+</sup>-mobilizing receptors have evolved diverse mechanisms for tight regulation that often include Calmodulin (CaM). TRPA1, an essential Ca<sup>2+</sup>-permeable ion channel involved in pain signaling and inflammation, exhibits complex Ca<sup>2+</sup> regulation with initial channel potentiation followed by rapid desensitization. The molecular mechanisms of TRPA1 Ca<sup>2+</sup> regulation and whether CaM plays a role remain elusive. We find that TRPA1 binds CaM best at basal Ca<sup>2+</sup> concentration, that they co-localize in resting cells, and that CaM suppresses TRPA1 activity. Combining biochemical, biophysical, modeling, and functional approaches, we identify an evolutionarily conserved, high-affinity CaM binding site (CaMBS) in the distal TRPA1 C-terminus. Genetic or biochemical perturbation of CaM binding to the TRPA1 CaMBS yields hyperactive channels that exhibit drastic slowing of desensitization with no effect to potentiation. TRPA1 regulation by CaM does not require the lower Ca<sup>2+</sup>-affinity N-lobe, suggesting that CaM does not directly communicate Ca<sup>2+</sup> binding to the channel. Higher extracellular Ca<sup>2+</sup> can partially rescue slowed desensitization suggesting that CaM binding to the TRPA1 CaMBS primes an intrinsic TRPA1 Ca<sup>2+</sup>-binding site that may be the true desensitization gate. Collectively, our results

identify a critical regulatory element in an unstructured TRPA1 region highlighting the importance of these domains, they reveal CaM is an essential TRPA1 auxiliary subunit required for desensitization that establishes proper channel function with implications for all future TRPA1 work, and they uncover a mechanism for receptor regulation by CaM that expands the scope of CaM biology.

## INTRODUCTION

$\text{Ca}^{2+}$  ( $\text{Ca}^{2+}$ ) is a unique ion since it regulates cell excitability and serves as a second messenger in signal transduction cascades involved in almost all aspects of cellular life<sup>1</sup>. Excessive  $\text{Ca}^{2+}$  entry is cytotoxic, and cells dedicate substantial resources to maintain a 20,000-fold lower cytoplasmic concentration than extracellular or endoplasmic reticulum stores<sup>1</sup>. Extracellular  $\text{Ca}^{2+}$  influx is facilitated by  $\text{Ca}^{2+}$ -permeable ion channels whose activity must be tightly controlled to prevent spurious initiation of  $\text{Ca}^{2+}$  signaling pathways and apoptosis. In the peptidergic C fiber subset of peripheral sensory neurons, extracellular  $\text{Ca}^{2+}$  influx triggers pain signals and the exocytotic release of neuropeptides that initiate neurogenic inflammation and neuronal hypersensitivity<sup>2-6</sup>. These processes are believed to play a role in the transition from acute to chronic pain<sup>7-9</sup>. Identifying the  $\text{Ca}^{2+}$ -permeable ion channels involved in initiating and maintaining neurogenic inflammation and determining their regulatory mechanisms could provide the basis for rational drug design to alleviate these symptoms.

A direct role for the wasabi receptor, TRPA1 (Transient Receptor Potential Ankyrin subtype 1), in human pain has been illustrated by the discovery and characterization of genetic variants that are associated with painful disorders<sup>10-12</sup>. TRPA1 is a homotetrameric  $\text{Ca}^{2+}$ -permeable non-selective cation channel that is expressed at the plasma membrane in a subset of peripheral sensory neurons originating from dorsal root, trigeminal, and nodose ganglia as well as non-neuronal tissues including airway epithelia, enterochromaffin cells, and cardiac tissue (**Fig. 1A-B**)<sup>13-18</sup>. Mammalian TRPA1 is a ligand-gated chemosensor that is activated by covalent modification of conserved cytoplasmic cysteine residues by environmental and endogenous electrophiles including allyl isothiocyanate (AITC),

cinnamaldehyde, and acrolein (**Fig. 1A**, grey circles)<sup>19-22</sup>. In sensory neurons, active TRPA1 channels then facilitate extracellular  $\text{Ca}^{2+}$  entry to initiate pain signals and neuropeptide release<sup>13,23-28</sup>. Neuropeptide-evoked immune responses release pro-inflammatory mediators that sensitize neurons to subsequent painful stimuli by activating or priming receptors including TRPA1<sup>13,29-31</sup>. The ability of TRPA1 to initiate pain and neurogenic inflammation as well as be sensitized by these signals places it in the center of a regulatory pathway that could go awry<sup>13</sup>. Accordingly, animal knockout studies show that TRPA1 plays a key role in the establishment of neurogenic inflammation and neuronal hypersensitivity making it a prime drug target for managing chronic pain and inflammation<sup>15,32-34</sup>.

TRPA1 exhibits complex  $\text{Ca}^{2+}$  regulation;  $\text{Ca}^{2+}$  entry initially enhances channel activity (*e.g.*, potentiation), but then causes rapid inactivation (*e.g.*, desensitization) as cytoplasmic  $\text{Ca}^{2+}$  rises<sup>21,35,36</sup>. TRPA1 electrophile agonist modifications can persist for at least 10 minutes, yet TRPA1 desensitizes on a millisecond timescale<sup>35,37</sup>. Thus,  $\text{Ca}^{2+}$  regulation is critical to limit the TRPA1 functional window, however, the mechanism underlying this regulation is poorly understood. Previous work suggests that TRPA1 potentiation and desensitization are independent regulatory events that may engage distinct channel machinery<sup>36,38</sup>. Direct  $\text{Ca}^{2+}$  binding sites have been proposed in TRPA1 cytoplasmic and transmembrane domains to control potentiation and/or desensitization, however, deep mechanistic insight is lacking to explain whether and how these sites affect  $\text{Ca}^{2+}$ -regulation and many of these sites remain controversial (**Fig. 1A-B**)<sup>38-40</sup>. Moreover, most of these elements reside within or near key TRPA1 structural domains that contribute to channel gating. Genetic perturbation in these elements might compromise intrinsic channel

structure or function, further complicating interpretation of their effects on  $\text{Ca}^{2+}$  regulation (**Fig. 1A-B**).

Ion channels can also be regulated by the universal  $\text{Ca}^{2+}$  sensor calmodulin (CaM), which was recently shown to bind TRPA1 in a  $\text{Ca}^{2+}$ -dependent manner and affect its  $\text{Ca}^{2+}$  regulation<sup>21,36,39-41</sup>. CaM was proposed to mediate these effects in part through a CaM binding domain (CaMBD) located adjacent to the TRP helix in the membrane proximal TRPA1 cytoplasmic C-terminus (**Fig. 1A-B**, CaMBD in pink and TRP helix in purple)<sup>41</sup>. Genetic perturbation of the CaMBD had modest effects on TRPA1  $\text{Ca}^{2+}$  regulation perhaps due to incomplete loss of CaM binding, which raised the intriguing possibility that TRPA1 contains another CaM binding site<sup>41</sup>. Here, we identify a previously unreported, highly conserved, high-affinity non-canonical CaM binding site (CaMBS) in the distal structurally unresolved TRPA1 C-terminus that we propose to be the main site for a TRPA1-CaM interaction (**Fig. 1A**, yellow oval). We show that TRPA1 binds CaM best at basal  $\text{Ca}^{2+}$  concentration through its CaMBS and that this interaction can be ablated with short truncations or single point mutations without affecting  $\text{Ca}^{2+}$ -independent channel activity, allowing us to decouple CaM binding and TRPA1 function for the first time. TRPA1 CaMBS mutants revealed that CaM binding to this site is dispensable for proper potentiation, but it is critically required for rapid desensitization providing further support for mechanistic independence of these two regulatory events. To date, all CaM regulated ion channels engage both the high  $\text{Ca}^{2+}$ -affinity C-lobe and the lower  $\text{Ca}^{2+}$ -affinity N-lobe wherein  $\text{Ca}^{2+}$ -mediated conformational changes in CaM confer  $\text{Ca}^{2+}$  sensing to the regulated channel<sup>42-46</sup>. In contrast, we find that only the high-affinity CaM C-lobe was necessary for TRPA1 regulation and thus CaM binding *per se* likely does not directly

trigger desensitization. Instead, we found desensitization resistant TRPA1 channels could be partially rescued by increasing the extracellular  $\text{Ca}^{2+}$  concentration available to permeate through open channels. Thus, we present a model that CaM acts as a long-range allosteric regulator to prime an intrinsic TRPA1  $\text{Ca}^{2+}$  binding site that is the true desensitization gate. In this way, we propose that CaM serves as a regulatory binding partner for TRPA1 akin to the auxiliary subunits of voltage-gated ion channels and establishes the proper TRPA1 functional window in cells<sup>47-51</sup>.

## RESULTS

### Calmodulin colocalizes with TRPA1 in cells and regulates its activity

To initially ask whether CaM can directly regulate TRPA1, wild type (WT) human TRPA1 (hTRPA1) was assayed for its ability to bind CaM-agarose at distinct  $\text{Ca}^{2+}$  concentrations. Consistent with literature precedence<sup>41</sup>, hTRPA1 failed to bind CaM in the absence of  $\text{Ca}^{2+}$  (**Fig. 1C and D**). Instead, a robust interaction with hTRPA1 was observed at resting, cytosolic  $\text{Ca}^{2+}$  concentration (0.1  $\mu\text{M}$ ) with a stepwise decrease in binding at intermediate (500  $\mu\text{M}$ ) and extracellular (2 mM)  $\text{Ca}^{2+}$  concentrations, suggesting that CaM differentially engages hTRPA1 under  $\text{Ca}^{2+}$  influx (**Fig. 1C and D**). The pronounced CaM binding at basal  $\text{Ca}^{2+}$  concentration raises the intriguing possibility that hTRPA1 and CaM form a stable complex at rest. Consistently, immunofluorescence (IF) confocal microscopy of Neuro2A cells revealed pronounced co-localization of hTRPA1 and CaM at the cell periphery in resting cells (**Fig. 1E**).

To next probe whether CaM regulates TRPA1 function, WT hTRPA1 was co-expressed in HEK293T cells with WT hCaM or a hCaM variant that has a point mutation in each EF hand that prevents  $\text{Ca}^{2+}$  binding (CaM<sub>1234</sub>), which was previously shown to be unable to

bind to TRPA1<sup>41</sup>, and channel activity was monitored by ratiometric Ca<sup>2+</sup> imaging. Cells co-expressing WT hCaM exhibited reduced AITC-evoked hTRPA1 activity at both sub-saturating and saturating agonist concentrations compared to cells co-expressing CaM<sub>1234</sub> (**Fig. 1F and G**). These differences in channel activity were not due to WT or mutant CaM-induced changes to hTRPA1 expression or subcellular localization (**Fig. 1H and S1**). Collectively, these results suggest hTRPA1 and hCaM form a tethered complex in resting cells and that hCaM suppresses channel activity. While HEK293T cells endogenously express WT hCaM, a large majority is likely pre-bound to other effector proteins leaving low levels of free CaM<sup>52</sup>. hTRPA1 overexpression seemingly overwhelms this free hCaM pool yielding enhanced channel activity, which can be rescued by concurrent overexpression of WT hCaM (**Fig. 1F**).

### **The TRPA1 distal C-terminus contains a critical Calmodulin binding element**

A CaM binding domain (CaMBD) was previously identified near the TRP helix, which is involved in channel gating and resides within the structurally resolved core of hTRPA1 (**Fig. 1A-B**)<sup>41</sup>. While the CaMBD was proposed to contribute to TRPA1 Ca<sup>2+</sup> regulation, mutagenesis of this site did not ablate CaM binding and suggested that TRPA1 contains another CaM binding element<sup>41</sup>. To ask whether and to what extent the CaMBD governs the hTRPA1-CaM interaction, a minimal hTRPA1 construct that was previously used for structural determination<sup>53</sup> and which retains the CaMBD was tested for CaM binding (hTRPA1<sup>S488-T1078</sup>, **Fig. 1A-B and S2**). However, this minimal hTRPA1 construct failed to bind CaM *in vitro* indicating that the CaMBD is not sufficient for mediating this interaction (**Fig. 2A**).

The hTRPA1<sup>S488-T1078</sup> construct truncates the disordered N-terminus (amino acids 1-61), the structurally unresolved ankyrin repeats (ARs, amino acids 61-447 containing AR1-11), and the structurally unresolved distal C-terminus (amino acids 1079-1119) suggesting one or more of these domains contain critical CaM binding sites (**Fig. 1A-B**). TRPA1 is unique among the mammalian TRP channels in that it has the largest N-terminal AR domain (ARD) consisting of 16 ARs (**Fig. 1A**)<sup>17,54</sup>. Though a functional or regulatory role for the large TRPA1 ARD is unclear, ARs are known to mediate protein-protein interactions raising the possibility that the TRPA1 ARD contains a CaM binding site<sup>55</sup>. Surprisingly, a hTRPA1 construct containing the full ARD but lacking the structurally unresolved N- and C-termini (hTRPA1<sup>M62-T1078</sup>) failed to bind CaM (**Fig. 2B**). Smaller hTRPA1 truncations lacking only the unresolved N- or C-termini (hTRPA1<sup>Δ1-61</sup> and hTRPA1<sup>Δ1079-1119</sup>, respectively) revealed that the unresolved C-terminus is critical for CaM binding (**Fig. 2C**).

The hTRPA1 unresolved C-terminus includes the terminal 41 amino acids, which accounts for only 3.7% of the channel sequence. An acidic cluster in this domain proximal to the coiled coil was previously proposed to be involved in Ca<sup>2+</sup> regulation indicating a role for the unresolved C-terminus in channel modulation<sup>38</sup>. To initially map the CaM binding site (CaMBS) within the unresolved C-terminus, a suite of truncations was built lacking sequential blocks of 10 residues (**Fig. 2D**) and assayed for CaM binding. Even the smallest of these constructs lacking only the terminal 11 amino acids (hTRPA1<sup>Δ1109-1119</sup>) failed to bind CaM at basal Ca<sup>2+</sup> concentration (**Fig. 2E**) indicating that at least part of the CaMBS resides within the extreme end of the hTRPA1 C-terminus.

### The TRPA1 distal C-terminus has a high affinity for Calmodulin

Quantitative binding assays with membrane proteins are particularly challenging, however, the hTRPA1 distal C-terminus may be amenable to production as an isolated element for such analyses. Maltose binding protein (MBP)-tagged versions of the full hTRPA1 unresolved C-terminus (hTRPA1<sup>1079-1119</sup>) and smaller fragments (hTRPA1<sup>1089-1119</sup> and hTRPA1<sup>1099-1119</sup>) were produced, expressed in HEK293T cells, and tested for their ability to bind CaM. Each bound CaM in a Ca<sup>2+</sup>-dependent manner with no binding observed with free MBP tag, confirming that the C-terminus contains a CaMBS (**Fig. 3A**). The hTRPA1<sup>1089-1119</sup> peptide was selected for binding studies as it afforded the highest-yield bacterial purifications (**Fig. S3A**). Importantly, the purified hTRPA1<sup>1089-1119</sup> peptide competed with WT hTRPA1 for CaM binding confirming that the isolated element can adopt a conformation amenable to CaM binding after bacterial purification and liberation from MBP (**Fig. S3B-C**).

To initially characterize the hTRPA1 CaMBS-hCaM interaction, hTRPA1<sup>1089-1119</sup> peptide and purified WT hCaM (**Fig. S3D**) were mixed in equimolar amounts (100  $\mu$ M each) in the presence of 2 mM free Ca<sup>2+</sup> and complexes were analyzed by size exclusion chromatography (SEC). While hTRPA1<sup>1089-1119</sup> and WT hCaM eluted as spatially separate peaks when analyzed independently (**Fig. 3B**, blue and yellow traces), mixed hTRPA1<sup>1089-1119</sup> and WT hCaM eluted as a single peak slightly larger than free WT hCaM with higher 280 nm absorbance indicating all available hTRPA1<sup>1089-1119</sup> peptide was bound in a stable complex with hCaM (**Fig. 3B**, green trace). This complex was disrupted by chelating Ca<sup>2+</sup> with 5 mM EGTA, confirming the Ca<sup>2+</sup>-dependence of the interaction (**Fig. 3C**, gray trace).

Fractions from the SEC runs revealed co-elution of the hTRPA1<sup>1089-1119</sup> peptide with WT hCaM in the presence, but not the absence of Ca<sup>2+</sup> (**Fig. 3D**). Similar experiments with purified hCaM<sub>12</sub> (**Fig. S3E**), a mutant hCaM that is incapable of binding Ca<sup>2+</sup> in its N-lobe and which simulates a low Ca<sup>2+</sup> environment<sup>56</sup>, revealed that it also forms a complex with all available hTRPA1<sup>1089-1119</sup> peptide (**Fig. 3E**, orange trace). These results suggest that Ca<sup>2+</sup> binding in the N-lobe is not required for the hTRPA1 CaMBS-hCaM interaction and that the hCaM C-lobe is likely responsible for mediating the Ca<sup>2+</sup>-dependent binding to the hTRPA1 distal C-terminus.

To quantitatively measure the hTRPA1<sup>1089-1119</sup> peptide-hCaM interaction for WT hCaM and hCaM<sub>12</sub> in the presence of 2 mM free Ca<sup>2+</sup> isothermal titration calorimetry (ITC) was used. Three independent runs of the TRPA1<sup>1089-1119</sup> peptide with WT hCaM and hCaM<sub>12</sub> revealed affinities centering on 613 nM and 100 nM, respectively (**Fig. 3F**, **S3F** and **G**). The ITC results were not due to titration artifacts from the peptide (**Fig. S3H**) and these binding affinities are within range of those reported for CaM-regulated ion channels<sup>57-61</sup>. Moreover, the higher affinity of hCaM<sub>12</sub> than WT hCaM for the hTRPA1<sup>1089-1119</sup> peptide is consistent with the IF imaging and CaM binding assays above suggesting hTRPA1 and hCaM form a stable complex at rest (**Fig. 1C-D**). Collectively, these results indicate that hTRPA1 is a physiologically relevant binding partner for hCaM, that the hCaM interaction may be predominantly mediated by the high Ca<sup>2+</sup> affinity C-lobe, and that hTRPA1 and hCaM may pre-associate in cells prior to channel activation.

### The TRPA1 Calmodulin binding site is highly conserved

To determine how the hTRPA1 distal C-terminus binds hCaM and to identify potential residues mediating this interaction, models of the hTRPA1<sup>1089-1119</sup> peptide in complex with hCaM were generated with AlphaFold2 Multimer<sup>62,63</sup>. Models with full-length hCaM were unsuccessful due to competition of the N- and C-lobes for the same binding site in the hTRPA1<sup>1089-1119</sup> peptide; however, high confidence models could be obtained with the hCaM N- and C-lobes, separately (**Fig. 4A-C** and **S4A-D**). Both models suggest that the hTRPA1<sup>1089-1119</sup> peptide associates with the hCaM lobes as an alpha helix (**Fig. S4C-D**). While the hTRPA1<sup>1089-1119</sup> peptide adopts an extended helical conformation with the hCaM C-lobe, it must adopt a bent helical conformation with the hCaM N-lobe to prevent steric clashing with hCaM K75 possibly resulting in a free energy penalty (**Fig. S4C-E**). These models support a more favorable binding mode of the hTRPA1<sup>1089-1119</sup> peptide to the hCaM C-lobe, which is consistent with the robust binding of hTRPA1 to hCaM at basal Ca<sup>2+</sup> concentration as well as Ca<sup>2+</sup>-dependent binding driven by the hCaM C-lobe observed above (**Fig. 1C-D** and **3F**).

The highest confidence model predicts that the hCaM C-lobe binds to the hTRPA1 C-terminal alpha helix at a motif spanning amino acids 1099-1111 (**Fig. 4A**, goldenrod). These residues forming the putative CaMBS contain a hydrophobic ridge comprised of residues W1103, V1106, L1107, and V1110 which bind the hydrophobic cleft of the hCaM C-lobe (**Fig. 4B**). This hydrophobic ridge is flanked on the N-terminal side by positively charged residues R1099 and R1102, and on the C-terminal side by K1111 with all three residues predicted to form salt bridges with glutamate residues from the hCaM C-lobe (**Fig. 4C**). This putative CaMBS is consistent with loss of CaM binding in the hTRPA1<sup>Δ1109-1119</sup>

truncation, which lacks the V1110 and K1111 residues (**Fig. 2E**). To discern which residues comprise the CaMBS, a suite of alanine mutations was generated in hTRPA1 and analyzed for hCaM binding. Individual mutation of W1103 or V1110 to alanine completely ablated hCaM binding at basal  $\text{Ca}^{2+}$  concentration with a partial reduction in binding by a L1107A mutant (**Fig. 4D-E**). Mutating all four hydrophobic residues (Quad) or the flanking R1102 and K1111 residues (RK/AA) to alanine similarly ablated hCaM binding at basal  $\text{Ca}^{2+}$  concentration (**Fig. 4D-E**). R1099 was not tested since it is poorly conserved (**Fig. 4F**, black arrow). These data support that R1102, W1103, V1106, L1107, V1110, and K1111 form the hTRPA1 CaMBS, consistent with the structural prediction (**Fig. 4F**, box).

Prior work demonstrated CaM regulates the mouse TRPA1 channel<sup>41</sup>. The hTRPA1 CaMBS identified in this study is highly conserved among vertebrate TRPA1 including the mouse orthologue, but it is absent from *C. elegans* TRPA1 (**Fig. 4F** and **S4F**). To ask whether the CaMBS governs CaM binding in other TRPA1 species orthologues, WT and partial CaMBS truncations of mouse, zebrafish, and *C. elegans* TRPA1 were analyzed for their hCaM binding ability. WT mouse and zebrafish TRPA1 constructs bound hCaM in a  $\text{Ca}^{2+}$ -dependent manner (**Fig. 4G**). In contrast, WT *C. elegans* TRPA1 and the partial CaMBS truncations of mouse and zebrafish TRPA1 failed to bind hCaM (**Fig. 4G**). These results are consistent with the CaMBS serving as a critical and highly conserved CaM binding element in TRPA1 channels.

### **Loss of Calmodulin binding is associated with hyperactive TRPA1 channels**

Identification of the CaMBS in the distal C-terminus far from the hTRPA1 core structure raises the intriguing possibility that hCaM binding could be selectively ablated without

compromising intrinsic channel function. Such a construct would facilitate a detailed characterization of whether and how hCaM regulates hTRPA1 without relying on hCaM mutants or inhibitors that may disrupt other aspects of CaM biology or that could indirectly impact channel function. Excitingly, the hTRPA1<sup>Δ1109-1119</sup> construct yielded functional channels with increased basal and agonist-evoked activity compared to WT hTRPA1 (**Fig. 5A-B**). The hTRPA1<sup>Δ1109-1119</sup> channels failed to co-localize with WT hCaM in Neuro2A cells, demonstrating that the loss of hCaM binding in pulldown experiments translates to a disruption of the protein-protein interaction in a cellular environment (**Fig. 5C**). This increase in channel activity was not due to an increase in mutant protein production or surface localization (**Fig. S1**) and instead suggests that loss of hCaM binding yields hyperactive hTRPA1 channels.

To directly test whether the hTRPA1<sup>Δ1109-1119</sup> construct relieves WT hCaM-mediated channel suppression, hTRPA1<sup>Δ1109-1119</sup> was co-expressed in HEK293T cells with WT hCaM or hCaM<sub>1234</sub>. Unlike WT hTRPA1 (**Fig. 1F-G**), hTRPA1<sup>Δ1109-1119</sup> channels were unaffected by hCaM co-expression (**Fig. 5D-E**) consistent with a loss of CaM binding capability (**Fig. 2E**). Akin to WT channels, WT hCaM and hCaM<sub>1234</sub> had no effect on hTRPA1<sup>Δ1109-1119</sup> expression or surface localization (**Fig. 5F and S1**). Together, these results demonstrate that the hTRPA1 distal C-terminus contains a critical CaMBS that is required for hCaM binding and its negative regulation of channel activity.

## CaM binding to the TRPA1 Calmodulin binding site is critical for channel desensitization

The preceding results suggest that hCaM is involved in an important aspect of hTRPA1 regulation which could be due to suppressed potentiation and/or enhanced desensitization. The canonical hTRPA1  $\text{Ca}^{2+}$  regulation profile can be observed in *Xenopus laevis* oocytes by two-electrode voltage clamp (TEVC), as previously reported (**Fig. 6A**)<sup>10,64</sup>. Thus, AITC-evoked WT and hTRPA1 <sup>$\Delta$ 1109-1119</sup> activity was compared by TEVC in the absence and presence of extracellular  $\text{Ca}^{2+}$  to directly discern how loss of CaM binding affects channel activity. Additionally, these channels were compared to W1103A hTRPA1, which represents a minimal hTRPA1 perturbation needed to ablate CaM binding (**Fig. 4D-E**). In the absence of extracellular  $\text{Ca}^{2+}$ , AITC evoked comparable currents from each channel population, suggesting that neither deletion of the terminal 11 amino acids nor the W1103A mutation inherently alter channel function (**Fig. 6A-D**, timepoint i). Application of extracellular  $\text{Ca}^{2+}$  triggered rapid potentiation of WT, hTRPA1 <sup>$\Delta$ 1109-1119</sup>, and W1103A hTRPA1 channels with comparable peak current amplitudes (**Fig. 6A-D**, timepoint ii). While WT hTRPA1 channels subsequently exhibited nearly complete desensitization within 25 seconds of extracellular  $\text{Ca}^{2+}$  addition (**Fig. 6A**, timepoint iii), hTRPA1 <sup>$\Delta$ 1109-1119</sup> and W1103A channels remained open with 20-30% or 10-20% their initial activity 5 minutes after extracellular  $\text{Ca}^{2+}$  application, respectively (**Fig. 6B-D**, timepoint iv). These residual activities could be inhibited with the TRPA1 antagonist A-967079, demonstrating that the ongoing activity was due to hTRPA1 channels (**Fig. 6B-C**, timepoint v).

To quantitatively characterize the effect of CaM binding on proper TRPA1  $\text{Ca}^{2+}$  regulation, rate constants for potentiation and desensitization were calculated from

baseline-corrected traces at -80 and +80 mV holding potentials. Such calculations reveal that WT hTRPA1 potentiated at a rate of 2.7 sec (-80 mV) and 2.2 sec (+80 mV) and desensitized at a rate of 11.9 sec (-80 mV) and 12.5 sec (+80 mV) following  $\text{Ca}^{2+}$  addition, consistent with literature precedence (**Fig. 6E-F**, black bars)<sup>36,38</sup>. In contrast, hTRPA1 <sup>$\Delta$ 1109-1119</sup> and W1103A hTRPA1 exhibited significantly delayed desensitization kinetics with 10- or 15-fold slowing to desensitization with inward currents (*e.g.*, -80 mV) and 16- or 20-fold slowing to desensitization kinetics with outward currents (*e.g.*, +80 mV), respectively, compared to WT hTRPA1 channels (**Fig. 6F**, red and blue bars, respectively). These fold-slowing to  $\text{Ca}^{2+}$ -dependent desensitization kinetics are on the order of that previously reported for a TRPA1 mutant exhibiting 100-fold reduced  $\text{Ca}^{2+}$  permeability and may, in part, reflect channel rundown independent of true  $\text{Ca}^{2+}$  desensitization<sup>36</sup>. Potentiation kinetics were more modestly slowed for hTRPA1 <sup>$\Delta$ 1109-1119</sup> and W1103A hTRPA1 compared to WT hTRPA1 (~3-fold each at -80 mV and ~1.8-fold each at +80 mV), though this can be largely accounted for by the greater effects to desensitization which would inherently provide more time for full potentiation (**Fig. 6E**, red and blue bars, respectively).

Such drastic delays to channel desensitization with hTRPA1 <sup>$\Delta$ 1109-1119</sup> and W1103A allows for sustained ion conduction through active mutant channels over a prolonged period, which could have significant physiological effects. hTRPA1 <sup>$\Delta$ 1109-1119</sup> channels exhibit a large, albeit nonsignificant increase in translocated charge at -80 mV and a significant, 5-fold increase at +80 mV (**Fig. 6G**, red bars). The W1103A hTRPA1 mutant exhibited significant, 20- and 10-fold increases in translocated charge at -80 and +80 mV, respectively (**Fig. 6G**, blue bars). These collective differences in mutant channel function are not due to changes in total protein expression (**Fig. 6H**).

To independently characterize the effect of CaM binding on hTRPA1 Ca<sup>2+</sup> regulation, the MBP-hTRPA1<sup>1089-1119</sup> peptide was used as an experimental tool to sequester endogenous CaM since this peptide competed with WT hTRPA1 in CaM binding assays (**Fig. S3B-C**). Co-expression of MBP-WT hTRPA1 with the MBP-hTRPA1<sup>1089-1119</sup> peptide in HEK293T cells yielded significantly enhanced basal and AITC-evoked activity by Ca<sup>2+</sup> imaging compared to channels co-expressed with free MBP, presumably due to endogenous hCaM sequestration and release from hCaM regulation (**Fig. S5A-C**). To ask how this impacted channel function, purified free MBP tag and MBP-hTRPA1<sup>1089-1119</sup> peptide were injected at a final concentration of 100 μM into oocytes expressing WT hTRPA1 one hour prior to TEVC recordings. WT hTRPA1 profiles from oocytes injected with free MBP were indistinguishable from those with WT hTRPA1 alone (compare **Fig. 6A** and **S5D**) and the channels exhibited similar desensitization rates (11.9 and 12.5 sec at -80 and +80 mV for WT hTRPA1, respectively versus 9.1 and 10.34 sec at -80 and +80 mV for WT hTRPA1 with free MBP, respectively). In contrast, WT hTRPA1 channels from oocytes injected with the MBP-hTRPA1<sup>1089-1119</sup> peptide exhibited 16- and 18-fold elongations to desensitization kinetics at -80 and +80 mV, respectively, compared to channels with free-MBP (**Fig. S5E-G**). Thus, the MBP-hTRPA1<sup>1089-1119</sup> peptide had a comparable effect on hTRPA1 activity as the W1103A mutant. Collectively, these results demonstrate that CaM is a critical regulator of hTRPA1 wherein CaM binding is required for proper hTRPA1 desensitization in intact cells while having no effect on potentiation. This also provides compelling evidence that potentiation and desensitization are independent regulatory events, as previously proposed<sup>36</sup>.

### The CaM C-lobe is sufficient to regulate TRPA1 activity

Engagement of the hTRPA1 CaMBS by the hCaM C-lobe is critical for proper channel desensitization, which raises mechanistic questions about how this binding event triggers desensitization. This could potentially be mediated by binding of the hCaM N-lobe to a different region in hTRPA1. Alternatively, desensitization could be controlled entirely by the hCaM C-lobe through binding at the hTRPA1 CaMBS. These two models differ in their requirement for the hCaM N-lobe. To determine which hCaM lobes are required, a suite of hCaM mutants was co-expressed with WT hTRPA1 in HEK293T cells and analyzed for their effect on AITC-evoked hTRPA1 activity by ratiometric  $\text{Ca}^{2+}$  imaging (**Fig. 7A**). Consistent with the results in **Fig. 1F-G**, WT hCaM significantly suppressed WT hTRPA1 activity compared to channels co-expressed with hCaM<sub>1234</sub> (**Fig. 7A-B**, solid black versus striped bars). A hCaM mutant that only retained a functional C-lobe (hCaM<sub>12</sub>) also significantly suppressed hTRPA1 activity, while a hCaM mutant that only retained a functional N-lobe (hCaM<sub>34</sub>) did not (**Fig. 7A-B**, black boxed versus carat bars). These results hint that the hCaM C-lobe is sufficient to mediate hTRPA1 regulation; however, it is possible that the hCaM N-lobe, independent of  $\text{Ca}^{2+}$  binding competency, is also required. Thus, the isolated hCaM C-lobe or a  $\text{Ca}^{2+}$ -binding deficient mutant (hCaM<sub>34</sub> C-lobe) were co-expressed with WT hTRPA1 and assayed for channel activity. Such experiments revealed that the hCaM C-lobe suppressed hTRPA1 activity akin to WT hCaM and hCaM<sub>12</sub>, while the hCaM<sub>34</sub> C-lobe mutant did not (**Fig. 7A-B**, gray versus white bars). Importantly, none of the hCaM constructs affected hTRPA1 expression (**Fig. 7C**). These results demonstrate that only the hCaM C-lobe is required for hTRPA1 regulation,

consistent with previous electrophysiological work showing that the CaM C-lobe enhances the rate of WT mouse TRPA1 desensitization<sup>41</sup>.

### **High extracellular Ca<sup>2+</sup> partially rescues desensitization-resistant TRPA1**

The hCaM C-lobe has a severely limited ability to respond to Ca<sup>2+</sup> flux compared to WT hCaM, which raises questions about how it could confer desensitization through binding at the hTRPA1 CaMBS. One possibility is that hCaM does not directly transmit a Ca<sup>2+</sup> signal to TRPA1, but instead its binding primes an intrinsic Ca<sup>2+</sup> binding site in TRPA1 that triggers channel desensitization. If true, desensitization of CaM binding deficient TRPA1 channels should be at least partially rescued by increasing the extracellular Ca<sup>2+</sup> concentration available to permeate through open channels. Consistent with literature precedence, WT hTRPA1 channels desensitized faster with 10 mM extracellular Ca<sup>2+</sup> than with 1.8 mM extracellular Ca<sup>2+</sup> (**Fig. 7D and F**)<sup>36,38</sup>. W1103A hTRPA1 channels were even more sensitive to extracellular Ca<sup>2+</sup> concentration exhibiting an approximately 3-fold faster desensitization rate with 10 mM extracellular Ca<sup>2+</sup> than with 1.8 mM extracellular Ca<sup>2+</sup> (**Fig. 7E and G**). Despite these enhanced rates, W1103A hTRPA1 channels were still approximately 4-fold slower to desensitize than WT hTRPA1 with 1.8 mM extracellular Ca<sup>2+</sup>. Collectively, these results are consistent with loss of CaM binding affecting a TRPA1 Ca<sup>2+</sup> binding site that can only be partially rescued by the higher intracellular Ca<sup>2+</sup> concentration permeated by W1103A hTRPA1 channels with 10 mM extracellular Ca<sup>2+</sup>. Future work will identify this intrinsic TRPA1 Ca<sup>2+</sup> binding site and its contribution to channel desensitization.

## DISCUSSION

TRPA1 is a  $\text{Ca}^{2+}$ -permeable ion channel implicated in chronic pain and inflammation whose activity is controlled by rapid desensitization following a cytosolic  $\text{Ca}^{2+}$  increase<sup>13,21,23-32,36,39-41</sup>. Despite the importance of desensitization to restricting proper TRPA1 functionality, this regulatory mechanism, and whether it involves the universal  $\text{Ca}^{2+}$  sensor CaM, has remained controversial<sup>36,39-41,65</sup>. Here, we find that CaM binds human TRPA1 best at basal  $\text{Ca}^{2+}$  concentration, co-localizes with TRPA1 at rest, and suppresses channel activity when co-expressed in heterologous cells, suggesting CaM is a *bona fide* TRPA1 regulator. CaM mediates this regulation through a previously unidentified, highly conserved, high-affinity binding site in the TRPA1 distal C-terminus that we have named the CaM binding site (CaMBS). The TRPA1 CaMBS resides in the final 18 amino acids of a 41-amino acid C-terminus that has yet to be resolved by structural studies (*e.g.*, the TRPA1 structurally unresolved C-terminus, **Fig. 1A**, yellow oval)<sup>39,66,67</sup>. Structure predictions and quantitative binding assays reveal that the TRPA1 CaMBS preferentially engages the high  $\text{Ca}^{2+}$ -affinity CaM C-lobe, supporting a pre-association of TRPA1 and CaM in cells. Mutation of putative TRPA1 CaMBS residues in the full-length channel or sequestration of CaM with a TRPA1 C-terminal peptide ablates CaM binding at basal  $\text{Ca}^{2+}$  concentration and yields hyperactive channels that exhibit a 10- to 20-fold slowing of  $\text{Ca}^{2+}$ -mediated desensitization and which can only be partially rescued by increased extracellular  $\text{Ca}^{2+}$  concentration (**Fig. 7H**, right). This functional perturbation is more drastic than that caused by all known TRPA1 channelopathic mutations and suggests that disruption of the TRPA1-CaM interaction would have profound neurological effects, which could provide a useful tool for studying TRPA1 hyperactivity in genetically tractable animal models<sup>10-12</sup>.

Indeed, some TRPV4 channelopathic mutations are thought to mimic loss of CaM binding<sup>68</sup>. Our work identifies the TRPA1 CaMBS as the main CaM binding element and reveals that CaM binding to this site is critically required for proper TRPA1 desensitization (**Fig. 7H**, left).

CaM binds and regulates the activity of hundreds of effector proteins including many ion channels through several types of binding motifs, requiring a remarkable degree of plasticity for a protein that is less than 17 kDa<sup>56,69,70</sup>. The canonical binding mode involves both lobes of Ca<sup>2+</sup>-bound CaM wrapping around a single effector protein alpha helix through a series of hydrophobic interactions with the CaM lobes' hydrophobic clefts<sup>44,56,71</sup>. The smallest class of CaM binding motifs is the 1-10 motif, which consists of 10 residues flanked by two hydrophobic anchors (*e.g.*, at positions 1 and 10) and that yields the most compact structure of CaM *via* the canonical binding mode<sup>70,72</sup>. The predicted TRPA1 CaMBS is also a 10-residue binding segment within a putative alpha helix with four hydrophobic residues at positions 2, 5, 6 and 9 and basic residues at positions 1 and 10 (**Fig. 4F**). The hydrophobic ridge spans the internal 8 amino acids, suggesting the TRPA1 CaMBS is too small to accommodate simultaneous engagement of both CaM lobes. Indeed, our binding studies and AlphaFold predictions show that the TRPA1 CaMBS binds only to the calcified CaM C-lobe adopting a non-canonical binding mode. Following naming conventions, the TRPA1 CaMBS is a 2-5-6-9 motif; it provides another example of CaM binding plasticity and it supports the growing body of literature that non-canonical CaM binding is more common than previously expected<sup>69</sup>.

Our data suggest that CaM forms a stable interaction with TRPA1 at rest through a Ca<sup>2+</sup>-dependent interaction between the TRPA1 CaMBS and the CaM C-lobe. These results raise

the intriguing possibility that CaM is the first discovered TRPA1 auxiliary subunit. Auxiliary subunits including CaM have been studied extensively and were shown to regulate ion channel folding, stability, trafficking, localization, stimulus sensitivity, and gating kinetics<sup>47-51,73</sup>. Our work reveals that CaM is an indispensable auxiliary subunit required for proper channel desensitization that effectively tightens the TRPA1 functional window and limits total ion influx (**Fig. 6G** and **7H**). In this way, CaM operates akin to the auxiliary subunits of voltage-gated ion channels<sup>47-51</sup>. Future *in vitro* work on TRPA1 should ensure that CaM is expressed at sufficient levels to initiate desensitization and to avoid artifactual results from hyperactive channels. This is particularly key for heterologous systems where endogenous CaM pools can be easily overwhelmed by overexpressed TRPA1 and must be supplemented by exogenous CaM.

We identified the TRPA1 CaMBS in the distal C-terminus, which has never been resolved structurally, and thus it is unknown where the CaMBS resides in relation to domains that govern channel gating<sup>39,66,67</sup>. This raises mechanistic questions about how CaM binding to the TRPA1 CaMBS could promote channel desensitization (**Fig. 1A-B**). An intriguing model is a coordinated response between the TRPA1 CaMBS and the previously identified CaM binding domain (CaMBD), which resides near the ion conduction pathway, through sequential binding of the CaM C- and N-lobes, respectively as intracellular Ca<sup>2+</sup> rises to trigger desensitization (**Fig. 7H**, left, dashed arrow). Such mechanisms involving disparate binding elements within the same channel for the CaM N- and C-lobes have been proposed for CaM- and Ca<sup>2+</sup>-mediated SK channel activation or TRPV5 inhibition<sup>42,43,45</sup>. However, we and others have shown that the CaM N-lobe is dispensable for TRPA1 regulation<sup>41</sup>. All CaM-regulated ion channels rely on

conformational changes in CaM upon  $\text{Ca}^{2+}$  binding to the N-lobe that either directly blocks the pore or induces a conformational change in the channel to regulate gating<sup>42-46</sup>. Thus, the lack of dependence here on the CaM N-lobe is strikingly distinct and suggests that CaM is not functioning as a direct  $\text{Ca}^{2+}$  sensor in TRPA1 desensitization. Our data also show that while ablation of CaM binding to the TRPA1 CaMBS drastically slows the desensitization rate, it does not completely ablate desensitization; permeating  $\text{Ca}^{2+}$  ions are, albeit inefficiently, able to desensitize TRPA1 and this slowed desensitization can be partially rescued by increasing the extracellular  $\text{Ca}^{2+}$  concentration (**Fig. 7H**, right, smaller red inhibition arrow). Collectively, our results support a model wherein CaM binding at the CaMBS primes the affinity of an intrinsic TRPA1  $\text{Ca}^{2+}$  binding site which serves as the desensitization gate (**Fig 7H**, left, larger red inhibition arrow). This model can explain why  $\text{Ca}^{2+}$  ions perfused directly onto the TRPA1 cytoplasmic domains in excised patches that were previously exposed to EGTA can still trigger desensitization<sup>36,40,65</sup>. CaM binding to the CaMBS may induce an allosteric conformational change that primes the intrinsic TRPA1  $\text{Ca}^{2+}$  binding site to readily respond to  $\text{Ca}^{2+}$  flux through the channel pore and trigger desensitization. Future structural and functional work are needed to identify this  $\text{Ca}^{2+}$  binding site, to determine how  $\text{Ca}^{2+}$  binding triggers TRPA1 desensitization, and to uncover how CaM affects this process. Finally, while the CaM N-lobe is not required for TRPA1 desensitization, it may serve to enhance TRPA1 binding through the CaMBD or other unidentified site, or it may remain available to interact with other local effectors and initiate  $\text{Ca}^{2+}$ - and CaM-dependent signaling<sup>74</sup>.

Collectively, we identified a highly conserved and critical CaM regulatory element in the human TRPA1 distal unstructured C-terminus that is required for proper channel

function. Localization of the TRPA1 CaMBS to the distal C-terminus is serendipitous since it allowed us to completely ablate CaM binding through genetic modification of TRPA1 without affecting intrinsic channel function (*e.g.*, WT and mutant TRPA1 channels exhibited similar activities in Ca<sup>2+</sup> free solution, **Fig. 6A-D**). Thus, we were able to directly reveal this critical role for CaM in TRPA1 regulation without relying on perturbation of CaM, which can have off-target effects. Moreover, our work demonstrates how short segments of structurally unresolved amino acids can drastically affect channel function in unexpected ways. Ion channels are highly enriched for intrinsically disordered segments at both their N- and C-termini with some of them, including TRPA1 as described here, shown to be indispensable for proper function<sup>75,76</sup>. For others, such as the related capsaicin receptor, TRPV1, a structurally unresolved element in the distal C-terminus governs phosphatidylinositol lipid regulation<sup>77,78</sup>. Perturbations therein promote TRPV1 sensitization and a splice variant that removes this regulatory element may underlie infrared detection capability in vampire bats<sup>77,79,80</sup>. Given their wide distribution amongst the ion channel proteome including the large TRP channel family, other intrinsically disordered segments are bound to have novel channel regulatory modes<sup>81</sup>. Such segments provide a ripe evolutionary source for new functionality as they are more permissive to mutations than structured regions, which is particularly useful for transmembrane proteins whose complex regulation has developed mainly through extra-membrane domains<sup>64,79,82-84</sup>. While the cryo-EM resolution revolution has been a boon for the ion channel and membrane protein fields, our work illustrates the need to study structurally unresolved and intrinsically disordered regions with renewed interest and vigor.

## METHODS

### Plasmid Construction

DNA sequences for human TRPA1, human TRPA1<sup>448-1078</sup>, and human Calmodulin were PCR amplified and subcloned into a p3xFLAG-eYFP-CMV-7.1 vector (Addgene) at the NotI/BamHI sites using In-Fusion EcoDry cloning (Takara) according to manufacturer protocols. Human TRPA1, mouse TRPA1, zebrafish TRPA1, and *C. elegans* TRPA1 were subcloned into 8xHis-MBP pFastBac1 modified with a CMV promoter (obtained from David Julius' lab) at the BamHI/NotI sites following the same protocol. 8xHis-MBP pFastBac1 modified with a CMV promoter human TRPA1<sup>1089-1119</sup> was created by introducing a BamHI site at the -1 position of the codon encoding TRPA1<sup>1089</sup> and digesting the plasmid with BamHI restriction enzyme followed by gel purification. The linearized vector segment was then transformed into XL-10 Gold cells resulting in a repaired vector. A similar strategy was followed for the creation of 8xHis-MBP pFastBac1 with a CMV promoter human TRPA1<sup>1079-1119</sup>, and human TRPA1<sup>1099-1119</sup>. For bacterial protein purification, DNA sequences for 8xHis-MBP TRPA1<sup>1089-1119</sup> and 3xFlag-6xHis-WT hCaM were PCR amplified and subcloned into a pET28a vector (Addgene) at the NcoI/NotI sites using In-Fusion EcoDry cloning. All mutants including hTRPA1<sup>Δ1109-1119</sup>, hTRPA1<sup>Δ1079-1119</sup>, hTRPA1<sup>Δ1089-1119</sup>, hTRPA1<sup>Δ1099-1119</sup>, and hTRPA1<sup>Δ1-61</sup>, TRPA1<sup>W1103A</sup>, TRPA1<sup>L1107A</sup>, TRPA1<sup>V1110A</sup>, TRPA1<sup>Quad</sup>, TRPA1<sup>RK/AA</sup>, CaM<sub>12</sub>, CaM<sub>34</sub>, and CaM<sub>1234</sub> were created using QuikChange Lightning site-directed mutagenesis (Agilent). V5-tagged hCaM was created by site-directed mutagenesis to replace the 3xFLAG-tag in the construct above. For expression in *Xenopus laevis* oocytes, 3xFLAG-hTRPA1 variant genes were subcloned

into the combined mammalian/oocyte expression vector pMO (obtained from David Julius' lab) prior to generating cRNAs.

All DNA primers were ordered from ThermoFisher and all constructs were sequence-verified using the Yale School of Medicine Keck DNA Sequencing Facility.

### **Mammalian Cell Culture and Protein Expression**

Human embryonic kidney cells (HEK293T, ATCC CRL-3216) were cultured in Dulbecco's modified Eagle's medium (DMEM; Invitrogen) supplemented with 10% calf serum and 1x Penicillin-Streptomycin (Invitrogen) at 37°C and 5% CO<sub>2</sub>. Neuro2A cells (ATCC CCL-131) were cultured in Dulbecco's modified Eagle's medium (DMEM; Invitrogen) supplemented with 10% fetal bovine serum and 1x Penicillin-Streptomycin (Invitrogen) at 37°C and 5% CO<sub>2</sub>. Cells were grown to ~85-95% confluence before splitting for experiments or propagation. HEK293T cells cultured to ~95% confluence were seeded at 1:10 or 1:20 dilutions into 6- or 12-well plates (Corning), respectively. After 1-5 hours recovery, cells were transiently transfected with 1 µg plasmid using jetPRIME (Polyplus) according to manufacturer protocols. For surface biotinylation experiments, cells were co-transfected with 0.5 µg 3xFLAG-tagged hTRPA1 variants and 0.5 µg 3xFLAG-hCaM variants.

### **Cell Lysis and Pulldown Experiments**

16-24 hours post-transfection, HEK293T cells were washed with PBS (Ca<sup>2+</sup> and magnesium free) and lysed in 75-150 µL of TRPA1 lysis buffer (40 mM Tris pH 8.0, 150

mM NaCl, 5 mM DDM, 500  $\mu$ M EGTA, EDTA-free cOmplete protease cocktail inhibitor tablet) at 4°C while gently nutating. Cell debris were pelleted from the resulting lysates by centrifugation at 15,000 RPM for 10 minutes at 4°C. Total protein concentration in lysates were quantified using a BCA assay (Pierce). Equal concentrations of protein lysate (100  $\mu$ g) from each experimental condition were added to resins as specified below. 10% of loaded protein amount was reserved as a whole-cell lysate loading control. Buffers were supplemented with free  $\text{Ca}^{2+}$  as indicated in each figure. Concentrations of  $\text{CaCl}_2$  required for each free  $\text{Ca}^{2+}$  concentration were calculated using Ca-EGTA calculator v1.3 using constants from Theo Schoenmakers' Chelator on the MaxChelator website<sup>85</sup>.

### **CaM-agarose Pulldown**

100  $\mu$ g lysates were incubated with 10  $\mu$ L of lysis buffer-equilibrated Calmodulin-agarose (Sigma-Aldrich) for 1 hour at 4°C with gentle nutation. Resin beads were washed 3-5 times with lysis buffer prior to elution; resin was pelleted, and bound proteins were eluted in TRPA1 lysis buffer supplemented with 5 mM EGTA for 30 minutes at 4°C with gentle nutation.

### **Surface Biotinylation Assay**

Surface biotinylation assays were conducted as previously reported<sup>10</sup>. Briefly, HEK293T cells were seeded in a 6-well plate pre-coated with Poly-L-Lysine (Sigma) and transfected with expression plasmids. 16-24 hours post-transfection, cells were washed with PBS, placed on ice, and incubated for 20 minutes with chilled 0.05 mg/mL Sulfo-NHS-LC-Biotin (ThermoFisher) in Ringer's solution. Cells were then washed with chilled wash

buffer (PBS + 100 mM Glycine) and the reaction was quenched on ice for 30 minutes with 100 mM Glycine and 0.5% BSA in PBS. Cells were then washed three times and lysed in TRPA1 lysis buffer containing 100 mM Glycine directly on the 6-well plate. Lysates were collected, protein concentration was determined by BCA assay, biotinylated proteins were isolated by Neutravidin pulldown and analyzed by immunoblot as described below. During quantification, any FLAG signal from CaM in the eluates were subtracted from all other conditions to account for probe internalization.

### **Neutravidin Pulldown**

Cell lysates that were generated following surface labeling experiments were incubated with 15  $\mu$ L of lysis buffer-equilibrated Neutravidin resin (Pierce) for 2 hours at 4°C with gentle nutation. The resin was then washed with lysis buffer three times, followed by a harsher wash with 1x PBS + 100 mM DTT. Resin was then washed once each with lysis buffer and 1x PBS. Biotinylated protein was eluted from the resin with a multi-step protocol to prevent TRPA1 aggregation while maximizing protein elution from the resin. First, resin was incubated with 10  $\mu$ L of biotin elution buffer (TRPA1 lysis buffer, 100 mM Glycine, 10 mM Biotin, 1% SDS) on ice for 10 min, followed by addition of 1  $\mu$ L  $\beta$ -mercaptoethanol (BME; Sigma) to each sample and incubation on ice for 5 minutes, and finally by addition of 4  $\mu$ L 4x Laemmli buffer + 10% BME with incubation at 65°C for 10 minutes. The resin was centrifuged, supernatant was removed and combined with additional 4  $\mu$ L Laemmli buffer + 10% BME for SDS-PAGE analysis.

### **SDS-PAGE and Immunoblot**

Samples were combined with Laemmli Sample buffer + 10% BME and separated on pre-cast 4-20% SDS-PAGE gels (Bio-Rad). Gels were transferred onto PVDF membranes (Bio-Rad) by semi-dry transfer at 15V for 40 minutes. Blots were blocked in 3% BSA prior to antibody probing. The following primary antibodies were used in PBST buffer (Boston Bioproducts): anti-MBP (mouse, 1:30,000, New England Biolabs), anti-FLAG (mouse, 1:30,000, Sigma), anti-tubulin (mouse, 1:5,000 in 3% BSA, Sigma). HRP-conjugated IgG secondary anti-mouse antibody was used as needed (rabbit, 1:25,000, Invitrogen). Membranes were developed using Clarity Western ECL substrate (Bio-Rad) and imaged using a Chemidoc Imaging System (Bio-Rad). Densitometric quantifications were performed with ImageJ software. All quantified band intensities for eluted samples were divided by their tubulin-normalized input band intensities.

### **Immunofluorescence Imaging**

Neuro2A cells transiently transfected with jetPRIME (Polyplus) according to manufacturer protocols were transferred to poly-L-lysine-coated cover slips and incubated for 16-20 hours prior to immunostaining. Cells were fixed on coverslips with 4% paraformaldehyde for 20 minutes, then permeabilized with 0.1% Triton in PBS for 10 min. Cells were then blocked in 4% BSA in PBS followed by incubation in primary anti-V5 monoclonal antibody (mouse, 1:500, Invitrogen) in 4% BSA in PBS at room temperature for 45 min. Cells were then washed with PBS and incubated with Alexa-Fluor488-conjugated secondary anti-mouse antibody in 4% BSA in PBS at room temperature for 45 min (goat, 1:700, Invitrogen), followed by PBS washes. Finally, cells were incubated in Cy3-conjugated anti-FLAG monoclonal antibody (mouse, 1:500, Sigma) in 4% BSA in PBS at

room temperature for 45 min. Images were acquired on a Zeiss Axio Observer Z1 inverted microscope using a Plan-Apochromat 63x/1.40 NA oil objective. Images were collected with ZEN 2.1 software.

### **Ratiometric Ca<sup>2+</sup> Imaging**

16-24 hours post-transfection, HEK293T cells were plated into isolated silicone wells (Sigma) on poly-L-lysine (Sigma)-coated cover glass (ThermoFisher). Remaining cells were lysed for anti-FLAG immunoblotting to ensure equivalent expression. 1 hour later, cells were loaded with 10 µg/mL Fura 2-AM (ION Biosciences) in Ringer's solution (Boston Bioproducts) with 0.025% Pluronic F-127 (Sigma) and incubated for 1 hour at room temperature, then rinsed twice with Ringer's solution. Ratiometric Ca<sup>2+</sup> imaging was performed using a Zeiss Axio Observer 7 inverted microscope with a Hamamatsu Flash sCMOS camera at 20x objective. Dual images (340 and 380 nm excitation, 510 nm emission) were collected and pseudocolour ratiometric images were monitored during the experiment (MetaFluor software). After stimulation with agonist, cells were observed for 45-100 s. AITC was purchased from Sigma and was freshly prepared as a stock at 4x the desired concentration in 1% DMSO and Ringer's solution. 5 µL of 4x agonist was added to wells containing 15 µL Ringer's solution to give the final 1x desired concentration. For all experiments, a minimum of 60-90 cells were selected per condition per replicate for ratiometric fluorescence quantification in MetaFluor with 3-5 replicates per experiment. Background signal was quantified from un-transfected cells and subtracted from quantified cells for normalization.

### **Bacterial Protein Expression and Purification**

Bacterial expression vectors were transformed into BL21(DE3) cells and plated on Kanamycin (Kan) LB agar plates. Individual colonies were selected to inoculate LB Kan overnight starter cultures from which 10 mL was used to inoculate 1 L of Terrific Broth (TB) Kan. Once the inoculated TB Kan reached an OD of 0.8-1.0, protein expression was induced using 1 mM IPTG (GoldBio). After 4 hours post-induction, bacteria were harvested at 3,000 rpm for 20 min, the supernatant was discarded, and cell pellets were snap frozen with liquid nitrogen and stored at -80°C. Bacteria were cultured at 37°C and 220 RPM for each step.

Bacterial pellets were thawed at 4°C and resuspended in bacterial lysis buffer (50 mM Tris pH 8.0, 500 mM NaCl, 2 mM CaCl<sub>2</sub>, 5 mM β-ME, 1 mM PMSF, 10% glycerol, and 5 mg bovine DNase I). Bacteria were lysed on ice using a FisherBrand Model 120 Sonic Dismembrator (Fisher Scientific). The sonicator was set to 50% amplitude and cycled between 1 minute on and 1 minute off for a total of 20 minutes. Bacterial debris were pelleted using an Eppendorf centrifuge 5810 R that had been cooled to 4°C at 3900 RPM for 30 minutes. All constructs contained either a 6xHis- or 8xHis-tag and were purified by gravity-flow immobilized metal affinity chromatography (IMAC) using lysis buffer-equilibrated HisPur Ni-NTA resin (ThermoFisher). To remove non-specifically bound proteins, the resin was washed with low-molar imidazole wash buffer (50 mM Tris pH 8.0, 150 mM NaCl, 5 mM β-ME, 0.1 mM PMSF, and 20 mM imidazole). Bound protein was eluted in 2 mL fractions with high-molar imidazole elution buffer (50 mM Tris pH 8.0, 150 mM NaCl, 2 mM CaCl<sub>2</sub>, 5 mM β-ME, 0.1 mM PMSF, and 300 mM imidazole) and an A<sub>280</sub>

measurement was taken for each fraction using a NanoDrop One (ThermoFisher). Protein-containing fractions were pooled, exchanged into storage buffer (50 mM Tris pH 8.0 150 mM NaCl, 2 mM CaCl<sub>2</sub>, and 0.1 mM PMSF) or oocyte injection buffer (50 mM Tris pH 8.0, 150 mM KCl, and 0.1 mM PMSF) by dialysis overnight and concentrated using Amicon Ultra centrifugal filter with a 10,000 Da molecular weight cutoff (Millipore). CaM and CaM<sub>12</sub> were further purified through size exclusion chromatography using a Superdex 75 Increase 10/300 GL (Cytiva). MBP-tagged TRPA1<sup>1089-1119</sup> was incubated with TEV protease overnight at 4°C to cleave the MBP tag. After TEV protease digestion, TRPA1<sup>1089-1119</sup> was isolated from free MBP using an Amicon Ultra centrifugal filter with a 30,000 Da molecular weight cutoff. SDS-Page and Coomassie staining was used for post-hoc analysis of each step of the purifications.

### **Size-Exclusion Chromatography Binding Assay**

Each condition was prepared using 100 μM of each purified protein in a total volume of 500 μL using storage buffer as described above and mixed by gentle nutation at 4°C for 5 minutes. Samples were then loaded onto a Superdex 75 Increase 10/300 GL column pre-equilibrated with either storage buffer or storage buffer supplemented with 5 mM EGTA and run at a flow rate of 0.5 mL/min. The A<sub>280</sub> signal was monitored by the ÄKTA pure chromatography system (Cytiva), and fractions corresponding to observed peaks were collected, concentrated with the appropriate Amicon Ultra cut-off spin filter, and subjected to Coomassie stain analysis.

### **Isothermal Titration Calorimetry**

All ITC experiments were carried out using a MicroCal VP-ITC (Malvern) at the Keck Biophysical Resource Center at Yale. The cell was loaded with 15  $\mu$ M hCaM or hCaM<sub>12</sub> and the titrant syringe with 810  $\mu$ M hTRPA1<sup>1089-1119</sup>. All proteins were buffer matched with storage buffer as described above. 35 injections of 3  $\mu$ L were performed with 240 seconds between each injection and a stir speed of 290 RPM. Data were analyzed with Origin7 software and fit using the one-site model.

### **Structure Prediction**

We used AlphaFold2-multimer with default parameters and Amber relaxation to generate all models<sup>62,63</sup>. Computation was performed on the Farnam cluster at Yale Center for Research Computing. hCaM amino acids 1 – 79 and 80 – 149 were used as the sequences for the calmodulin N- and C-lobe, respectively. For human TRPA1, aa. 993 – 1010, aa. 977 – 1010, and aa. 1092 – 1119 were used as the sequences for the CaMBD, TRP-CaMBD, and CaMBS respectively. Sequences for Human CaM and TRPA1 were retrieved from Uniprot with accession code P0DP23 and O75762. After obtaining predictions from AlphaFold, we used the model with the highest confidence, as judged by average pLDDT, for all further analysis.

### **Oocyte electrophysiology**

Experiments were conducted as previously reported<sup>10</sup>. pMO vectors carrying 3 $\times$ FLAG-tagged hTRPA1 constructs were linearized with PmeI, cRNAs were generated by *in vitro* transcription with the mMessage mMachine T7 transcription kit (Thermo) according to the manufacturer's protocol and were purified with a RNeasy kit (Qiagen). cRNA transcripts

were microinjected into surgically extracted *Xenopus laevis* oocytes (Ecocyte) with a Nanoject III (Harvard Apparatus). Oocytes were injected with 0.25 ng (WT hTRPA1) or 0.1 ng (CaMBS variants) of cRNA per cell, and whole-cell currents were measured 24h post-injection using two-electrode voltage clamp (TEVC). Currents were measured using an OC-725D amplifier (Warner Instruments) delivering a ramp protocol from  $-100$  mV to  $+100$  mV applied every second. Microelectrodes were pulled from borosilicate glass capillary tubes and filled with 3 M KCl. Microelectrode resistances of 0.7–1.2 M $\Omega$  were used for all experiments. Bath solution contained (in mM) 93.5 NaCl, 2 KCl, 2 MgCl<sub>2</sub>, 0.1 BaCl<sub>2</sub>, and 5 HEPES (pH 7.5). For experiments in the presence of Ca<sup>2+</sup>, BaCl<sub>2</sub> was replaced with 1.8 mM CaCl<sub>2</sub>. For experiments comparing 1.8 and 10 mM extracellular Ca<sup>2+</sup>, BaCl<sub>2</sub> was replaced with 1.8 or 10 mM CaCl<sub>2</sub> and supplemented with 125  $\mu$ M niflumic acid (NFA) to inhibit endogenous Ca<sup>2+</sup>-activated chloride channels. For experiments in Fig. S5, the purified free MBP tag or MBP-hTRPA1<sup>1089-1119</sup> peptide in oocyte injection buffer were microinjected at least 1 hour prior to recording with a final concentration of 100  $\mu$ M assuming an oocyte volume of 1  $\mu$ L. Data were subsequently analyzed using pClamp11 software (Molecular Devices). Oocytes were individually collected after recordings, lysed in 20  $\mu$ L TRPA1 lysis buffer, and subjected to anti-FLAG immunoblot analysis to confirm construct expression.

### **Sequence alignment**

The sequence alignment in Figure 4F was built by aligning the mouse, rat, chicken, fruit bat, ball python snake, boa snake, rat snake, and *Drosophila melanogaster* TRPA1 C-terminal sequences to residues 1089-1112 of human TRPA1 in Sequence Logo.

### **Statistical Analysis**

All data quantification was performed in Microsoft Excel. Quantified data presentation and statistical analyses were performed in GraphPad Prism. Criterion for statistical significance for all tests was  $p < 0.05$ .

### **Data Availability**

The data that support the findings of this study are available from the corresponding author upon reasonable request. The 6V9W (<https://www.rcsb.org/structure/6v9w>) PDB file was used in this study. Models were built with UCSF Chimera version 16.1 or ChimeraX version 1.6.1.

### **Acknowledgements**

We thank Wendy Gilbert, Franziska Bleichert, Lily Kabeche, Tony Koleske, and Yong Xiong for constructive suggestions, Fred Sigworth, and members of the Paulsen lab for helpful discussions and for critical reading of the manuscript, and Grover Paulsen-Sharpe and Marilee Pawsen for moral support. We thank Ewa Folta-Stogniew for technical assistance with ITC experiments. J.H.S. is supported by an NIH NINDS NRSA pre-doctoral fellowship (1F31NS122412) and a Cellular and Molecular Biology pre-doctoral training grant (T32GM007223). A.B. is supported by a Biophysics pre-doctoral training grant (5T32GM008283-33). This research was supported by an International Association for the Study of Pain Early Career Research Grant, a Rita Allen Foundation and American Pain Society Pain Scholar Award, and by NIH grant R35GM142825 to C.E.P. The content is solely the responsibility of the authors and does not necessarily represent the official views of the National Institutes of Health.

**Author Contributions:** J.H.S. and C.E.P. planned the project, designed experiments, cloned all constructs used in the study, and carried out Ca<sup>2+</sup> imaging. J.H.S., G.A.A., and C.E.P. carried out Calmodulin binding assays. J.H.S. carried out surface biotinylation, protein purifications, size exclusion chromatography assays, isothermal titration calorimetry, and two-electrode voltage clamp work. A.B. carried out immunostainings. Y.Z. ran the AlphaFold2 Multimer predictions. J.H.S. and C.E.P. wrote the manuscript with input from G.A.A., A.B., and Y.Z.

**Competing Interests:** The authors declare no competing interests.

## REFERENCES

- 1 Clapham, D. E. Ca<sup>2+</sup> signaling. *Cell* **131**, 1047-1058 (2007).
- 2 Averbek, B. in *Encyclopedia of Pain* 1320-1322 (Springer, 2007).
- 3 Chiu, I. M., von Hehn, C. A. & Woolf, C. J. Neurogenic inflammation and the peripheral nervous system in host defense and immunopathology. *Nat Neurosci* **15**, 1063-1067 (2012).
- 4 Ji, R. R., Nackley, A., Huh, Y., Terrando, N. & Maixner, W. Neuroinflammation and Central Sensitization in Chronic and Widespread Pain. *Anesthesiology* **129**, 343-366 (2018).
- 5 Matsuda, M., Huh, Y. & Ji, R. R. Roles of inflammation, neurogenic inflammation, and neuroinflammation in pain. *J Anesth* **33**, 131-139 (2019).
- 6 Richardson, J. D. & Vasko, M. R. Cellular mechanisms of neurogenic inflammation. *J Pharmacol Exp Ther* **302**, 839-845 (2002).
- 7 Gao, R. *et al.* Potent analgesic effects of a store-operated Ca<sup>2+</sup> channel inhibitor. *Pain* **154**, 2034-2044 (2013).
- 8 Hagenston, A. M. & Simonetti, M. Neuronal Ca<sup>2+</sup> signaling in chronic pain. *Cell Tissue Res* **357**, 407-426 (2014).
- 9 Yousuf, M. S. *et al.* Endoplasmic reticulum stress in the dorsal root ganglia regulates large-conductance potassium channels and contributes to pain in a model of multiple sclerosis. *FASEB J* **34**, 12577-12598 (2020).
- 10 Bali, A. *et al.* Molecular mechanism of hyperactivation conferred by a truncation of TRPA1. *Nat Commun* **14**, 2867 (2023).
- 11 Kremeyer, B. *et al.* A gain-of-function mutation in TRPA1 causes familial episodic pain syndrome. *Neuron* **66**, 671-680 (2010).
- 12 Nirenberg, M. J., Chaouni, R., Biller, T. M., Gilbert, R. M. & Paisan-Ruiz, C. A novel TRPA1 variant is associated with carbamazepine-responsive cramp-fasciculation syndrome. *Clin Genet* **93**, 164-168 (2018).
- 13 Bautista, D. M., Pellegrino, M. & Tsunozaki, M. TRPA1: A gatekeeper for inflammation. *Annu Rev Physiol* **75**, 181-200 (2013).
- 14 Chen, J. & Hackos, D. H. TRPA1 as a drug target--promise and challenges. *Naunyn Schmiedebergs Arch Pharmacol* **388**, 451-463 (2015).
- 15 Grace, M. S., Baxter, M., Dubuis, E., Birrell, M. A. & Belvisi, M. G. Transient receptor potential (TRP) channels in the airway: role in airway disease. *Br J Pharmacol* **171**, 2593-2607 (2014).
- 16 Julius, D. TRP channels and pain. *Annu Rev Cell Dev Biol* **29**, 355-384 (2013).
- 17 Talavera, K. *et al.* Mammalian Transient Receptor Potential TRPA1 Channels: From Structure to Disease. *Physiol Rev* **100**, 725-803 (2020).
- 18 Zhang, X. Targeting TRP ion channels for itch relief. *Naunyn Schmiedebergs Arch Pharmacol* **388**, 389-399 (2015).
- 19 Bandell, M. *et al.* Noxious cold ion channel TRPA1 is activated by pungent compounds and bradykinin. *Neuron* **41**, 849-857 (2004).
- 20 Hinman, A., Chuang, H. H., Bautista, D. M. & Julius, D. TRP channel activation by reversible covalent modification. *Proc Natl Acad Sci U S A* **103**, 19564-19568 (2006).
- 21 Jordt, S. E. *et al.* Mustard oils and cannabinoids excite sensory nerve fibres through the TRP channel ANKTM1. *Nature* **427**, 260-265 (2004).
- 22 Macpherson, L. J. *et al.* Noxious compounds activate TRPA1 ion channels through covalent modification of cysteines. *Nature* **445**, 541-545 (2007).
- 23 Andre, E. *et al.* Cigarette smoke-induced neurogenic inflammation is mediated by alpha,beta-unsaturated aldehydes and the TRPA1 receptor in rodents. *J Clin Invest* **118**, 2574-2582 (2008).

- 24 Balestrini, A. *et al.* A TRPA1 inhibitor suppresses neurogenic inflammation and airway contraction for asthma treatment. *J Exp Med* **218** (2021).
- 25 Gouin, O. *et al.* TRPV1 and TRPA1 in cutaneous neurogenic and chronic inflammation: pro-inflammatory response induced by their activation and their sensitization. *Protein Cell* **8**, 644-661 (2017).
- 26 Kunkler, P. E., Ballard, C. J., Oxford, G. S. & Hurley, J. H. TRPA1 receptors mediate environmental irritant-induced meningeal vasodilatation. *Pain* **152**, 38-44 (2011).
- 27 Meseguer, V. *et al.* TRPA1 channels mediate acute neurogenic inflammation and pain produced by bacterial endotoxins. *Nat Commun* **5**, 3125 (2014).
- 28 Trevisani, M. *et al.* 4-Hydroxynonenal, an endogenous aldehyde, causes pain and neurogenic inflammation through activation of the irritant receptor TRPA1. *Proc Natl Acad Sci U S A* **104**, 13519-13524 (2007).
- 29 Fernandes, E. S., Fernandes, M. A. & Keeble, J. E. The functions of TRPA1 and TRPV1: moving away from sensory nerves. *Br J Pharmacol* **166**, 510-521 (2012).
- 30 Julius, D. & Basbaum, A. I. Molecular mechanisms of nociception. *Nature* **413**, 203-210 (2001).
- 31 Nassini, R., Materazzi, S., Benemei, S. & Geppetti, P. The TRPA1 channel in inflammatory and neuropathic pain and migraine. *Rev Physiol Biochem Pharmacol* **167**, 1-43 (2014).
- 32 Asgar, J. *et al.* The role of TRPA1 in muscle pain and mechanical hypersensitivity under inflammatory conditions in rats. *Neuroscience* **310**, 206-215 (2015).
- 33 Holzer, P. TRP channels in the digestive system. *Curr Pharm Biotechnol* **12**, 24-34 (2011).
- 34 Wang, Z. *et al.* The TRPA1 Channel in the Cardiovascular System: Promising Features and Challenges. *Front Pharmacol* **10**, 1253 (2019).
- 35 Nagata, K., Duggan, A., Kumar, G. & Garcia-Anoveros, J. Nociceptor and hair cell transducer properties of TRPA1, a channel for pain and hearing. *J Neurosci* **25**, 4052-4061 (2005).
- 36 Wang, Y. Y., Chang, R. B., Waters, H. N., McKemy, D. D. & Liman, E. R. The nociceptor ion channel TRPA1 is potentiated and inactivated by permeating  $\text{Ca}^{2+}$  ions. *J Biol Chem* **283**, 32691-32703 (2008).
- 37 Conaway, C. C., Krzeminski, J., Amin, S. & Chung, F. L. Decomposition rates of isothiocyanate conjugates determine their activity as inhibitors of cytochrome p450 enzymes. *Chem Res Toxicol* **14**, 1170-1176 (2001).
- 38 Sura, L. *et al.* C-terminal acidic cluster is involved in  $\text{Ca}^{2+}$ -induced regulation of human transient receptor potential ankyrin 1 channel. *J Biol Chem* **287**, 18067-18077 (2012).
- 39 Zhao, J., Lin King, J. V., Paulsen, C. E., Cheng, Y. & Julius, D. Irritant-evoked activation and  $\text{Ca}^{2+}$  modulation of the TRPA1 receptor. *Nature* **585**, 141-145 (2020).
- 40 Zurborg, S., Yurgionas, B., Jira, J. A., Caspani, O. & Heppenstall, P. A. Direct activation of the ion channel TRPA1 by  $\text{Ca}^{2+}$ . *Nat Neurosci* **10**, 277-279 (2007).
- 41 Hasan, R., Leeson-Payne, A. T., Jaggar, J. H. & Zhang, X. Calmodulin is responsible for  $\text{Ca}^{2+}$ -dependent regulation of TRPA1 Channels. *Sci Rep* **7**, 45098 (2017).
- 42 Dang, S. *et al.* Structural insight into TRPV5 channel function and modulation. *Proc Natl Acad Sci U S A* **116**, 8869-8878 (2019).
- 43 Hughes, T. E. T. *et al.* Structural insights on TRPV5 gating by endogenous modulators. *Nat Commun* **9**, 4198 (2018).
- 44 Kovalevskaya, N. V. *et al.* Structural analysis of calmodulin binding to ion channels demonstrates the role of its plasticity in regulation. *Pflugers Arch* **465**, 1507-1519 (2013).
- 45 Lee, C. H. & MacKinnon, R. Activation mechanism of a human SK-calmodulin channel complex elucidated by cryo-EM structures. *Science* **360**, 508-513 (2018).

- 46 Singh, A. K., McGoldrick, L. L., Twomey, E. C. & Sobolevsky, A. I. Mechanism of calmodulin inactivation of the Ca<sup>2+</sup>-selective TRP channel TRPV6. *Sci Adv* **4**, eaau6088 (2018).
- 47 Campiglio, M. & Flucher, B. E. The role of auxiliary subunits for the functional diversity of voltage-gated Ca<sup>2+</sup> channels. *J Cell Physiol* **230**, 2019-2031 (2015).
- 48 Deutsch, C. Potassium channel ontogeny. *Annu Rev Physiol* **64**, 19-46 (2002).
- 49 Dolphin, A. C. Voltage-gated Ca<sup>2+</sup> channels and their auxiliary subunits: physiology and pathophysiology and pharmacology. *J Physiol* **594**, 5369-5390 (2016).
- 50 Isom, L. L., De Jongh, K. S. & Catterall, W. A. Auxiliary subunits of voltage-gated ion channels. *Neuron* **12**, 1183-1194 (1994).
- 51 Yu, F. H. & Catterall, W. A. Overview of the voltage-gated sodium channel family. *Genome Biol* **4**, 207 (2003).
- 52 Wu, X. & Bers, D. M. Free and bound intracellular calmodulin measurements in cardiac myocytes. *Cell Ca<sup>2+</sup>* **41**, 353-364 (2007).
- 53 Liu, C. *et al.* A Non-covalent Ligand Reveals Biased Agonism of the TRPA1 Ion Channel. *Neuron* **109**, 273-284 e274 (2021).
- 54 Meents, J. E., Ciotu, C. I. & Fischer, M. J. M. TRPA1: a molecular view. *J Neurophysiol* **121**, 427-443 (2019).
- 55 Gaudet, R. A primer on ankyrin repeat function in TRP channels and beyond. *Mol Biosyst* **4**, 372-379 (2008).
- 56 Chin, D. & Means, A. R. Calmodulin: a prototypical Ca<sup>2+</sup> sensor. *Trends Cell Biol* **10**, 322-328 (2000).
- 57 Bate, N. *et al.* A Novel Mechanism for Calmodulin-Dependent Inactivation of Transient Receptor Potential Vanilloid 6. *Biochemistry* **57**, 2611-2622 (2018).
- 58 Chen, W. *et al.* Calmodulin binds to Drosophila TRP with an unexpected mode. *Structure* **29**, 330-344 e334 (2021).
- 59 Lau, K., Chan, M. M. & Van Petegem, F. Lobe-specific calmodulin binding to different ryanodine receptor isoforms. *Biochemistry* **53**, 932-946 (2014).
- 60 Marques-Carvalho, M. J. *et al.* Molecular Insights into the Mechanism of Calmodulin Inhibition of the EAG1 Potassium Channel. *Structure* **24**, 1742-1754 (2016).
- 61 Sarhan, M. F., Van Petegem, F. & Ahern, C. A. A double tyrosine motif in the cardiac sodium channel domain III-IV linker couples Ca<sup>2+</sup>-dependent calmodulin binding to inactivation gating. *J Biol Chem* **284**, 33265-33274 (2009).
- 62 Evans, R. *et al.* Protein complex prediction with AlphaFold-Multimer. *bioRxiv* (2021). <https://doi.org/https://doi.org/10.1101/2021.10.04.463034>
- 63 Jumper, J. *et al.* Highly accurate protein structure prediction with AlphaFold. *Nature* **596**, 583-589 (2021).
- 64 Cordero-Morales, J. F., Gracheva, E. O. & Julius, D. Cytoplasmic ankyrin repeats of transient receptor potential A1 (TRPA1) dictate sensitivity to thermal and chemical stimuli. *Proc Natl Acad Sci U S A* **108**, E1184-1191 (2011).
- 65 Doerner, J. F., Gisselmann, G., Hatt, H. & Wetzl, C. H. Transient receptor potential channel A1 is directly gated by Ca<sup>2+</sup> ions. *J Biol Chem* **282**, 13180-13189 (2007).
- 66 Paulsen, C. E., Armache, J. P., Gao, Y., Cheng, Y. & Julius, D. Structure of the TRPA1 ion channel suggests regulatory mechanisms. *Nature* **520**, 511-517 (2015).
- 67 Suo, Y. *et al.* Structural Insights into Electrophile Irritant Sensing by the Human TRPA1 Channel. *Neuron* **105**, 882-894 e885 (2020).
- 68 Loukin, S. H., Teng, J. & Kung, C. A channelopathy mechanism revealed by direct calmodulin activation of TrpV4. *Proc Natl Acad Sci U S A* **112**, 9400-9405 (2015).
- 69 Tidow, H. & Nissen, P. Structural diversity of calmodulin binding to its target sites. *FEBS J* **280**, 5551-5565 (2013).
- 70 Yap, K. L. *et al.* Calmodulin target database. *J Struct Funct Genomics* **1**, 8-14 (2000).

- 71 Meador, W. E., Means, A. R. & Quioco, F. A. Target enzyme recognition by calmodulin: 2.4 A structure of a calmodulin-peptide complex. *Science* **257**, 1251-1255 (1992).
- 72 Rellos, P. *et al.* Structure of the CaMKIIdelta/calmodulin complex reveals the molecular mechanism of CaMKII kinase activation. *PLoS Biol* **8**, e1000426 (2010).
- 73 Saimi, Y. & Kung, C. Calmodulin as an ion channel subunit. *Annu Rev Physiol* **64**, 289-311 (2002).
- 74 Li, J. *et al.* Research Progress on TRPA1 in Diseases. *J Membr Biol* (2023).
- 75 Lobley, A., Swindells, M. B., Orengo, C. A. & Jones, D. T. Inferring function using patterns of native disorder in proteins. *PLoS Comput Biol* **3**, e162 (2007).
- 76 Magidovich, E., Orr, I., Fass, D., Abdu, U. & Yifrach, O. Intrinsic disorder in the C-terminal domain of the Shaker voltage-activated K<sup>+</sup> channel modulates its interaction with scaffold proteins. *Proc Natl Acad Sci U S A* **104**, 13022-13027 (2007).
- 77 Cao, E., Cordero-Morales, J. F., Liu, B., Qin, F. & Julius, D. TRPV1 channels are intrinsically heat sensitive and negatively regulated by phosphoinositide lipids. *Neuron* **77**, 667-679 (2013).
- 78 Chuang, H. H. *et al.* Bradykinin and nerve growth factor release the capsaicin receptor from PtdIns(4,5)P<sub>2</sub>-mediated inhibition. *Nature* **411**, 957-962 (2001).
- 79 Gracheva, E. O. *et al.* Ganglion-specific splicing of TRPV1 underlies infrared sensation in vampire bats. *Nature* **476**, 88-91 (2011).
- 80 Prescott, E. D. & Julius, D. A modular PIP<sub>2</sub> binding site as a determinant of capsaicin receptor sensitivity. *Science* **300**, 1284-1288 (2003).
- 81 Goretzki, B., Guhl, C., Tebbe, F., Harder, J. M. & Hellmich, U. A. Unstructural Biology of TRP Ion Channels: The Role of Intrinsically Disordered Regions in Channel Function and Regulation. *J Mol Biol* **433**, 166931 (2021).
- 82 Allard, C. A. H. *et al.* Structural basis of sensory receptor evolution in octopus. *Nature* **616**, 373-377 (2023).
- 83 Bellono, N. W., Leitch, D. B. & Julius, D. Molecular basis of ancestral vertebrate electroreception. *Nature* **543**, 391-396 (2017).
- 84 Kang, G. *et al.* Sensory specializations drive octopus and squid behaviour. *Nature* **616**, 378-383 (2023).
- 85 Schoenmakers, T. J., Visser, G. J., Flik, G. & Theuvsen, A. P. CHELATOR: an improved method for computing metal ion concentrations in physiological solutions. *Biotechniques* **12**, 870-874, 876-879 (1992).

## Figures

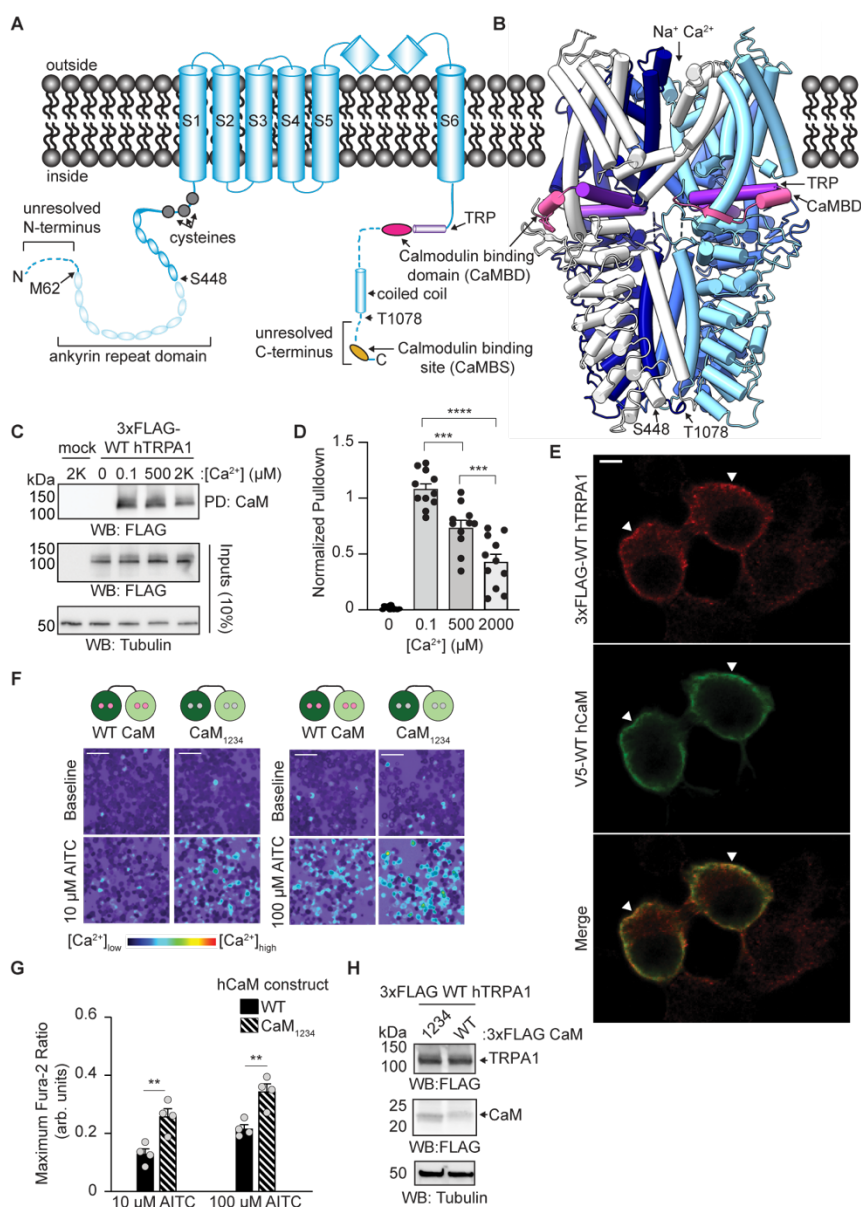


**Figure 1.** TRPA1 activity is regulated by Calmodulin binding in cells. **(A)** Cartoon schematic of a full-length hTRPA1 monomeric subunit with relevant structural features, a previously identified Calmodulin binding domain (CaMBD, pink), and the Calmodulin binding site (CaMBS, yellow) identified in this study denoted. Dashes and transparencies denote unresolved regions in Cryo-EM structures. Residues indicated with arrows denote

positions of truncations used in this study. **(B)** Ribbon diagram of WT hTRPA1 atomic model for residues S448-T1078 from the homotetrameric channel (PDB: 6V9W). Each subunit is colored differently for clarity. The CaMBD and TRP helix are colored as in (A). **(C)** Immunoblotting analysis of 3xFLAG-WT hTRPA1 after CaM-agarose pulldown at the indicated  $\text{Ca}^{2+}$  concentrations from lysates of HEK293T cells transfected with 3xFLAG-WT hTRPA1 or empty vector (mock). Samples were probed using an HRP-conjugated anti-FLAG antibody. Tubulin from whole cell lysates (10%, inputs) was the loading control. **(D)** Quantitative analysis of CaM-agarose enrichment of 3xFLAG-WT hTRPA1 at the indicated  $\text{Ca}^{2+}$  concentrations relative to the maximum enrichment within each replicate. Data represent mean  $\pm$  SEM. \*\*\* $p=0.0003$  (0.1 versus 500  $\mu\text{M}$   $\text{Ca}^{2+}$ ), \*\*\* $p=0.0008$  (500 versus 2000  $\mu\text{M}$   $\text{Ca}^{2+}$ ), \*\*\*\* $p<0.0001$  (0.1 versus 2000  $\mu\text{M}$   $\text{Ca}^{2+}$ ).  $n=11$ , one-way ANOVA with Tukey's *post hoc* analysis. **(E)** Representative immunofluorescence images of Neuro2A cells transiently co-transfected with 3xFLAG-WT hTRPA1 and V5-WT hCaM. Cells were stained with anti-FLAG (red) and anti-V5 (green) antibodies. Regions of co-localization appear as yellow in the merged images. White arrowheads denote cells exhibiting co-localization. Scale bar indicates 5  $\mu\text{m}$ . Images are representative of three independent experiments. **(F)** Ratiometric  $\text{Ca}^{2+}$  imaging of HEK293T cells co-transfected with 3xFLAG-WT hTRPA1 and 3xFLAG-WT or a  $\text{Ca}^{2+}$  binding-deficient ( $\text{CaM}_{1234}$ ) hCaM. Cells were stimulated with AITC (10 or 100  $\mu\text{M}$ ). Images are representative of four independent experiments. Scale bars indicate 50  $\mu\text{m}$ . **(G)** Quantification of 10  $\mu\text{M}$  and 100  $\mu\text{M}$  AITC-evoked change in Fura-2 ratio of data from panels (F) of cells co-expressing WT hTRPA1 and WT hCaM (black bars) or  $\text{CaM}_{1234}$  (striped bars). Data represent mean  $\pm$  SEM. \*\* $p=0.0066$  (10  $\mu\text{M}$  AITC) or \*\* $p=0.0048$  (100  $\mu\text{M}$  AITC).  $n=4$  independent

experiments,  $n \geq 90$  cells per transfection condition per experiment, two-tailed Student's t-test. **(H)** Representative immunoblotting analysis of the cells used for  $\text{Ca}^{2+}$  imaging in (F). Samples were probed as in (C).

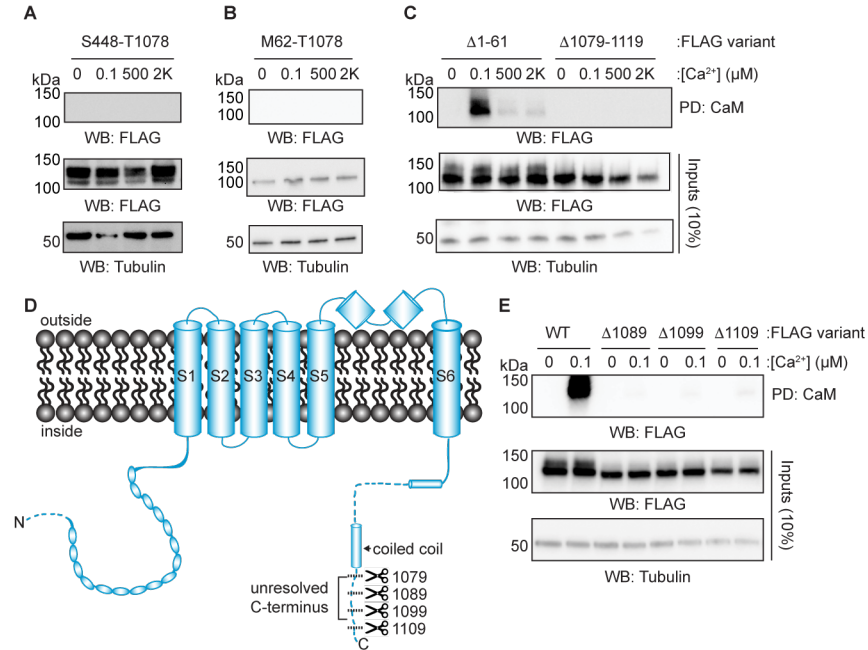


**Figure 2.** Identification of a CaM binding element in the TRPA1 unresolved C-terminus. (A-C, E) Representative immunoblotting analysis of 3xFLAG-hTRPA1 truncation constructs after CaM-agarose pulldown at the indicated Ca<sup>2+</sup> concentrations from lysates of transfected HEK293T cells. Samples were probed as in Fig. 1C. Data are representative of three independent experiments. (D) Cartoon schematic of a suite of hTRPA1 unresolved C-terminus truncations.

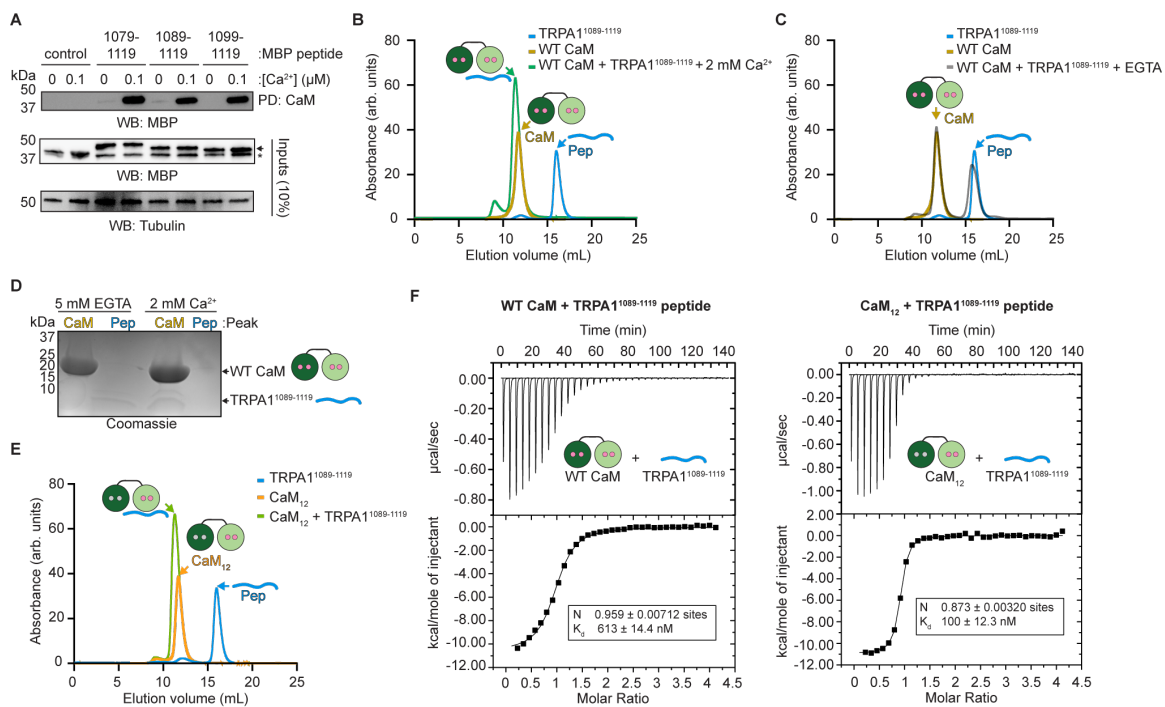


**Figure 3.** The TRPA1 distal C-terminus contains a high affinity CaM binding site. **(A)** Immunoblotting analysis of the indicated MBP-tagged hTRPA1 peptide constructs after CaM-agarose pulldown in the absence or presence of Ca<sup>2+</sup> from lysates of HEK293T cells transfected with free MBP (control), MBP-tagged hTRPA1<sup>1079-1119</sup>, hTRPA1<sup>1089-1119</sup>, or hTRPA1<sup>1099-1119</sup> peptides. Samples were probed using an anti-MBP primary antibody and an HRP-conjugated anti-mouse secondary antibody. Tubulin from whole cell lysates (10%, inputs) was the loading control. Asterisk (\*) denotes free MBP. Arrow denotes MBP-tagged peptide. **(B and C)** Superdex 75 chromatograms of WT hCaM alone (yellow), hTRPA1<sup>1089-1119</sup> peptide alone (blue), WT hCaM with hTRPA1<sup>1089-1119</sup> in the presence of 2 mM Ca<sup>2+</sup> (green, B) or 5 mM EGTA (black, C). **(D)** Coomassie stain of fractions collected from C (5 mM EGTA, black trace) and B (2 mM Ca<sup>2+</sup>, green trace). Fractions were taken from the elution volumes for hCaM (indicated in yellow) and hTRPA1<sup>1089-1119</sup> peptide (indicated in

blue) alone. **(E)** Superdex 75 chromatograms of hCaM<sub>12</sub> alone (orange), hTRPA1<sup>1089-1119</sup> alone (blue), and hCaM<sub>12</sub> with hTRPA1<sup>1089-1119</sup> in the presence of 2 mM Ca<sup>2+</sup> (green). Chromatograms in B, C and E were generated from 100 μM protein for each construct. **(F)** Representative isothermal titration calorimetry plots of WT hCaM (left) or hCaM<sub>12</sub> (right) titrated by hTRPA1<sup>1089-1119</sup> peptide at 2 mM Ca<sup>2+</sup> and fitted using the one-site binding model. Values for the number of binding sites (N) and the binding constant K<sub>d</sub> are shown. **(B-C and E-F)** Data are representative of three independent replicates.

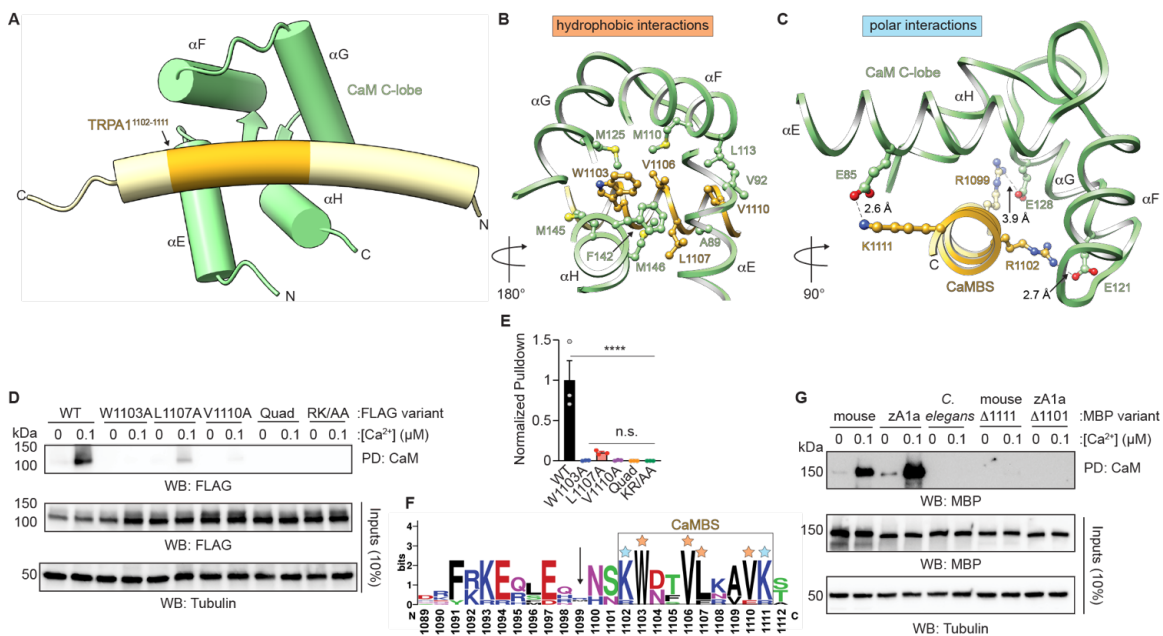


**Figure 4.** Identification of key and conserved TRPA1 CaMBS residues involved in CaM binding. **(A)** Ribbon diagram of the hCaM C-lobe atomic model (green, residues 79-148) in complex with part of the TRPA1 C-terminus (yellow, residues 1089-1119) as predicted by AlphaFold2 Multimer<sup>62,63</sup>. The region proposed to be the CaM binding site (CaMBS, hTRPA1 residues R1102-K1111) is indicated in goldenrod. **(B and C)** Ribbon diagrams from panel (A) with residues mediating hydrophobic (B) and polar (C) interactions depicted as balls and sticks. **(D)** Immunoblotting analysis of the indicated 3xFLAG-hTRPA1 constructs after CaM-agarose pulldown in the absence or presence of Ca<sup>2+</sup> from lysates of HEK293T cells transfected with 3xFLAG-WT, W1103A, L1107A, V1110A, W1103A/V1106A/L1107A/V1110A (Quad), or R1102A/K1111A (RK/AA) hTRPA1. Blot is representative of three independent experiments. Samples were probed as in Fig. 1C. **(E)** Quantification of CaM-agarose pulldowns represented in (D). Pulldown was normalized to the WT hTRPA1 with Ca<sup>2+</sup> average. Data represent mean  $\pm$  SEM. \*\*\*\*p<0.0001, n.s. not

significant ( $p > 0.05$ ).  $n = 3$  independent experiments, one-way ANOVA with Tukey's *post hoc* analysis. (F) Sequence alignment of 9 TRPA1 orthologues aligned to residues 1089-1112 of hTRPA1. Alignment generated with Sequence Logo. Arrow denotes poorly conserved hTRPA1 R1099. Box denotes TRPA1 CaMBS. Hydrophobic (orange) and polar (blue) residues proposed to form the CaMBS are denoted with stars. (G) Immunoblotting analysis of the indicated MBP-TRPA1 species orthologue constructs after CaM-agarose pulldown in the absence or presence of  $\text{Ca}^{2+}$  from lysates of HEK293T cells transfected with MBP-WT mouse, zebrafish TRPA1a isoform (zA1a), or *C. elegans* TRPA1 or the  $\Delta 1109$ -1119 equivalents of mouse ( $\Delta 1111$ -1125) or zebrafish ( $\Delta 1101$ -1115) TRPA1. Blot is representative of four independent experiments. Samples were probed as in Fig. 3A.

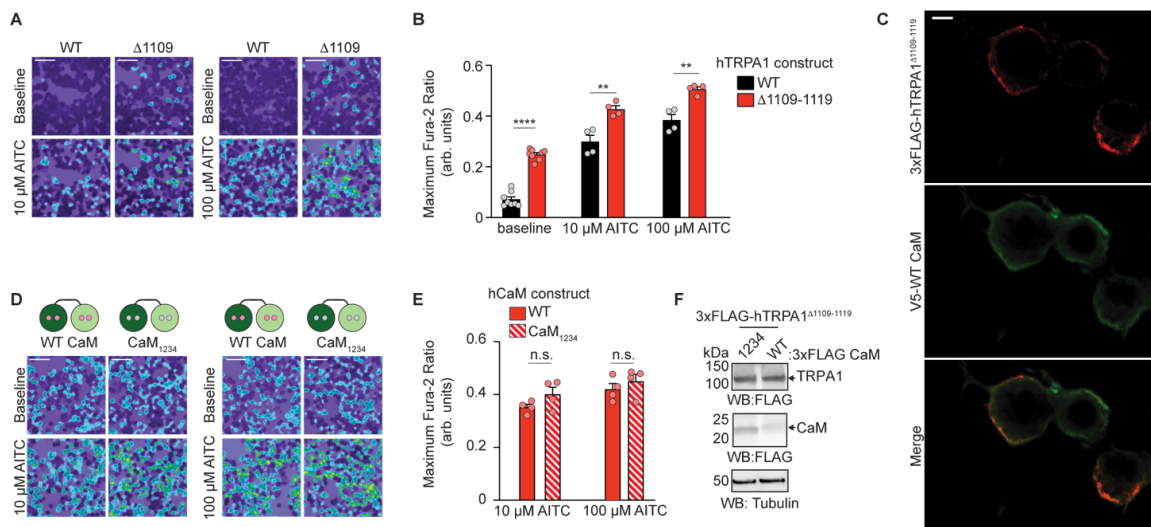


**Figure 5.** Functional consequence of loss of CaM binding on TRPA1. **(A)** Ratiometric  $\text{Ca}^{2+}$  imaging of HEK293T cells transfected with 3xFLAG-WT hTRPA1 or hTRPA1 $^{\Delta 1109-1119}$ . Cells were stimulated with AITC (10 or 100  $\mu\text{M}$ ). Images are representative of four independent experiments. Scale bars indicate 50  $\mu\text{m}$ . **(B)** Quantification of baseline, 10  $\mu\text{M}$  or 100  $\mu\text{M}$  AITC-evoked change in Fura-2 ratio from cells in (A) transfected with WT hTRPA1 (black) or hTRPA1 $^{\Delta 1109-1119}$  (red). Data represent mean  $\pm$  SEM. \*\*\*\* $p < 0.0001$  (baseline), \*\* $p = 0.0043$  (10  $\mu\text{M}$  AITC), and \*\* $p = 0.0025$  (100  $\mu\text{M}$  AITC).  $n = 4$  independent experiments,  $n \geq 90$  cells per transfection condition per experiment, two-tailed Student's  $t$ -test. **(C)** Representative immunofluorescence images of Neuro2A cells transiently co-transfected with 3xFLAG-hTRPA1 $^{\Delta 1109-1119}$  and V5-WT hCaM. Cells were stained as in Fig. 1E. Regions of co-localization appear as yellow in the merged images. Scale bar indicates 5  $\mu\text{m}$ . Images are representative of three independent experiments. **(D)** Ratiometric  $\text{Ca}^{2+}$  imaging of HEK293T cells co-transfected with 3xFLAG-hTRPA1 $^{\Delta 1109-1119}$  and 3xFLAG-WT hCaM or CaM $_{1234}$ . Cells were stimulated with AITC (10 or 100  $\mu\text{M}$ ). Images are representative of four independent experiments. Scale bars indicate 50  $\mu\text{m}$ . **(E)**

Quantification of 10  $\mu\text{M}$  and 100  $\mu\text{M}$  AITC-evoked change in Fura-2 ratio of data from panels (D) of cells co-expressing hTRPA1 $^{\Delta 1109-1119}$  and WT hCaM (red bars) or CaM<sub>1234</sub> (striped bars). Data represent mean  $\pm$  SEM. n.s. not significant ( $p > 0.05$ ).  $n = 4$  independent experiments,  $n \geq 90$  cells per transfection condition per experiment, two-tailed Student's *t*-test. (F) Representative immunoblotting analysis of the cells used for Ca<sup>2+</sup> imaging in (D). Samples were probed as in Fig. 1D.

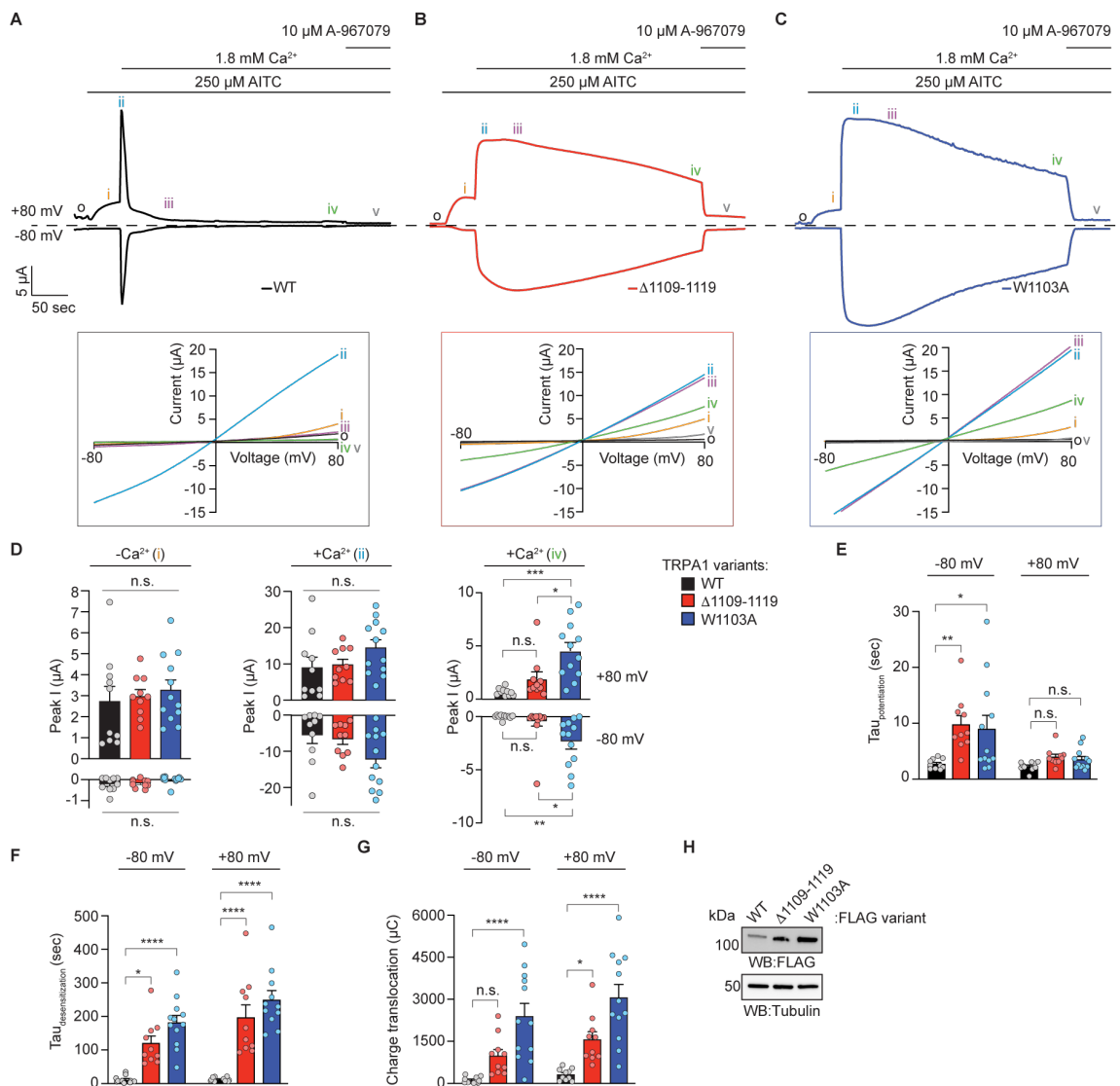


**Figure 6.** CaM binding is critical for TRPA1 desensitization. (A-C) Representative time-traces at -80 and +80 mV holding potentials from oocytes expressing WT (A, black),  $\Delta 1109-1119$  (B, red), or W1103A hTRPA1 (C, blue). Current evoked with 250  $\mu\text{M}$  AITC in the absence (orange i) and presence (blue ii) of 1.8 mM extracellular  $\text{Ca}^{2+}$ . Channels were blocked with 10  $\mu\text{M}$  A-967079 (grey v). Dashed line denotes 0  $\mu\text{A}$  current. Protocol of condition application indicated above. Boxed below are the corresponding current-voltage relationships from timepoints indicated by black o (baseline), orange i (AITC without  $\text{Ca}^{2+}$ ), blue ii (AITC with  $\text{Ca}^{2+}$ ), purple iii (25 seconds after  $\text{Ca}^{2+}$  addition), green

iv (5 minutes after  $\text{Ca}^{2+}$  addition), and grey v (A-967079 inhibited). **(D)** Quantification of peak current amplitudes at +80 mV (above) and -80 mV (below) before (orange i, left), 25 seconds after (blue ii, middle), and 5 minutes after (green iv, right)  $\text{Ca}^{2+}$  addition. Colors as indicated in A-C. Data represent mean  $\pm$  SEM. \*\*\* $p=0.0002$ , \*\* $p=0.0026$ , \* $p=0.0132$  or  $0.0217$  (+80 and -80 mV, respectively), n.s. not significant ( $p>0.05$ ). **(E and F)** Calculated time constants of potentiation (E) and desensitization (F) at -80 mV (left) and +80 mV (right) from fitting data as in A-C to a single-exponential function. Data represent mean  $\pm$  SEM. \* $p=0.0135$  (WT versus W1103A, -80 mV, tau potentiation), \*\* $p=0.0069$  (WT versus  $\Delta 1109-1119$ , -80 mV, tau potentiation), \*\*\*\* $p<0.0001$ , \* $p=0.0189$  (WT versus  $\Delta 1109-1119$ , -80 mV, tau desensitization), n.s. not significant ( $p>0.05$ ). **(G)** Quantification of charge translocation ( $\mu\text{A}\cdot\text{s}$ ,  $\mu\text{C}$ , *e.g.*, area under the curve) at -80 mV (left) and +80 mV (right) from oocytes used as in A-C. Data represent mean  $\pm$  SEM. \* $p=0.0408$  (WT versus  $\Delta 1109-1119$ , -80 mV), \*\*\*\* $p<0.0001$ , n.s. not significant ( $p>0.05$ ). **(D-G)**  $n=10$  (WT and  $\Delta 1109-1119$  hTRPA1) or  $12$  (W1103A hTRPA1) oocytes per condition, one-way ANOVA with Bonferroni's *post hoc* analysis. **(H)** Western blot of lysates from oocytes used for recordings in A-C expressing 3xFLAG-tagged hTRPA1 variants, probed as in Fig. 1D.

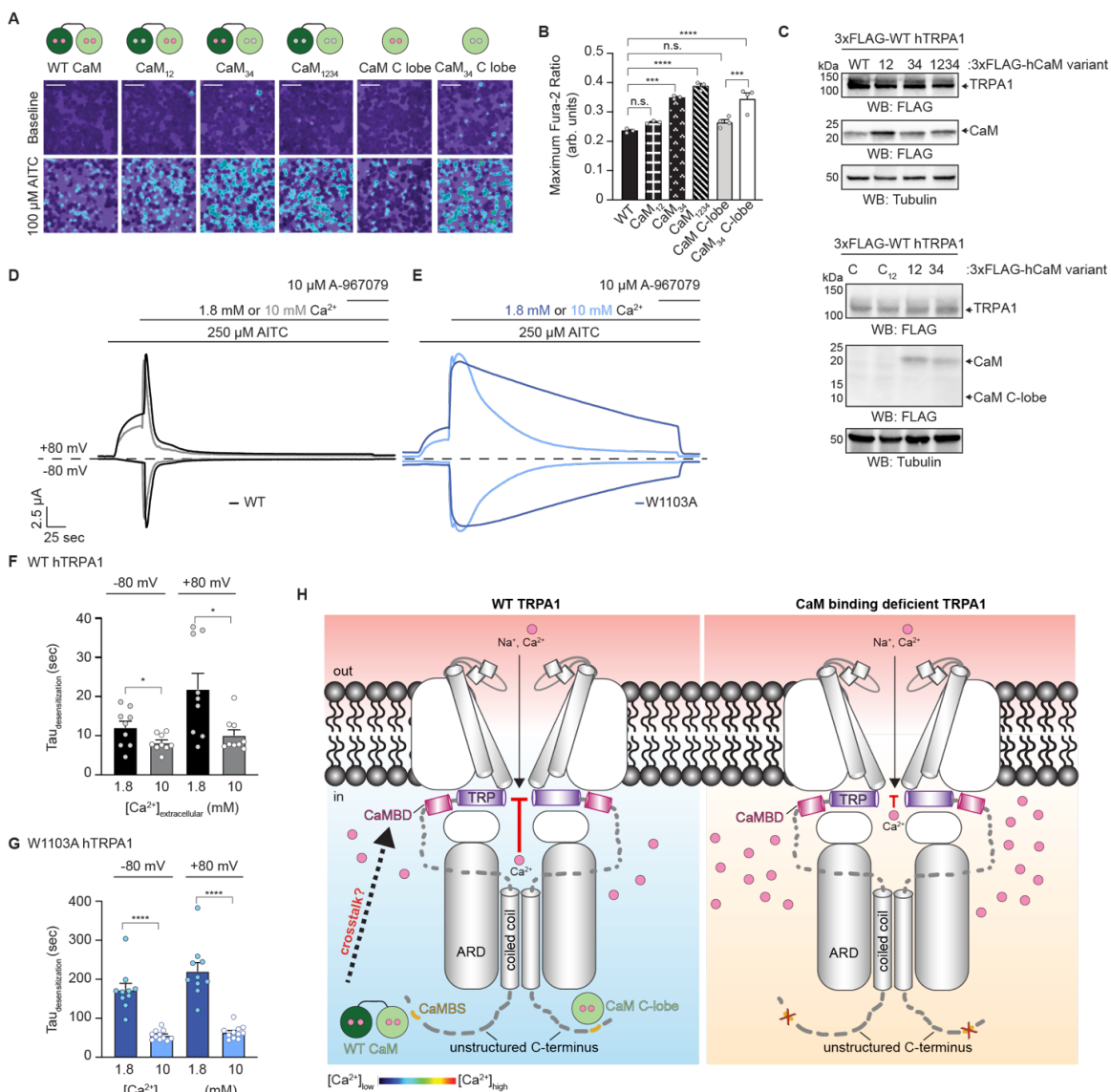


**Figure 7.** Requirement of the CaM C-lobe for TRPA1 regulation and model. (A) Ratiometric Ca<sup>2+</sup> imaging of HEK293T cells transfected with WT hTRPA1 and WT or the indicated hCaM mutants. Cells were stimulated with 100  $\mu$ M AITC. Images are representative of three (WT CaM, CaM<sub>12</sub>, CaM<sub>34</sub>, and CaM<sub>1234</sub>) or four (CaM C-lobe and CaM<sub>34</sub> C-lobe) independent experiments. Scale bars indicate 50  $\mu$ m. (B) Quantification of 100  $\mu$ M AITC-evoked change in Fura-2 ratio of data from panel (A). Data represent mean  $\pm$  SEM. \*\*\*\*,  $p < 0.0001$ , \*\*\* $p = 0.001$  (WT CaM versus CaM<sub>34</sub>) or 0.0007 (CaM C-lobe

versus CaM<sub>34</sub> C-lobe), n.s. not significant  $p > 0.05$ ).  $n = 3$  (WT CaM, CaM<sub>12</sub>, CaM<sub>34</sub>, and CaM<sub>1234</sub>) or 4 (CaM C-lobe and CaM<sub>34</sub> C-lobe) independent replicates, one-way ANOVA with Tukey's *post hoc* analysis. (C) Representative immunoblotting analysis of the cells used for Ca<sup>2+</sup> imaging in (A). Samples were probed as in Fig. 1D. (D-E) Representative time-traces at -80 and +80 mV holding potentials from oocytes expressing WT (D) or W1103A hTRPA1 (E). Current evoked with 250  $\mu$ M AITC in the absence and presence of 1.8 mM (black/dark blue) or 10 mM (grey/light blue) extracellular Ca<sup>2+</sup>. Channels were blocked with 10  $\mu$ M A-967079. Dashed line denotes 0  $\mu$ A current. Protocol of condition application indicated above. Extracellular solutions contained 125  $\mu$ M niflumic acid (NFA). (F-G) Calculated time constants of desensitization from fitting data as in D-E at 1.8 or 10 mM extracellular Ca<sup>2+</sup> to a single-exponential function. Data represent mean  $\pm$  SEM. \*\*\*\* $p < 0.001$ , \* $p = 0.0424$  (WT hTRPA1, -80 mV) or 0.0146 (WT hTRPA1, +80 mV).  $n = 9$  (WT), 10 (W1103A, 1.8 mM Ca<sup>2+</sup>) or 11 (W1103A, 10 mM Ca<sup>2+</sup>) oocytes per condition, two-tailed Student's t-test.

(H) Cartoon model illustrating Ca<sup>2+</sup> desensitization of TRPA1 (red inhibition arrow) in a WT channel (left) versus a CaM binding deficient channel (right). Two subunits are shown for clarity. Channel activation facilitates permeation of sodium and Ca<sup>2+</sup> ions into the cytoplasm. WT CaM (dumbbell) or the CaM C-lobe (green circle) binding to the TRPA1 CaMBS (yellow) in the unstructured C-terminus primes TRPA1 for rapid desensitization following Ca<sup>2+</sup> permeation (left, blue color on the Ca<sup>2+</sup> concentration heat map). When the TRPA1-CaM interaction is disrupted, channels remain active allowing intracellular Ca<sup>2+</sup> concentrations to rise (right, orange color on the Ca<sup>2+</sup> concentration heat map) before incomplete desensitization is observed. Aspects of TRPA1 regulation by CaM may involve

concerted binding of the CaM N-lobe to the CaMBD (red crosstalk) or to an unknown second site.

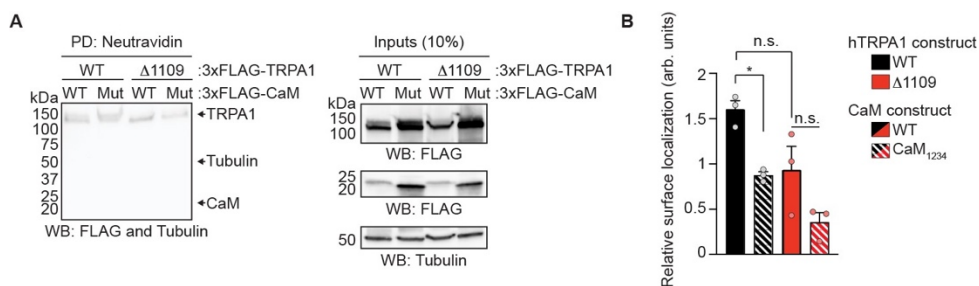


**Figure S1.** Effect of CaM or CaM<sub>1234</sub> co-expression on TRPA1 surface localization. **(A)** Immunoblotting analysis of 3xFLAG-WT hTRPA1, 3xFLAG-hTRPA1<sup>Δ1109-1119</sup>, 3xFLAG-WT CaM or 3xFLAG-CaM<sub>1234</sub> protein expression in biotin-labeled plasma membranes from transfected cells. Biotinylated proteins were precipitated by Neutravidin resin pulldown and probed as in Fig. 1F. CaM and Tubulin were the negative controls for plasma membrane localization. **(B)** Quantitative analysis of the plasma membrane localization of 3xFLAG-WT hTRPA1 or hTRPA1<sup>Δ1109-1119</sup> proteins relative to Tubulin. Data represent mean ± SEM. \*p < 0.05, n.s. not significant. n=3, one-way ANOVA with Tukey's *post hoc* analysis.

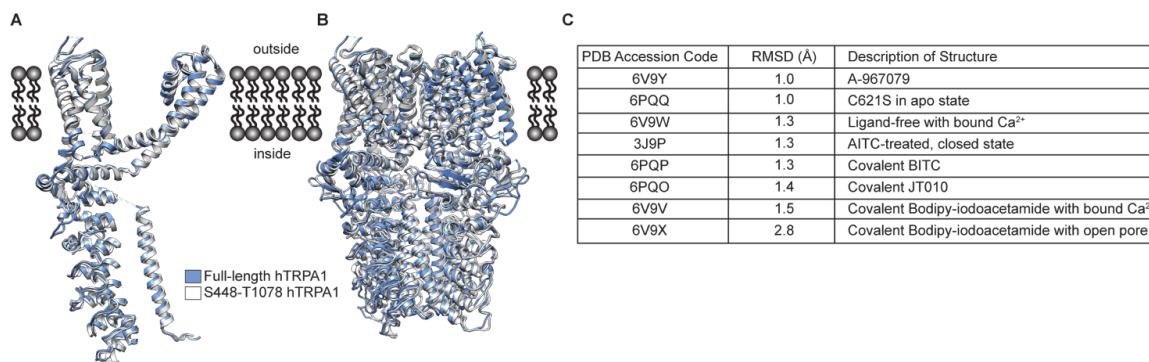


**Figure S2.** Structural conservation of WT hTRPA1 and minimal hTRPA1<sup>448-1078</sup>. (A and B) Ribbon diagram of WT hTRPA1 monomeric (A) or tetrameric (B) atomic models for residues S448-T1078 (blue) overlaid with minimal hTRPA1<sup>448-1078</sup> construct (white). Models built with the human hTRPA1 Cryo-EM structure (PDB: 6V9W) or the minimal hTRPA1<sup>448-1078</sup> construct (PDB: 6X2J) in ChimeraX. Models were aligned in real space. (C) RMSD of TRPA1<sup>488-1078</sup> against all available full-length TRPA1 structures. Calculations were performed by the Dali server using TRPA1<sup>488-1078</sup> as the search model in a heuristic PDB search.

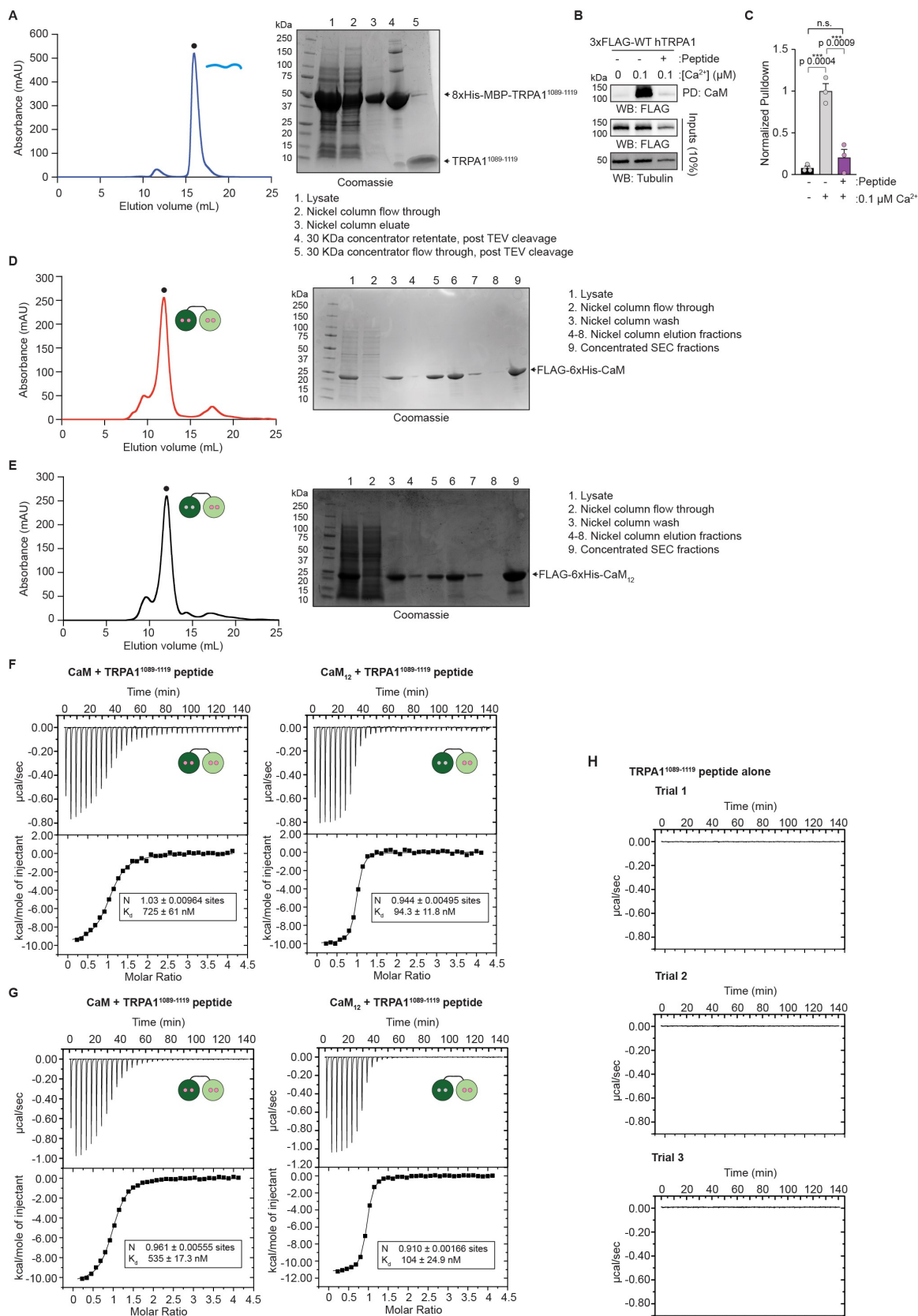


**Figure S3.** Purifications of (A) the hTRPA1<sup>1089-1119</sup> peptide, (D) WT hCaM, and (E) hCaM<sub>12</sub> for size exclusion chromatography and isothermal calorimetry. Representative Superdex 75 chromatograms (left) and Coomassie gels (right) from a purification for each. The peak corresponding to each protein is indicated (black dot). (B) Immunoblotting analysis of 3xFLAG-WT hTRPA1 after CaM-agarose pulldown at the indicated Ca<sup>2+</sup> concentrations in presence or absence of 10 μM hTRPA1<sup>1089-1119</sup> peptide. Samples were probed as in Fig. 1F. Blot is representative of three independent experiments. (C) Quantification of CaM-agarose pulldowns represented in (B). Pulldown was normalized to the WT hTRPA1 with Ca<sup>2+</sup> and without hTRPA1<sup>1089-1119</sup> peptide average. Data represent mean ± SEM. \*\*\*p<0.001, \*p<0.05, n.s. not significant. n = 3 independent experiments, one-way ANOVA with Tukey's *post hoc* analysis. (F and G) Replicates 2 (F) and 3 (G) of isothermal calorimetry plots of WT hCaM (left) or hCaM<sub>12</sub> (right) titrated by TRPA1<sup>1089-1119</sup> at 2 mM Ca<sup>2+</sup> and fitted using the one-site binding model. Values for the number of binding sites (N) and the binding constant K<sub>d</sub> are shown. (H) Three control isothermal calorimetry plots for buffer titrated by TRPA1<sup>1089-1119</sup> at 2 mM Ca<sup>2+</sup>.

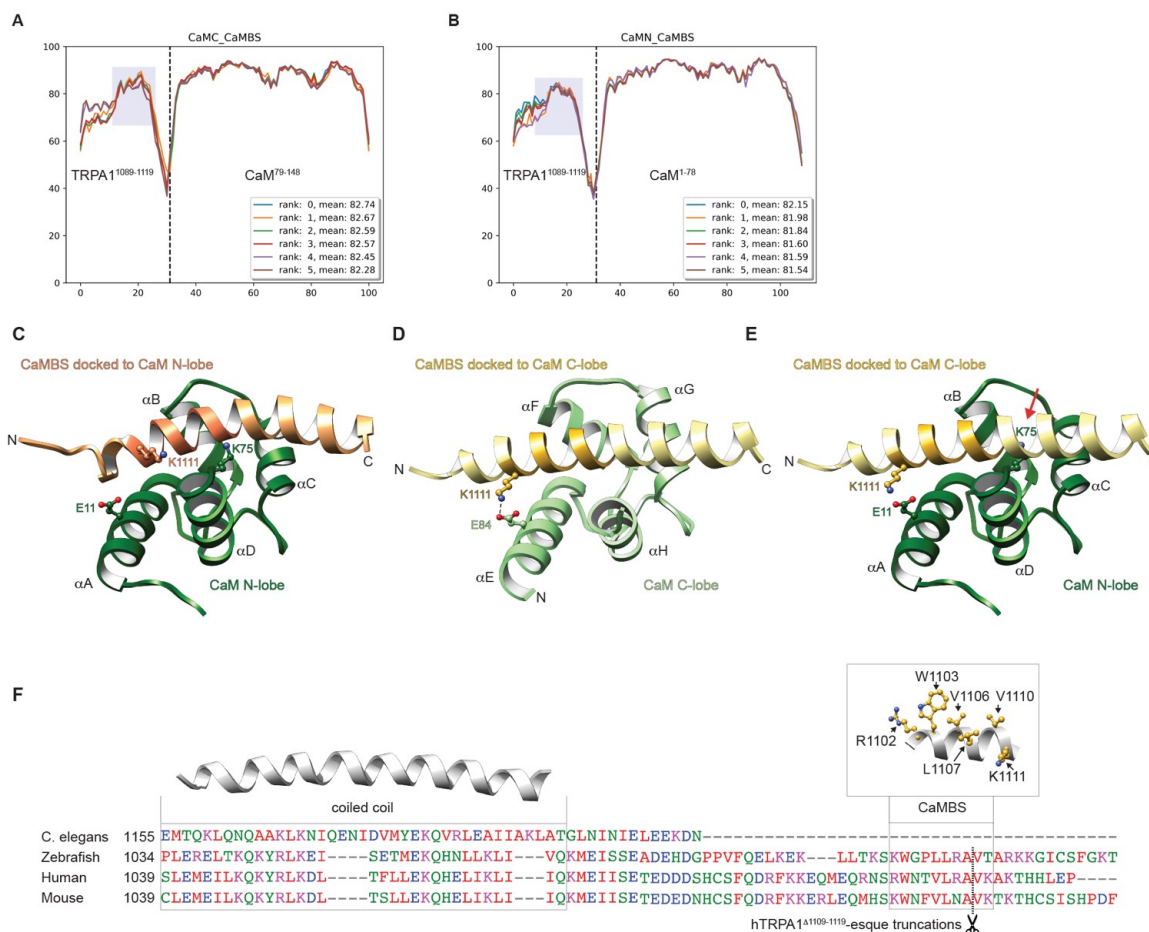


**Figure S4.** Structural models and sequence conservation of the TRPA1 CaMBS. (A and B) Confidence measurements (pLDDT plots) of AlphaFold2 Multimer models for the hTRPA1<sup>1089-1119</sup> peptide docked to the CaM C- (A) or N- (B) lobe. For each, the top five generated models are plotted. Rank 0 models were used for models in **Fig. 5A-C** and (C-E). (A) hTRPA1<sup>1089-1119</sup> docked to the CaM C-lobe (residues 79-148) used in **Figure 5**. (B) hTRPA1<sup>1089-1119</sup> docked to the CaM N-lobe (residues 1-78). (C-E) Proposed rationale for CaMBS specificity for the CaM C-lobe. Panels built in ChimeraX. (C) Ribbon diagram of the hCaM N-lobe atomic model (dark green, residues 1-78) in complex with the hTRPA1<sup>1089-1119</sup> peptide (orange) as predicted by AlphaFold2. The region proposed to be the CaMBS (hTRPA1 residues 1102-1111) is indicated in deep orange. CaMBS K1111,

CaM E11, and CaM K75 residues are shown as balls and sticks. **(D)** Ribbon diagram of the hCaM C-lobe atomic model (light green, residues 79-148) in complex with the hTRPA1<sup>1089-1119</sup> peptide (yellow) as predicted by AlphaFold2. The region proposed to be the CaMBS (hTRPA1 residues R1102-K1111) is indicated in goldenrod. CaMBS K1111 and CaM E84 are shown as balls and sticks. **(E)** Ribbon diagram of the hTRPA1<sup>1089-1119</sup> peptide from panel (D) overlaid with the CaM N-lobe model from panel (C). Steric clash between the CaMBS and CaM K75 side chain is indicated with a red arrow. **(F)** Alignment of mouse, zebrafish TRPA1a isoform, and *C. elegans* TRPA1 with the hTRPA1 protein sequence for the coiled coil and structurally unresolved distal C-terminus. Regions of the coiled coil and the novel CaMBS identified in this study are boxed and indicated above. Residues that contribute to CaM binding are indicated as balls and sticks in yellow. Alignment was built with Clustal Omega. The coiled coil helix was built with the human TRPA1 Cryo-EM structure (PDB: 6V9W) and the CaMBS was built with the human TRPA1 AlphaFold deposited structure in ChimeraX. Scissors denote the hTRPA1<sup>Δ1109-1119</sup> truncation point.

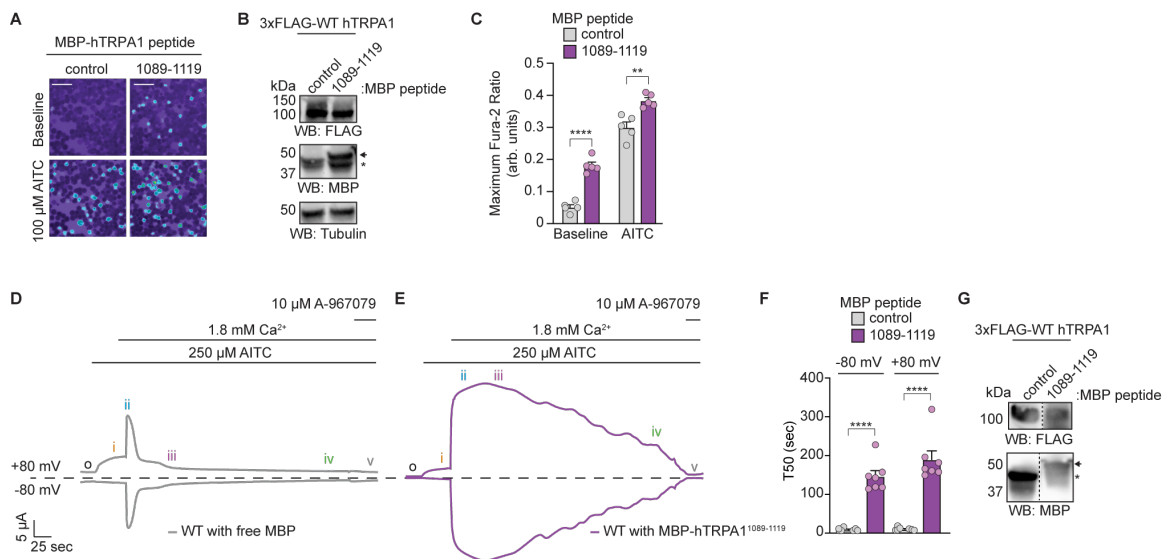


**Figure S5.** CaM sequestration with a TRPA1 C-terminal peptide slows channel

desensitization. **(A)** Ratiometric Ca<sup>2+</sup> imaging of HEK293T cells co-transfected with WT hTRPA1 and free MBP (control) or MBP-hTRPA1<sup>1089-1119</sup>. Cells were stimulated with 100  $\mu$ M AITC. Images are representative of five independent experiments. Scale bars indicate 50  $\mu$ m. **(B)** Representative immunoblotting analysis of the cells used for Ca<sup>2+</sup> imaging in **(A)**. Samples were probed using an HRP-conjugated anti-FLAG antibody or an anti-MBP primary antibody and an HRP-conjugated anti-mouse secondary antibody. Tubulin was the loading control. Asterisk (\*) denotes free MBP. Arrow denotes MBP-tagged peptide. **(C)** Quantification of 100  $\mu$ M AITC-evoked change in Fura-2 ratio of data from panel **(A)**. WT hTRPA1 co-expressed with free MBP indicated in grey, WT hTRPA1 co-expressed with MBP-hTRPA1<sup>1089-1119</sup> peptide indicated in purple. Data represent mean  $\pm$  SEM. \*\*\*\*p<0.0001, \*\*p=0.0018. n = 5 independent experiments, n  $\geq$  90 cells per transfection condition per experiment, two-tailed Student's t-test. **(D-E)** Representative time-traces at -80 and +80 mV holding potentials from oocytes expressing WT hTRPA1 and injected with 100  $\mu$ M free MBP **(D)**, grey) or MBP-hTRPA1<sup>1089-1119</sup> peptide **(E)**, purple) one hour prior to recordings. Current evoked with 250  $\mu$ M AITC in

the absence (orange i) and presence (blue ii) of 1.8 mM extracellular  $\text{Ca}^{2+}$ . Channels were blocked with 10  $\mu\text{M}$  A-967079 (grey v). Dashed line denotes 0  $\mu\text{A}$  current. Protocol of condition application indicated above. (F) Calculated time constants of desensitization (T50) at -80 mV (left) and +80 mV (right) from fitting data as in D-E to a linear regression function. Data represent mean  $\pm$  SEM. \*\*\*\* $p < 0.0001$ , twotailed Student's t-test.  $n = 7$  oocytes per injection type. Colors as in (C). (G) Western blot of lysates from oocytes used for recordings in D-E probed as in (B).

### **Chapter 3: Contribution of S2-S3 CBS and CaMBD to TRPA1 Ca<sup>2+</sup> Regulation**

#### **Introduction**

We have shown that the CaMBS within the distal, disordered C-terminus is a high affinity CaM binding site which recruits CaM to act as an auxiliary subunit. The CaMBS binds CaM through its C-lobe, and the C-lobe alone is able to initiate Ca<sup>2+</sup>-dependent desensitization. Without an intact CaMBS CaM no longer acts as an auxiliary subunit, and TRPA1 loses the ability to rapidly desensitize upon influx of extracellular Ca<sup>2+</sup>. Even without CaM acting as an auxiliary subunit, desensitization can be sped up by introducing higher concentrations of extracellular Ca<sup>2+</sup> demonstrating that an unknown Ca<sup>2+</sup> coordination site within TRPA1 is the likely desensitization gate with enhanced affinity for Ca<sup>2+</sup> upon CaM binding. While this is a major advancement in our understanding of TRPA1 Ca<sup>2+</sup> regulation, there are still several questions left unanswered. The most obvious question is what mediates Ca<sup>2+</sup>-dependent potentiation? Loss of CaM as an auxiliary subunit showed no discernible effect on potentiation suggesting that direct coordination of Ca<sup>2+</sup> by TRPA1 must be responsible for initiating potentiation. Given how rapid both potentiation and desensitization occur in wild-type TRPA1, this Ca<sup>2+</sup> coordination site would need to have a high affinity for Ca<sup>2+</sup> to ensure a potentiated state can be reached before desensitization begins. Of the three proposed Ca<sup>2+</sup> binding sites the S2-S3 CBS is most likely to contribute to potentiation<sup>1-4</sup> (**Fig. 1**). The effects of the putative EF-hand domain within ankyrin repeat 12 has not been replicated by other labs and the acidic cluster is located within the distal C-terminus making it the mostly likely candidate to work in concert with CaM and the CaMBS to initiate desensitization (**Fig. 1B**). However, the S2-S3 CBS is located next to the exit of the ion conduction pathway in prime position to

respond to permeating  $\text{Ca}^{2+}$  ions (**Fig. 1C**). The purification method for the solved structures containing  $\text{Ca}^{2+}$  bound within the S2-S3 loop suggest this site is indeed a high affinity  $\text{Ca}^{2+}$  binding site, but the affinity for  $\text{Ca}^{2+}$  in the S2-S3 loop may be so high that it is always occupied and simply stabilizes the structure of TRPA1 rather than acting as a  $\text{Ca}^{2+}$  sensor. Even if the S2-S3 CBS coordinates  $\text{Ca}^{2+}$  to stabilize TRPA1, it could still affect  $\text{Ca}^{2+}$  regulation through the CaMBD given their close proximity within the structure.

The next question that comes from our work on the CaMBS is how the CaMBD fits into regulation of TRPA1 channel activity. It was previously reported that CaM binding through the CaMBD influenced both potentiation and desensitization of TRPA1 which is difficult to reconcile with the data we have collected<sup>5</sup>. We show that loss of CaM binding under basal cellular conditions has no effect on potentiation while dramatically slowing desensitization. It is possible the CaMBD acts independently of the CaMBS and binds CaM after  $\text{Ca}^{2+}$  begins to permeate through the TRPA1 pore to initiate potentiation. However, for similar reasons outlined above potentiation occurs on such a rapid timescale making it unlikely that dynamic recruitment of CaM to the CaMBD could be responsible for controlling potentiation.

CaM and the CaMBD do not appear to play a role in potentiation, but it is possible the CaMBS and CaMBD work together to control desensitization. CaM bridging the distal CaMBS and the CaMBD located within the allosteric nexus provides an appealing model to explain the role of the CaM N-lobe in  $\text{Ca}^{2+}$ -mediated desensitization<sup>6-12</sup>. While we were able to demonstrate that CaM C-lobe binding to the CaMBS is able to initiate desensitization in HEK293T cells using  $\text{Ca}^{2+}$  imaging, we were unable to perform CaM mutant experiments in oocytes using TEVC. Total CaM concentrations in *Xenopus laevis*

oocytes are 2 to 3-fold higher compared to HEK293 cells which is high enough to saturate or nearly saturate TRPA1 while transient transfection of exogenous CaM is required to saturate TRPA1 expressed in HEK293 cells<sup>13-16</sup>. Since we had to rely on crude Ca<sup>2+</sup> imaging experiments, it was not possible to determine if the C-lobe of CaM could desensitize TRPA1 at the same rate as full-length CaM.

We demonstrate that the S2-S3 CBS is most likely binding Ca<sup>2+</sup> under basal cellular conditions to structurally stabilize the transmembrane region and allosteric nexus of TRPA1 including the CaMBD. Using AlphaFold and CaM binding experiments we find that residues from the C-terminal end of the TRP-like helix enhance the CaM binding capability of the CaMBD while residues within the  $\beta$ -strand likely do not directly interact with CaM and instead stabilize the S1-S4 helical bundle. TEVC studies of TRP-CaMBD mutants show that desensitization is slightly slowed by perturbing the CaMBD but is much less drastic compared to CaMBS mutants. We propose the CaMBD is functioning in an ancillary role that augments TRPA1 CaM binding, but the CaMBS serves as both the primary recruiter of CaM and primes the channel for desensitization.

## **Results**

### **Ablating the S2-S3 CBS destabilizes TRPA1**

It was reported that the S2-S3 triple mutant did not possess Ca<sup>2+</sup>-mediated potentiation or desensitization, but the magnitude of the currents it produced was not compared to wild type TRPA1 channels<sup>1</sup>. To assess the effects of the S2-S3 CBS on overall TRPA1 channel activity, we performed fura-2 Ca<sup>2+</sup> imaging experiments on the S2-S3 triple mutant (E788S, Q791S, and N805S) which completely ablates Ca<sup>2+</sup> binding. If the S2-S3 CBS acts as a

Ca<sup>2+</sup> sensor controlling potentiation and desensitization, ablation of Ca<sup>2+</sup> binding should lead to an increase in overall channel activity as loss of the potentiated state is more than compensated for by impaired desensitization<sup>17,18</sup>. However, the loss of a structurally important site would destabilize the channel and lead to a decrease in overall channel activity. In HEK293T cells expressing the S2-S3 triple mutant we observed a significant decrease in AITC-evoked TRPA1 activity compared to cells expressing wild type TRPA1 suggesting the S2-S3 CBS is not involved in desensitization and is likely a structural site (**Fig. 2A-C**). However, we cannot rule out the possibility this reduction in activity is due to the loss of Ca<sup>2+</sup>-mediated potentiation while retaining desensitization.

Given its proximity to both the allosteric nexus and the CaMBD, we hypothesized the S2-S3 CBS might influence CaM binding. To test the effect of the S2-S3 CBS on CaM binding, we performed CaM-agarose binding assays to compare wild type TRPA1 and the S2-S3 triple mutant at Ca<sup>2+</sup> concentrations of 0  $\mu$ M Ca<sup>2+</sup> (negative control), 0.1  $\mu$ M Ca<sup>2+</sup> (basal concentration), 500  $\mu$ M Ca<sup>2+</sup> (nanodomain concentration), and 2000  $\mu$ M Ca<sup>2+</sup> (saturating concentration)<sup>19,20</sup>. Consistent with our work shown in Chapter 2, wild type TRPA1 and the S2-S3 triple mutant have negligible binding to CaM-agarose resin in the absence of Ca<sup>2+</sup>. At 0.1  $\mu$ M Ca<sup>2+</sup> the S2-S3 triple mutant demonstrated significant reduction in the ability to bind CaM (~30% lower) compared to wild type TRPA1 (**Fig. 2D-E**). However, at Ca<sup>2+</sup> concentrations of 500  $\mu$ M and 2000  $\mu$ M, the S2-S3 triple mutant showed only a slight reduction in CaM binding which were statistically non-significant compared to wild type TRPA1. This suggests the S2-S3 CBS influences CaM binding at basal Ca<sup>2+</sup> concentrations with little effect under conditions of Ca<sup>2+</sup> influx which is consistent with our hypothesis that the S2-S3 CBS imparts structural stability rather than acting as a Ca<sup>2+</sup>

sensor. The change in CaM binding is presumably due to structural destabilization affecting the CaMBD.

### **The TRP-like helix enhances Calmodulin binding of the CaMBD**

Several elements of the putative CaMBD are unusual for a CaM binding region. Typically, CaM binds to one or two  $\alpha$ -helices using exposed hydrophobic grooves within their N and C-lobes, but the proposed CaMBD includes a  $\beta$ -strand<sup>5,7,9,21-25</sup>. Moreover, V1005 and P1007 within this  $\beta$ -strand were identified as being critical to CaM binding but are facing away from the cytosol on the opposite face of W993 which was also predicted to be involved in CaM binding. Both V1005 and P1007 are packed against E705 of the pre-S1 helix suggesting they help stabilize the transmembrane domain (**Fig. 3A**). Without a significant rearrangement these sidechains would not be available to participate in CaM binding interactions. We hypothesized the nearby TRP-like helix may be interacting with the CaMBD instead of the  $\beta$ -strand. To initially gauge this possibility, we used AlphaFold2 multimer to generate models of CaM interacting with the TRP-CaMBD (AA 976-1008)<sup>26,27</sup>. The model with the highest confidence score showed the TRP-CaMBD bound within the hydrophobic groove of the CaM N-lobe while maintaining the same helix-loop-helix structure observed in the cryo-EM structures as opposed to the CaMBS which binds as a single  $\alpha$ -helix in the C-lobe (**Fig. 3 B-C**). This is an atypical calmodulin interaction, but a similar helix-loop-helix interaction with CaM has been observed in structures of SK2/SK4 channels<sup>7,23</sup>. The most significant interactions between the TRP-CaMBD and CaM were localized to the C-terminal end of the TRP-like domain and the N-terminal end of the CaMBD  $\alpha$ -helix (**Fig. 3C**). There is no contribution from residues that form the  $\beta$ -

strand within the full-length TRPA1 structure supporting our hypothesis that V1005 and P1007 mutants affect CaM binding through local structural rearrangements.

To assess the effects of the TRP-like helix on CaM binding, we expressed MBP-tagged constructs of hTRPA1<sup>1089-1119</sup>, the originally proposed CaMBD, and the TRP-CaMBD in HEK293T cells and performed CaM-agarose binding assays using 0  $\mu\text{M}$   $\text{Ca}^{2+}$ , 0.1  $\mu\text{M}$   $\text{Ca}^{2+}$ , and 2000  $\mu\text{M}$   $\text{Ca}^{2+}$  concentrations. For both the CaMBD and TRP-CaMBD there was low binding at 0.1  $\mu\text{M}$   $\text{Ca}^{2+}$ , but at 2000  $\mu\text{M}$   $\text{Ca}^{2+}$  there was a marked increase in TRP-CaMBD binding to CaM-agarose relative to the CaMBD suggesting the TRP-like helix interacts with CaM and enhances the binding potential of the CaMBD (**Fig. 3D-E**). To ensure this interaction occurs in cells, we performed Fura-2  $\text{Ca}^{2+}$  imaging on HEK293T cells co-expressing TRPA1 and either MBP-tagged hTRPA1<sup>1089-1119</sup> or MBP-tagged TRP-CaMBD (**Fig. 3F-H**). We observed an increase in both baseline and AITC-evoked TRPA1 activity in TRP-CaMBD expressing cells relative to MBP controls although this was only statistically significant for baseline measurements. However, MBP-tagged hTRPA1<sup>1089-1119</sup> expressing cells had a greater increase in both baseline and AITC-evoked TRPA1 activity relative to MBP controls suggesting it has a greater ability to sequester CaM compared to the TRP-CaMBD consistent with our model that the CaMBS is the primary site of CaM binding.

### **The TRP-CaMBD influences Calmodulin binding of full-length hTRPA1**

To assess the effect of the TRP-CaMBD on CaM binding within full-length hTRPA1, we designed two mutants using our AlphaFold2 multimer model as a guide. Since the TRP-CaMBD lies within a structurally important region near the allosteric nexus, we avoided mutating hydrophobic sidechains that are more likely to be involved in stabilizing potential structural rearrangements and focused on positively charged sidechains that are often required for CaM binding<sup>8-10,21,22,24,25,28</sup>. We identified three lysine sidechains (K989, K997, K1001) predicted to form salt bridges with glutamate sidechains from the N-lobe of CaM, and an arginine residue (R996) hydrogen bond with a threonine residue from CaM (**Fig. 3C**). We mutated each of these residues to serine (herein referred to as the 4S mutant) and performed CaM-agarose pulldowns at 0  $\mu\text{M}$   $\text{Ca}^{2+}$ , 0.1  $\mu\text{M}$   $\text{Ca}^{2+}$ , and 2000  $\mu\text{M}$   $\text{Ca}^{2+}$  concentrations with wild type hTRPA1, W1103A, 4S, and 4S + W1103A (**Fig. 4A-B**). The 4S mutant had an approximately 40% reduction in CaM binding capability at basal and saturating  $\text{Ca}^{2+}$  concentrations relative to wild-type TRPA1. This is similar to results obtained with the S2-S3 triple mutant suggesting the CBS does influence the CaMBD (**Fig. 2D-E**). The W1103A mutant has no binding at basal  $\text{Ca}^{2+}$  concentrations as shown in Chapter 2 but regains approximately 30% of CaM binding capability relative to wild-type TRPA1 at saturating  $\text{Ca}^{2+}$  concentrations. However, the combination of the 4S and W1103A mutation resulted in a near total loss of CaM binding regardless of  $\text{Ca}^{2+}$  concentration indicating that both the CaMBS and the CaMBD contribute to CaM binding within hTRPA1.

**Calmodulin binding at the CaMBD slightly enhances  $\text{Ca}^{2+}$ -mediated desensitization**

To assess the role of the CaMBD on hTRPA1 activity, we performed TEVC experiments on oocytes expressing the 4S mutant (**Fig. 4C-F**). AITC-evoked peak currents remained largely similar between wild type hTRPA1 and the 4S mutant, but Ca<sup>2+</sup>-mediated desensitization of the 4S mutant was slightly slower compared to hTRPA1. Consistent with our prior work, the CaMBD does not appear to be necessary for rapid Ca<sup>2+</sup>-mediated desensitization but mutagenesis of the CaMBD slightly delays desensitization (**Fig. 4D&F**). This likely occurs by stabilizing the preceding CaM binding event at the CaMBS through interactions with the available CaM N-lobe.

TRPA1 possesses remarkably complex Ca<sup>2+</sup> regulation mechanisms that allow for precise control of channel activity by potentiating currents at low concentrations of intracellular Ca<sup>2+</sup> and rapidly desensitizing as Ca<sup>2+</sup> concentrations increase. While we showed that CaM binding at the CaMBS is required for rapid desensitization in Chapter 2, it was difficult to create a model that incorporated the CaMBS, the S2-S3 CBS, and the CaMBD based on previously published data. To better understand how each individual component works together we performed our own CaM binding and activity assays on S2-S3 CBS and CaMBD mutants. In our new model we propose the S2-S3 CBS is not a Ca<sup>2+</sup> sensor but binds Ca<sup>2+</sup> under basal cellular conditions to stabilize the S1-S4 helix and allosteric nexus including the CaMBD. The CaMBS acts as the high affinity recruiting site for the CaM C-lobe which is sufficient to induce rapid Ca<sup>2+</sup>-mediated desensitization. However, the CaMBD is able to increase the overall affinity of TRPA1 for CaM by binding the unoccupied N-lobe resulting in a faster desensitization on a population level. It is also possible this interaction initiates a 2<sup>nd</sup> stage of the desensitization process.

The S2-S3 CBS was the first  $\text{Ca}^{2+}$  binding site in TRPA1 to be identified using biophysical and structural techniques, and its location near the transmembrane domain and allosteric nexus suggested it may play a role in regulating channel activity. While prior literature on the S2-S3 CBS claimed it was a  $\text{Ca}^{2+}$  sensor to initiate  $\text{Ca}^{2+}$ -mediated potentiation and desensitization, our research suggests the S2-S3 CBS plays a structural role consistent with its apparent high affinity for  $\text{Ca}^{2+}$ . However, this does not preclude a potential role in regulating TRPA1 activity. It is possible that channel activity can be negatively regulated by stripping the  $\text{Ca}^{2+}$  from S2-S3 CBS and destabilizing the channel. Inositol hexaphosphate (IP6) is a polyanion cofactor that was found to bind TRPA1 between the coiled-coil and the ARD stabilizing the channel<sup>29,30</sup>. Polyanions like IP6 have a high affinity for  $\text{Ca}^{2+}$  ions and form insoluble aggregates with  $\text{Ca}^{2+}$  at biologically relevant pH<sup>31-33</sup>. It is possible that TRPA1 may undergo conformational changes that can release IP6 or another bound polyanion cofactor which could go on to strip the  $\text{Ca}^{2+}$  from S2-S3 CBS ultimately destabilizing the channel.

CaM binding through the CaMBD was proposed to regulate both  $\text{Ca}^{2+}$ -mediated potentiation and desensitization. However, our work on the CaMBS suggests it is highly unlikely that CaM is involved in mediating potentiation, and the CaMBS is able to induce robust desensitization without the need for a bridging interaction with the CaMBD. The proposed CaMBD was also extremely unusual compared to other CaM binding regions in that it included a  $\beta$ -strand with proposed interacting residues packed against structurally important sites of the transmembrane domain. To resolve these questions, we used AlphaFold to generate models of CaM interacting with the CaMBD and found the TRP-like helix and the helical section of the CaMBD have a helix-loop-helix interaction with

the N-lobe of CaM. The  $\beta$ -strand residues did not interact with the N-lobe in our model, and CaM-agarose pulldowns indicate the TRP-CaMBD has higher CaM binding ability than the CaMBD alone. It is likely the previously reported effects on CaM binding from mutagenesis in this region was due to local structural changes rather than a loss of a true CaM interacting residue. Within the context of full-length TRPA1 the CaMBD appears to have a relatively minor contribution to CaM binding and desensitization compared to the CaMBS. However, acting as an ancillary binding site for CaM might be important *in vivo* as it provides an overall increase in binding affinity for CaM in an environment where competition for CaM binding is much greater. Additionally, full desensitization may require interaction with the CaMBD.

## **METHODS**

### **Plasmid Construction**

DNA sequences for human TRPA1 were PCR amplified and subcloned into a p3xFLAG-eYFP-CMV-7.1 vector (Addgene) at the NotI/BamHI sites using In-Fusion EcoDry cloning (Takara) according to manufacturer protocols. 8xHis-MBP pFastBac1 modified with a CMV promoter human TRPA1<sup>1089-1119</sup> was created by introducing a BamHI site at the -1 position of the codon encoding TRPA1<sup>1089</sup> and digesting the plasmid with BamHI restriction enzyme followed by gel purification. The linearized vector segment was then transformed into XL-10 Gold cells resulting in a repaired vector. A modified strategy was followed for the creation of 8xHis-MBP pFastBac1 with a CMV promoter CaMBD, and TRP-CaMBD. A BamHI site was placed at the -1 position of the codon encoding for TRPA1<sup>976</sup> for the TRP-CaMBD and TRPA1<sup>992</sup> for the CaMBD. Each of these plasmids

were digested with BamHI restriction enzymes followed by gel purifications. The linearized vector segments were then transformed into XL-10 Gold cells resulting in a repaired vector. In each of the repaired vectors a NotI site was introduced at the +1 position of the codon encoding for TRPA1<sup>1008</sup>. Each of these plasmids were digested with NotI restriction enzymes followed by gel purifications. The linearized vector segments were then transformed into XL-10 Gold cells resulting in the final repaired vector. For expression in *Xenopus laevis* oocytes, 3xFLAG-hTRPA1 variant genes were subcloned into the combined mammalian/oocyte expression vector pMO (obtained from David Julius' lab) prior to generating cRNAs.

All DNA primers were ordered from ThermoFisher and all constructs were sequence-verified using the Yale School of Medicine Keck DNA Sequencing Facility.

### **Mammalian Cell Culture and Protein Expression**

Human embryonic kidney cells (HEK293T, ATCC CRL-3216) were cultured in Dulbecco's modified Eagle's medium (DMEM; Invitrogen) supplemented with 10% calf serum and 1x Penicillin-Streptomycin (Invitrogen) at 37°C and 5% CO<sub>2</sub>. Cells were grown to ~85-95% confluence before splitting for experiments or propagation. HEK293T cells cultured to ~95% confluence were seeded at 1:10 or 1:20 dilutions into 6- or 12-well plates (Corning), respectively. After 1-5 hours recovery, cells were transiently transfected with 1 µg plasmid using jetPRIME (Polyplus) according to manufacturer protocols.

### **Cell Lysis and Pulldown Experiments**

16-24 hours post-transfection, HEK293T cells were washed with PBS ( $\text{Ca}^{2+}$  and magnesium free) and lysed in 75-150  $\mu\text{L}$  of TRPA1 lysis buffer (40 mM Tris pH 8.0, 150 mM NaCl, 5 mM DDM, 500  $\mu\text{M}$  EGTA, EDTA-free cOmplete protease cocktail inhibitor tablet) at  $4^\circ\text{C}$  while gently nutating. Cell debris were pelleted from the resulting lysates by centrifugation at 15,000 RPM for 10 minutes at  $4^\circ\text{C}$ . Total protein concentration in lysates were quantified using a BCA assay (Pierce). Equal concentrations of protein lysate (100  $\mu\text{g}$ ) from each experimental condition were added to resins as specified below. 10% of loaded protein amount was reserved as a whole-cell lysate loading control. Buffers were supplemented with free  $\text{Ca}^{2+}$  as indicated in each figure. Concentrations of  $\text{CaCl}_2$  required for each free  $\text{Ca}^{2+}$  concentration were calculated using Ca-EGTA calculator v1.3 using constants from Theo Schoenmakers' Chelator on the MaxChelator website.

### **CaM-agarose Pulldown**

100  $\mu\text{g}$  lysates were incubated with 10  $\mu\text{L}$  of lysis buffer-equilibrated Calmodulin-agarose (Sigma-Aldrich) for 1 hour at  $4^\circ\text{C}$  with gentle nutation. Resin beads were washed 3-5 times with lysis buffer prior to elution; resin was pelleted, and bound proteins were eluted in TRPA1 lysis buffer supplemented with 5 mM EGTA for 30 minutes at  $4^\circ\text{C}$  with gentle nutation.

### **SDS-PAGE and Immunoblot**

Samples were combined with Laemmli Sample buffer + 10% BME and separated on pre-cast 4-20% SDS-PAGE gels (Bio-Rad). Gels were transferred onto PVDF membranes (Bio-Rad) by semi-dry transfer at 15V for 40 minutes. Blots were blocked in 3% BSA prior

to antibody probing. The following primary antibodies were used in PBST buffer (Boston Bioproducts): anti-MBP (mouse, 1:30,000, New England Biolabs), anti-FLAG (mouse, 1:30,000, Sigma), anti-tubulin (mouse, 1:5,000 in 3% BSA, Sigma). HRP-conjugated IgG secondary anti-mouse antibody was used as needed (rabbit, 1:25,000, Invitrogen). Membranes were developed using Clarity Western ECL substrate (Bio-Rad) and imaged using a Chemidoc Imaging System (Bio-Rad). Densitometric quantifications were performed with ImageJ software. All quantified band intensities for eluted samples were divided by their tubulin-normalized input band intensities.

### **Ratiometric Ca<sup>2+</sup> Imaging**

16-24 hours post-transfection, HEK293T cells were plated into isolated silicone wells (Sigma) on poly-L-lysine (Sigma)-coated cover glass (ThermoFisher). Remaining cells were lysed for anti-FLAG immunoblotting to ensure equivalent expression. 1 hour later, cells were loaded with 10 µg/mL Fura 2-AM (ION Biosciences) in Ringer's solution (Boston Bioproducts) with 0.025% Pluronic F-127 (Sigma) and incubated for 1 hour at room temperature, then rinsed twice with Ringer's solution. Ratiometric Ca<sup>2+</sup> imaging was performed using a Zeiss Axio Observer 7 inverted microscope with a Hamamatsu Flash sCMOS camera at 20x objective. Dual images (340 and 380 nm excitation, 510 nm emission) were collected and pseudocolour ratiometric images were monitored during the experiment (MetaFluor software). After stimulation with agonist, cells were observed for 45-100 s. AITC was purchased from Sigma and was freshly prepared as a stock at 4x the desired concentration in 1% DMSO and Ringer's solution. 5 µL of 4x agonist was added to wells containing 15 µL Ringer's solution to give the final 1x desired concentration. For

all experiments, a minimum of 60-90 cells were selected per condition per replicate for ratiometric fluorescence quantification in MetaFluor with 3-5 replicates per experiment. Background signal was quantified from un-transfected cells and subtracted from quantified cells for normalization.

### **Structure Prediction**

We used AlphaFold2-multimer with default parameters and Amber relaxation to generate all models. Computation was performed on the Farnam cluster at Yale Center for Research Computing. hCaM amino acids 1 – 149 were used as the sequences for Calmodulin. For human TRPA1, aa. 993 – 1010, aa. 977 – 1010, and aa. 1092 – 1119 were used as the sequences for the CaMBD, TRP-CaMBD, and CaMBS respectively. Sequences for Human CaM and TRPA1 were retrieved from Uniprot with accession code P0DP23 and O75762. After obtaining predictions from AlphaFold, we used the model with the highest confidence, as judged by average pLDDT, for all further analysis.

### **Oocyte electrophysiology**

Experiments were conducted as previously reported. pMO vectors carrying 3×FLAG-tagged hTRPA1 constructs were linearized with PmeI, cRNAs were generated by *in vitro* transcription with the mMessage mMachine T7 transcription kit (Thermo) according to the manufacturer's protocol and were purified with a RNeasy kit (Qiagen). cRNA transcripts were microinjected into surgically extracted *Xenopus laevis* oocytes (Ecocyte) with a Nanoject III (Harvard Apparatus). Oocytes were injected with 0.25 ng (WT hTRPA1) or 0.1 ng (CaMBD variant) of cRNA per cell, and whole-cell currents were measured 24h

post-injection using two-electrode voltage clamp (TEVC). Currents were measured using an OC-725D amplifier (Warner Instruments) delivering a ramp protocol from  $-100$  mV to  $+100$  mV applied every second. Microelectrodes were pulled from borosilicate glass capillary tubes and filled with 3 M KCl. Microelectrode resistances of  $0.7$ – $1.2$  M $\Omega$  were used for all experiments. Bath solution contained (in mM) 93.5 NaCl, 2 KCl, 2 MgCl<sub>2</sub>, 0.1 BaCl<sub>2</sub>, and 5 HEPES (pH 7.5). For experiments in the presence of Ca<sup>2+</sup>, BaCl<sub>2</sub> was replaced with 1.8 mM CaCl<sub>2</sub>. Data were subsequently analyzed using pClamp11 software (Molecular Devices). Oocytes were individually collected after recordings, lysed in 20  $\mu$ L TRPA1 lysis buffer, and subjected to anti-FLAG immunoblot analysis to confirm construct expression.

### Statistical Analysis

All data quantification was performed in Microsoft Excel. Quantified data presentation and statistical analyses were performed in GraphPad Prism. Criterion for statistical significance for all tests was  $p < 0.05$ .

### References

1. Zhao, J., Lin King, J.V., Paulsen, C.E., Cheng, Y. & Julius, D. Irritant-evoked activation and calcium modulation of the TRPA1 receptor. *Nature* **585**, 141-145 (2020).
2. Zurborg, S., Yurgionas, B., Jira, J.A., Caspani, O. & Heppenstall, P.A. Direct activation of the ion channel TRPA1 by Ca. *Nature Neuroscience* **10**, 277-279 (2007).

3. Doerner, J.F., Gisselmann, G., Hatt, H. & Wetzel, C.H. Transient receptor potential channel  $\alpha 1$  is directly gated by calcium ions. *Journal of Biological Chemistry* **282**, 13180-13189 (2007).
4. Sura, L. et al. C-terminal Acidic Cluster Is Involved in Calcium-induced Regulation of Human Transient Receptor Potential Ankyrin 1 Channel. *Journal of Biological Chemistry* **287**, 18067-18077 (2012).
5. Hasan, R., Leeson-Payne, A.T.S., Jaggar, J.H. & Zhang, X.M. Calmodulin is responsible for  $\text{Ca}^{2+}$ -dependent regulation of TRPA1 Channels. *Scientific Reports* **7**(2017).
6. Mandala, V.S. & MacKinnon, R. Voltage-sensor movements in the Eag Kv channel under an applied electric field. *Proceedings of the National Academy of Sciences of the United States of America* **119**(2022).
7. Lee, C.H. & MacKinnon, R. Activation mechanism of a human SK-calmodulin channel complex elucidated by cryo-EM structures. *Science* **360**, 508-+ (2018).
8. Hughes, T.E.T. et al. Structural insights on TRPV5 gating by endogenous modulators. *Nature Communications* **9**(2018).
9. Singh, A.K., McGoldrick, L.L., Twomey, E.C. & Sobolevsky, A.I. Mechanism of calmodulin inactivation of the calcium-selective TRP channel TRPV6. *Science Advances* **4**(2018).
10. Dang, S.Y. et al. Structural insight into TRPV5 channel function and modulation. *Proceedings of the National Academy of Sciences of the United States of America* **116**, 8869-8878 (2019).
11. Melville, Z. et al. A drug and ATP binding site in type 1 ryanodine receptor. *Structure* **30**, 1025-+ (2022).
12. Haji-Ghassemi, O. et al. Cryo-EM analysis of scorpion toxin binding to Ryanodine Receptors reveals subconductance that is abolished by PKA phosphorylation. *Science Advances* **9**(2023).
13. Cartaud, A., Ozon, R., Walsh, M.P., Haiech, J. & Demaille, J.G. *Xenopus laevis* oocyte calmodulin in the process of meiotic maturation. *J Biol Chem* **255**, 9404-8 (1980).
14. Cicirelli, M.F. & Smith, L.D. Calmodulin synthesis and accumulation during oogenesis and maturation of *Xenopus laevis* oocytes. *Dev Biol* **113**, 174-81 (1986).
15. Black, D.J., Tran, Q.K. & Persechini, A. Monitoring the total available calmodulin concentration in intact cells over the physiological range in free  $\text{Ca}^{2+}$ . *Cell Calcium* **35**, 415-425 (2004).
16. Wu, X. & Bers, D.M. Free and bound intracellular calmodulin measurements in cardiac myocytes. *Cell Calcium* **41**, 353-364 (2007).
17. Wang, Y.Y., Chang, R.B., Waters, H.N., Mckemy, D.D. & Liman, E.R. The Nociceptor Ion Channel TRPA1 Is Potentiated and Inactivated by Permeating Calcium Ions. *Journal of Biological Chemistry* **283**, 32691-32703 (2008).
18. Nagata, K., Duggan, A., Kumar, G. & García-Añoveros, J. Nociceptor and hair cell transducer properties of TRPA1, a channel for pain and hearing. *Journal of Neuroscience* **25**, 4052-4061 (2005).
19. Naraghi, M. & Neher, E. Linearized buffered  $\text{Ca}^{2+}$  diffusion in microdomains and its implications for calculation of  $[\text{Ca}^{2+}]$  at the mouth of a calcium channel. *J Neurosci* **17**, 6961-73 (1997).
20. Tadross, M.R., Tsien, R.W. & Yue, D.T.  $\text{Ca}^{2+}$  channel nanodomains boost local  $\text{Ca}^{2+}$  amplitude. *Proc Natl Acad Sci U S A* **110**, 15794-9 (2013).
21. Rhoads, A.R. & Friedberg, F. Sequence motifs for calmodulin recognition. *Faseb Journal* **11**, 331-340 (1997).
22. Yap, K.L. et al. Calmodulin target database. *J Struct Funct Genomics* **1**, 8-14 (2000).

23. Schumacher, M.A., Rivard, A.F., Bächinger, H.P. & Adelman, J.P. Structure of the gating domain of a Calcium-activated K-channel complexed with Calcium/calmodulin. *Nature* **410**, 1120-1124 (2001).
24. Saimi, Y. & Kung, C. Calmodulin as an ion channel subunit. *Annual Review of Physiology* **64**, 289-311 (2002).
25. Tidow, H. & Nissen, P. Structural diversity of calmodulin binding to its target sites. *Febs Journal* **280**, 5551-5565 (2013).
26. Jumper, J. et al. Highly accurate protein structure prediction with AlphaFold. *Nature* **596**, 583-589 (2021).
27. Liu, J. et al. Enhancing alphafold-multimer-based protein complex structure prediction with MULTICOM in CASP15. *Commun Biol* **6**, 1140 (2023).
28. Zhu, M.X. Multiple roles of calmodulin and other Calcium-binding proteins in the functional regulation of TRP channels. *Pflugers Archiv-European Journal of Physiology* **451**, 105-115 (2005).
29. Paulsen, C.E., Armache, J.P., Gao, Y., Cheng, Y. & Julius, D. Structure of the TRPA1 ion channel suggests regulatory mechanisms. *Nature* **525**, 552 (2015).
30. Kim, D. & Cavanaugh, E.J. Requirement of a soluble intracellular factor for activation of transient receptor potential A1 by pungent chemicals: Role of inorganic polyphosphates. *Journal of Neuroscience* **27**, 6500-6509 (2007).
31. Cheryan, M. Phytic Acid Interactions in Food Systems. *Crc Critical Reviews in Food Science and Nutrition* **13**, 297-335 (1980).
32. Graf, E. Calcium-Binding to Phytic Acid. *Journal of Agricultural and Food Chemistry* **31**, 851-855 (1983).
33. Dendougui, F. & Schwedt, G. In vitro analysis of binding capacities of calcium to phytic acid in different food samples. *European Food Research and Technology* **219**, 409-415 (2004).

## Figures

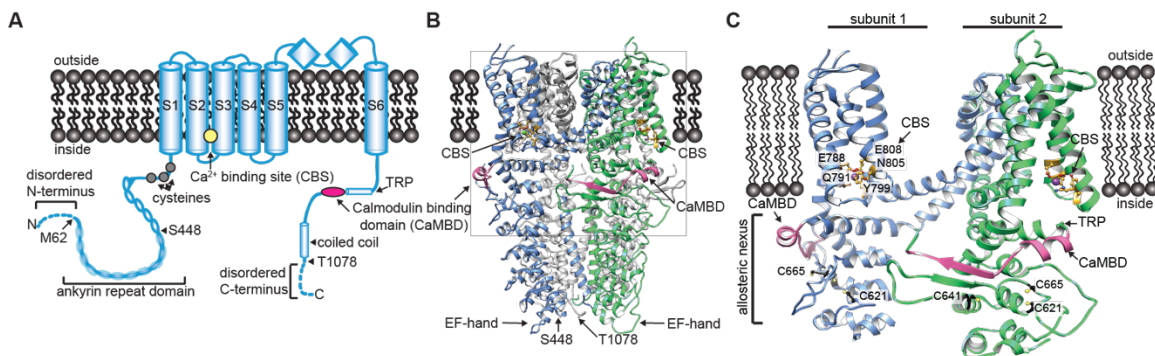


**Figure 1.** Potential crosstalk between the S2-S3 CBS and CaMBD. **(A)** Cartoon schematic of a full-length hTRPA1 monomeric subunit with relevant structural features, a previously identified Calmodulin binding domain (CaMBD, pink) and S2-S3 Ca<sup>2+</sup> binding site (S2-S3 CBS, yellow). Dashes and transparencies denote unresolved regions in Cryo-EM structures. **(B)** Cartoon diagram of WT hTRPA1 atomic model for residues S448-T1078 from the homotetrameric channel (PDB: 6V9W). Each subunit is colored differently for clarity with the CaMBD and S2-S3 CBS colored as in (A). **(C)** Inset of the allosteric nexus from the box denoted in (B). Reactive cysteines and Ca<sup>2+</sup> coordinating residues from each subunit are labeled and shown as sticks.

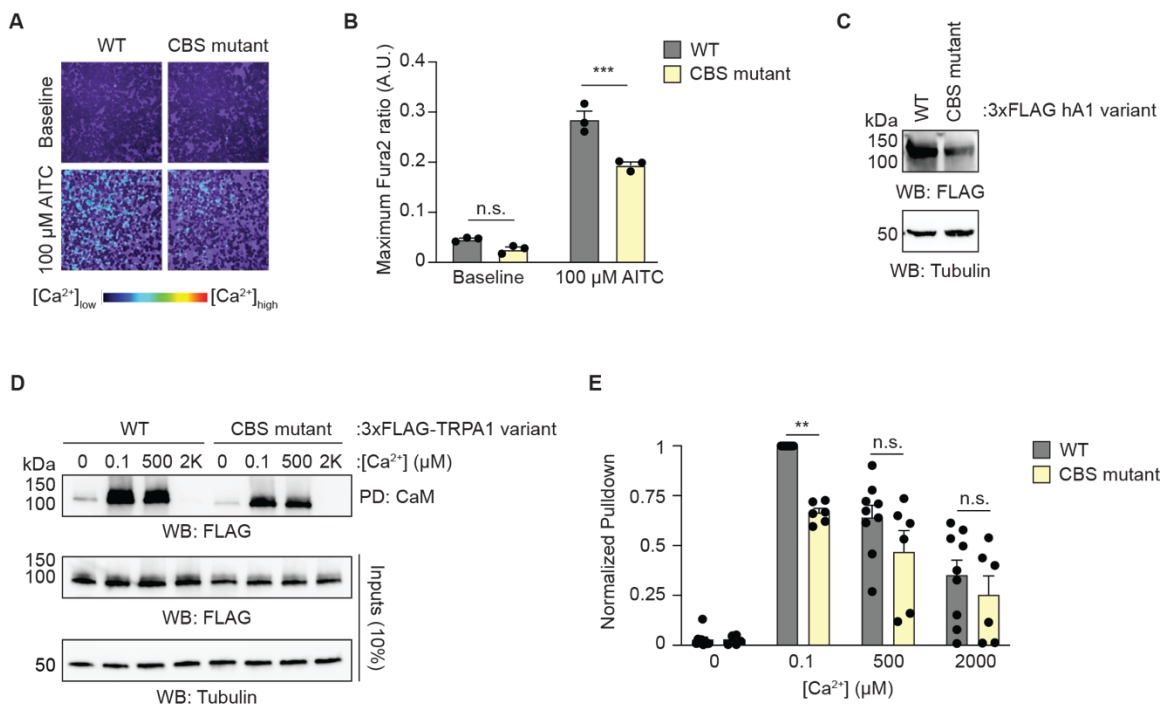


**Figure 2.** The S2-S3 CBS stabilizes TRPA1. **(A)** Ratiometric  $Ca^{2+}$  imaging of HEK293T cells transfected with WT hTRPA1 and the S2-S3 triple mutant. Cells were stimulated with 100  $\mu$ M AITC. Images are representative of three independent experiments. **(B)** Quantification of 100  $\mu$ M AITC-evoked change in Fura-2 ratio of data from panel (A). Data represent mean  $\pm$  SEM. \*\*\*  $p < 0.001$  (WT vs S2-S3 triple mutant, 100  $\mu$ M AITC) or n.s. (not significant)  $p > 0.05$  (WT vs S2-S3 triple mutant, baseline). Two-tailed Student's t-test was used for statistical analysis. **(C)** Representative immunoblotting analysis of the cells used for  $Ca^{2+}$  imaging in (A). **(D)** Immunoblotting analysis of WT hTRPA1 and S2-S3 triple mutant after CaM-agarose pulldown at the indicated  $Ca^{2+}$  concentrations from lysates of transfected HEK293T cells. Samples were probed using an HRP-conjugated anti-FLAG antibody. Tubulin from whole cell lysates (10%, inputs) was the loading control. **(E)** Quantitative analysis of CaM-agarose enrichment from (D) Data represent mean  $\pm$  SEM. \*\* $p < 0.01$ , n.s. (non-significant).  $n = 6$ , two-tailed Student's t-test.

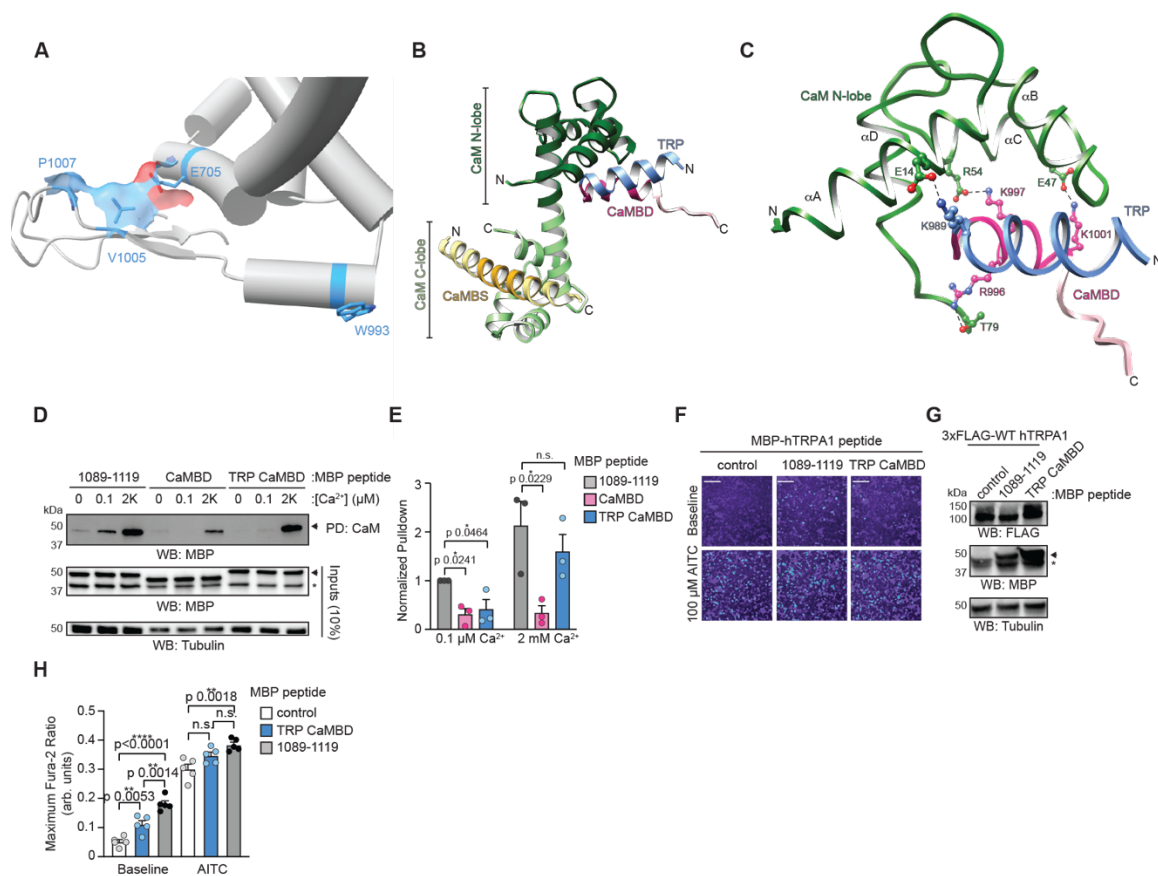


**Figure 3.** The TRP-like helix enhances the CaMBD. **(A)** Cartoon tube representation of TRPA1 with residues important to the CaMBD highlighted in blue. E705, V1005, and P1007 are also given a transparent surface rendering to illustrate van der Waals interactions. **(B)** Cartoon diagram of the hCaM atomic model (dark green, residues 1-78, light green, residues 79-148) in complex with part of the TRPA1 C-terminus including the CaMBS (yellow, residues 1089-1119), TRP-like helix (blue, residues 976-990), and CaMBD (purple, residues 991-1008) as predicted by AlphaFold2 Multimer. **(C)** Ribbon diagram of the CaM N-lobe and TRP-CaMBD from panel (B). Interacting residues are labeled and depicted as balls and sticks. **(D)** Immunoblotting analysis of the indicated MBP-tagged hTRPA1 peptide constructs after CaM-agarose pulldown in the absence of Ca<sup>2+</sup>, 0.1 μM Ca<sup>2+</sup>, or 2000 μM Ca<sup>2+</sup> from lysates of HEK293T cells transfected with hTRPA1<sup>1089-1119</sup>,

the CaMBD, or TRP-CaMBD peptides. Samples were probed using an anti-MBP primary antibody and an HRP-conjugated anti-mouse secondary antibody. Tubulin from whole cell lysates (10%, inputs) was the loading control. (E) Quantitative analysis of CaM-agarose enrichment of MBP-tagged peptides at the indicated  $\text{Ca}^{2+}$  concentrations relative to the enrichment of hTRPA1<sup>1089-1119</sup> at 0.1  $\mu\text{M}$   $\text{Ca}^{2+}$ . hTRPA1<sup>1089-1119</sup> represented by grey bars, CaMBD represented by pink bars, and TRP-CaMBD represented by blue bars. Data represent mean  $\pm$  SEM. \*  $p=0.0241$  (hTRPA1<sup>1089-1119</sup> vs CaMBD 0.1  $\mu\text{M}$   $\text{Ca}^{2+}$ ), \*  $p=0.0464$  (hTRPA1<sup>1089-1119</sup> vs TRP-CaMBD 0.1  $\mu\text{M}$   $\text{Ca}^{2+}$ ), \*  $p=0.0229$  (hTRPA1<sup>1089-1119</sup> vs CaMBD 2000  $\mu\text{M}$   $\text{Ca}^{2+}$ ), n.s (hTRPA1<sup>1089-1119</sup> vs TRP-CaMBD 2000  $\mu\text{M}$   $\text{Ca}^{2+}$ ).  $n=3$ , one-way ANOVA with Tukey's *post hoc* analysis. (F) Ratiometric  $\text{Ca}^{2+}$  imaging of HEK293T cells co-transfected with WT hTRPA1 and free MBP (control), MBP-hTRPA1<sup>1089-1119</sup>, or MBP-TRP-CaMBD. Cells were stimulated with 100  $\mu\text{M}$  AITC. Images are representative of five independent experiments. Scale bars denote 50  $\mu\text{M}$  (G) Representative immunoblotting analysis of the cells used for  $\text{Ca}^{2+}$  imaging in (F). Samples were probed using an HRP-conjugated anti-FLAG antibody or an anti-MBP primary antibody and an HRP-conjugated anti-mouse secondary antibody. Tubulin was the loading control. Asterisk (\*) denotes free MBP. Arrow denotes MBP-tagged peptide. (H) Quantification of 100  $\mu\text{M}$  AITC-evoked change in Fura-2 ratio of data from panel (F). WT hTRPA1 co-expressed with free MBP indicated in white, WT hTRPA1 co-expressed with MBP-hTRPA1<sup>1089-1119</sup> peptide indicated in grey, WT hTRPA1 co-expressed with MBP-TRP-CaMBD indicated in blue. Data represent mean  $\pm$  SEM. \*\*\*\* $p<0.0001$ , \*\* $p<0.01$ , n.s (non-significant)  $n = 5$  independent experiments,  $n \geq 90$  cells per transfection condition per experiment, one-way ANOVA with Tukey's *post hoc* test.

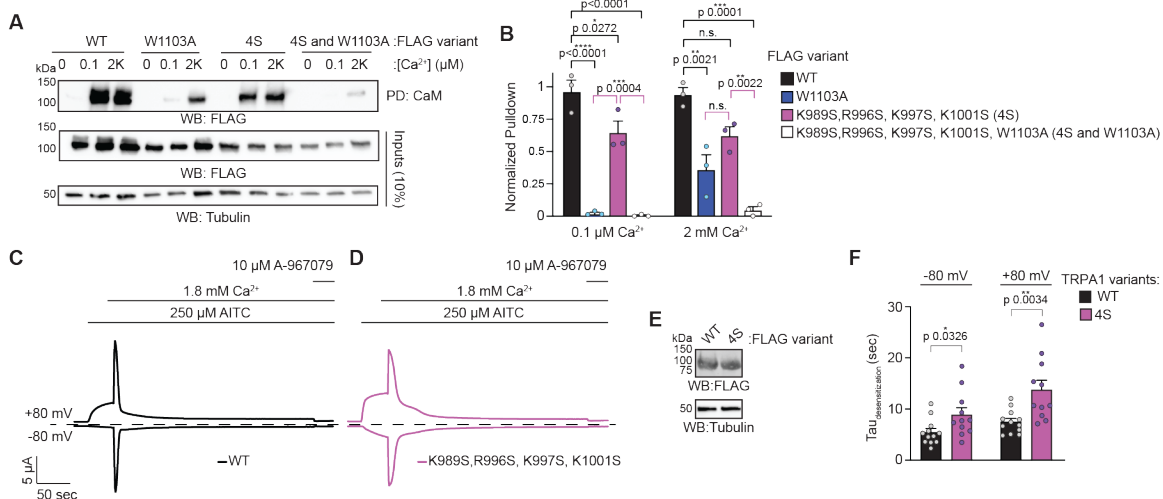


**Figure 4.** Effect of the TRP-CaMBD on full-length TRPA1. **(A)** Immunoblotting analysis of the indicated 3xFLAG-hTRPA1 constructs after CaM-agarose pulldown in the absence of Ca<sup>2+</sup>, 0.1 μM Ca<sup>2+</sup>, or 2000 μM Ca<sup>2+</sup> from lysates of HEK293T cells transfected with 3xFLAG-WT, W1103A, 4S, or 4S with W1103A. Blot is representative of three independent experiments. **(B)** Quantification of CaM-agarose pulldowns represented in (A). Pulldown was normalized to the WT hTRPA1 with 0.1 μM Ca<sup>2+</sup> average. Data represent mean ± SEM. \*\*\*\*p<0.0001, \*\*\* p<0.001, \*\* p<0.01, \* p<0.05, n.s. not significant (p>0.05). n = 3 independent experiments, one-way ANOVA with Tukey's *post hoc* analysis. **(C-D)** Representative time-traces at -80 and +80 mV holding potentials from oocytes expressing WT hTRPA1 or 4S. Current evoked with 250 μM AITC in the absence and presence of 1.8 mM extracellular Ca<sup>2+</sup>. Channels were blocked with 10 μM A-967079. Dashed line denotes 0 μA current. Protocol of condition application indicated above. **(E)** Western blot of lysates from oocytes used for recordings in C-E. **(F)** Calculated time constants of desensitization from (C and D) at -80 mV (left) and +80 mV (right) from fitting data a single-exponential function. Data represent mean ± SEM. \*p=0.0326 (WT versus

4S, -80 mV, tau desensitization), \*\* $p=0.0034$  (WT versus 4S, +80 mV, tau desensitization).

n=12 WT TRPA1, n=11 4S, two-tailed Student's t-test.

## **Chapter 4: Conclusions and Future Directions**

TRPA1 is a nociceptive ion channel that is involved in initiating and maintaining pain and inflammation across various tissues and organ systems<sup>1-51</sup>. Because of this TRPA1 has evolved an intricate  $\text{Ca}^{2+}$  regulation system to control its activity tightly and precisely<sup>1,51-62</sup>. The effects of  $\text{Ca}^{2+}$  on TRPA1 activity have been well described, but determining the mechanism of action has been difficult for the field. While several sites of  $\text{Ca}^{2+}$  regulation have been proposed, there is weak and conflicting evidence to support their proposed roles in TRPA1  $\text{Ca}^{2+}$  regulation. For my thesis I sought to clarify the roles of these proposed sites and put forth a unified and cohesive model of TRPA1 calcium regulation.

Under basal cellular conditions hTRPA1 is in a closed conformation with only transitory openings (**Fig. 1A**). The S2-S3 CBS contains a bound  $\text{Ca}^{2+}$  ion, and a polyanion compound, potentially IP6, is bound between the ARD and the coiled-coil<sup>61,63,64</sup>. We have shown that the S2-S3 CBS is important for stabilizing the channel, likely through the transmembrane domain and allosteric nexus, and prior literature has identified IP6 or similar polyanion cofactors as being necessary for channel stability. The calcified C-lobe of CaM is bound to the CaMBS in the unstructured C-terminus and serves as an auxiliary subunit that primes TRPA1 channels to respond to an influx of  $\text{Ca}^{2+}$  ions.

Covalent modification of TRPA1 by reactive electrophiles stabilizes the open state of the channel allowing an influx of  $\text{Na}^+$  and  $\text{Ca}^{2+}$  ions (**Fig. 1B**)<sup>3,7</sup>. With a slight increase in local  $\text{Ca}^{2+}$  concentration, channel activity is rapidly potentiated through an unknown mechanism. Given how quickly potentiation takes place in the presence of physiologically relevant extracellular  $\text{Ca}^{2+}$  concentrations, this mechanism likely involves a high affinity  $\text{Ca}^{2+}$  binding site which has yet to be identified.

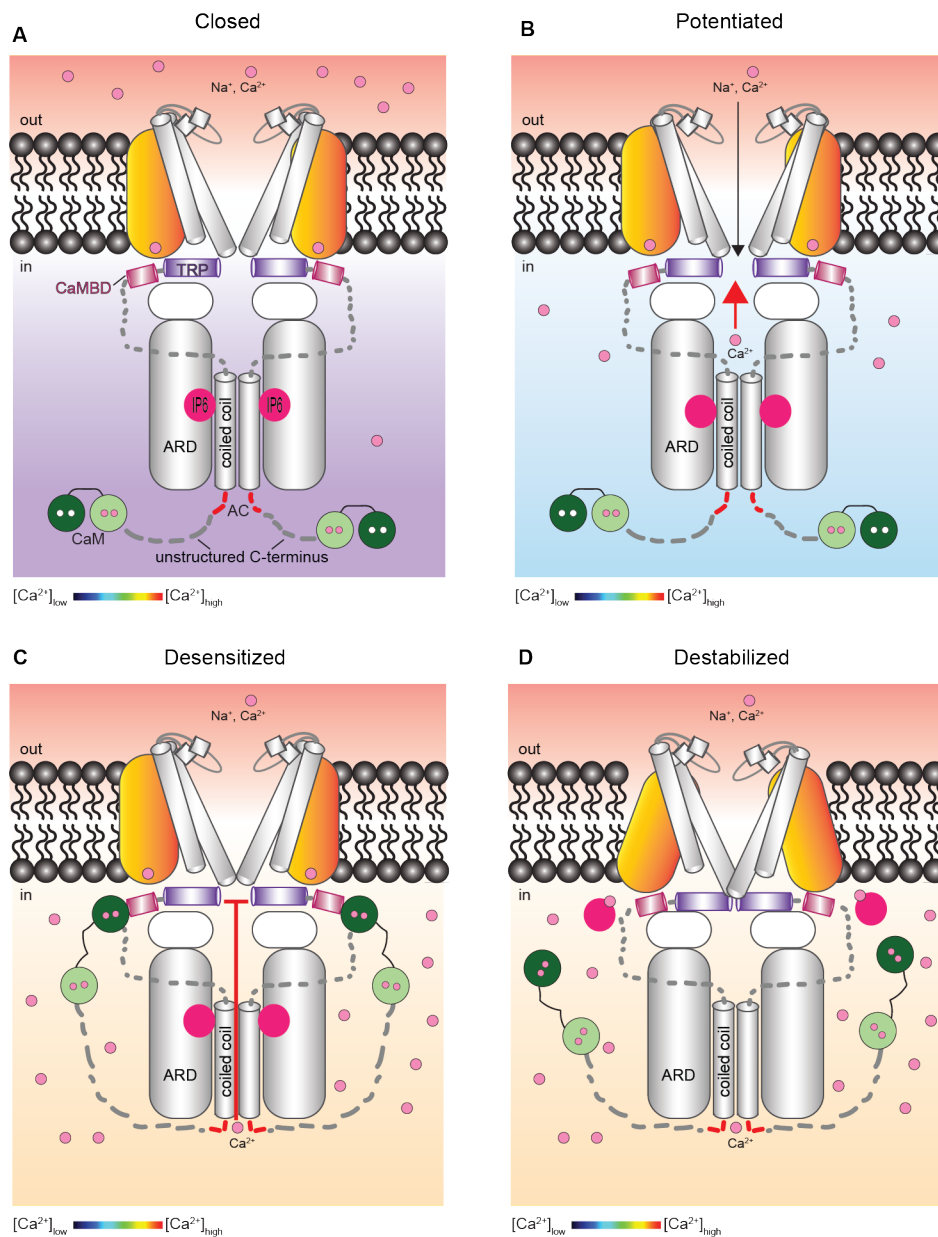


**Figure 1.** Cartoon model of TRPA1 calcium regulation. **(A)** Light purple gradient represents basal calcium concentrations. TRPA1 is closed with calcium bound at the S2-S3 CBS, CaM C-lobe (light green) bound at the unstructured C-terminus, and IP6 bound between the ARD and coiled-coil. AC is the acidic cluster (red dashes) TRP helix is purple, CaMBD is magenta, and S1-S4 helical bundle is orange gradient. **(B)** TRPA1 in an open state just after agonist activation allowing influx of cations. Light blue gradient represents low increase in calcium concentrations. Calcium likely binds to an unknown site to initiate rapid potentiation as denoted by red arrow. **(C)** Accumulation of

calcium around TRPA1 triggers desensitization. High concentration of calcium denoted by orange gradient background. CaM C-lobe binding primes the acidic cluster to bind calcium. Upon AC binding calcium the ARD and coiled-coil cage induces channel closure and enters a desensitized state. CaM N-lobe becomes calcified and binds to the CaMBD stabilizing the CaM interaction and slightly enhancing channel desensitization. **(D)** Increasing calcium concentrations and movement of the ARD Coiled-coil cage causes displacement of the polyanion cofactor destabilizing the channel. The freed polyanion has the potential to strip the S2-S3 CBS of its bound calcium further stabilizing the channel.

As local calcium concentrations continue to increase, TRPA1 is rapidly desensitized **(Fig. 1C)**. This occurs through calcium binding at an unconfirmed site, but I believe the acidic cluster just below the coiled coil is the mostly likely calcium binding site to trigger desensitization. Dense areas of negative charge in flexible regions have been shown to bind  $\text{Ca}^{2+}$  ions<sup>65</sup>, and the CaMBS is just downstream of the acidic cluster putting it in a plausible position to modify the properties of the acidic cluster. Additionally, the acidic cluster makes several interactions with the bottom of the coiled-coil and ankyrin repeat 12, so calcium binding at the acidic cluster could readily be communicated through the ARD and the coiled-coil cage. With the increase in  $\text{Ca}^{2+}$  concentration the N-lobe of CaM will become calcified<sup>66</sup> and undergo conformational changes that allow it to bind the CaMBD further enhancing the rapid desensitization of TRPA1.

Prior literature as well as our own data shows that TRPA1 can remain active for long periods of time in the absence of  $\text{Ca}^{2+}$ , yet the presence of extracellular  $\text{Ca}^{2+}$  results in both rapid desensitization and a pronounced tachyphylaxis. Given that TRPA1 can be activated by electrophilic compounds that can modify the reactive cysteines for upwards of 10

minutes or even irreversibly, it is possible TRPA1 has evolved to only open for a short period of time followed by channel desensitization and destabilization to prevent spurious activity (**Fig. 1D**). Destabilization could take place by dislodging the polyanion cofactor either through calcium binding to the polyanion or after conformational changes associated with desensitization. Once free, the polyanion cofactor would be in close proximity to the S2-S3 CBS and could potentially strip the bound calcium. While parts of this model are speculative, it provides testable hypotheses moving forward.

Perhaps the most difficult aspect of TRPA1 calcium regulation left to solve is potentiation, since the previously proposed  $\text{Ca}^{2+}$  binding sites do not seem to be responsible for initiating potentiation. However, previous research suggests that potentiation is almost certainly caused by direct calcium binding. TRPA1 pore mutants with significantly impaired  $\text{Ca}^{2+}$  permeability no longer goes through potentiation when exposed to extracellular  $\text{Ca}^{2+57}$ . Photo uncaging experiments of chelated intracellular  $\text{Ca}^{2+}$  show that potentiation of TRPA1 can also occur without permeation of extracellular  $\text{Ca}^{2+}$ , and potentiated currents can be stable as long as intracellular  $\text{Ca}^{2+}$  concentrations are held constant. Taken together, this indicates that a novel, high affinity  $\text{Ca}^{2+}$  binding site can exist anywhere within the intracellular region of TRPA1 and potentiate channel activity. While there is not an obvious candidate for a potential high affinity  $\text{Ca}^{2+}$  binding site that can potentiate TRPA1 currents, a rigorous structural and evolutionary analysis to design potential  $\text{Ca}^{2+}$  binding impaired mutants along with electrophysiology studies may provide the answers to TRPA1 calcium-mediated potentiation.

The identification of CaM as a key component in TRPA1 calcium-mediated desensitization represents a step forward for the field, but there are still several lingering

questions. While CaM is able to drastically speed up desensitization, increasing  $\text{Ca}^{2+}$  concentrations alone are also able to speed up desensitization. We propose this is due to an interplay between CaM binding at the CaMBS and  $\text{Ca}^{2+}$  binding to the nearby acidic cluster where CaM binding enhances the acidic cluster's affinity for  $\text{Ca}^{2+}$  ions. This is a unique model for CaM regulation since it appears CaM is outsourcing calcium sensitivity to its effector essentially subverting its established role as the universal  $\text{Ca}^{2+}$  sensor. Moreover, there is no biochemical or biophysical evidence supporting the acidic cluster's ability to bind  $\text{Ca}^{2+}$ . The first step in verifying this model will require confirmation that the acidic cluster is capable of binding  $\text{Ca}^{2+}$  which can be done by expressing soluble fragments of TRPA1 that include the acidic cluster. These same fragments can then be used to gauge the effect of CaM on acidic cluster  $\text{Ca}^{2+}$  binding.

The use of patch clamping in HEK293 cells will be critical to understanding the full mechanism of TRPA1 regulation by CaM. Our TEVC work was limited by the fact we could only obtain whole-cell macroscopic currents and could not use exogenous CaM mutants<sup>67,68</sup>. By patch clamping wild type TRPA1 and TRPA1 CaM binding mutants in HEK293 cells, we could obtain microscopic currents showing how CaM affects TRPA1 at a single channel level. Additionally, this technique provides the ability to pull excised patches allowing for a much greater control of the "intracellular" environment. Excised patches containing TRPA1 could have endogenously bound CaM removed by chelating available calcium and replaced with purified CaM mutants. This would allow us to investigate how each CaM lobe and each CaM EF-hand is involved in the desensitization process.

The majority of our work focused on the distal and disordered C-terminus and the CaMBS within it, but the key to identifying all of the components involved in calcium-mediated desensitization may lie within the unstructured N-terminus of rattlesnake TRPA1 (rsTRPA1). hTRPA1 functions as a chemosensor in peripheral sensory neurons, but rsTRPA1 functions as a heat sensor expressed in pit organs to provide infrared detection<sup>69,70</sup>. In addition to the differing mechanisms of activation, rsTRPA1 also lacks calcium-mediated desensitization<sup>69</sup>. It was found that heat sensitivity could be conferred to the pore region of hTRPA1 by making chimeric TRPA1 channels where the ARD of hTRPA1 was replaced with the ARD from rsTRPA1. However, with more conservative chimeras where only 4 ankyrin repeats of hTRPA1 are replaced with rsTRPA1 ankyrins, chemosensitivity was maintained and calcium-mediated desensitization was ablated. Each of these constructs retained the S2-S3 CBS, the CaMBD, the acidic cluster, and the CaMBS demonstrating these components are not sufficient to induce calcium-mediated desensitization, and some component of the ARD is critical for this process. From the published literature it appears that ankyrin repeat 11 is the critical component for ARD-mediated desensitization. This is the last unstructured ankyrin repeat in the available cryo-EM structures suggesting it would be in close proximity to both the coiled-coil and the CaMBS. It is possible that ankyrin repeat 11 is somehow involved with CaM-dependent effects given their close proximity to each other. Regardless, rsTRPA1 and our work on the CaMBS provide us with an exciting launching point to begin to fully unravel the mechanism of TRPA1 calcium-mediated desensitization.

## References

1. Bandell, M. et al. Noxious cold ion channel TRPA1 is activated by pungent compounds and bradykinin. *Neuron* **41**, 849-857 (2004).
2. Kwan, K.Y. et al. TRPA1 contributes to cold, mechanical, and chemical Nociception but is not essential for hair-cell transduction. *Neuron* **50**, 277-289 (2006).
3. Hinman, A., Chuang, H.H., Bautista, D.M. & Julius, D. TRP channel activation by reversible covalent modification. *Proceedings of the National Academy of Sciences of the United States of America* **103**, 19564-19568 (2006).
4. Bautista, D.M. et al. TRPA1 mediates the inflammatory actions of environmental irritants and proalgesic agents. *Cell* **124**, 1269-1282 (2006).
5. Trevisani, M. et al. 4-Hydroxynonenal, an endogenous aldehyde, causes pain and neurogenic inflammation through activation of the irritant receptor TRPA1. *Proceedings of the National Academy of Sciences of the United States of America* **104**, 13519-13524 (2007).
6. Petrus, M. et al. A role of TRPA1 in mechanical hyperalgesia is revealed by pharmacological inhibition. *Molecular Pain* **3**(2007).
7. Macpherson, L.J. et al. Noxious compounds activate TRPA1 ion channels through covalent modification of cysteines. *Nature* **445**, 541-545 (2007).
8. Dai, Y. et al. Sensitization of TRPA1 by PAR2 contributes to the sensation of inflammatory pain. *Journal of Clinical Investigation* **117**, 1979-1987 (2007).
9. Taylor-Clark, T.E. et al. Relative contributions of TRPA1 and TRPV1 channels in the activation of vagal bronchopulmonary C-fibres by the endogenous autacoid 4-oxononenal. *Journal of Physiology-London* **586**, 3447-3459 (2008).
10. Cruz-Orengo, L. et al. Cutaneous nociception evoked by 15-delta PGJ2 via activation of ion channel TRPA1. *Mol Pain* **4**, 30 (2008).
11. Taylor-Clark, T.E. et al. Prostaglandin-induced activation of nociceptive neurons via direct interaction with transient receptor potential A1 (TRPA1). *Mol Pharmacol* **73**, 274-81 (2008).
12. Materazzi, S. et al. Cox-dependent fatty acid metabolites cause pain through activation of the irritant receptor TRPA1. *Proceedings of the National Academy of Sciences of the United States of America* **105**, 12045-12050 (2008).
13. André, E. et al. Cigarette smoke-induced neurogenic inflammation is mediated by  $\alpha,\beta$ -unsaturated aldehydes and the TRPA1 receptor in rodents. *Journal of Clinical Investigation* **118**, 2574-2582 (2008).
14. Wang, S. et al. Phospholipase C and protein kinase A mediate bradykinin sensitization of TRPA1: a molecular mechanism of inflammatory pain. *Brain* **131**, 1241-1251 (2008).
15. Taylor-Clark, T.E., Ghatta, S., Bettner, W. & Udem, B.J. Nitrooleic Acid, an Endogenous Product of Nitritative Stress, Activates Nociceptive Sensory Nerves via the Direct Activation of TRPA1. *Molecular Pharmacology* **75**, 820-829 (2009).
16. Ro, J.Y., Lee, J.S. & Zhang, Y.P. Activation of TRPV1 and TRPA1 leads to muscle nociception and mechanical hyperalgesia. *Pain* **144**, 270-277 (2009).
17. Caceres, A.I. et al. A sensory neuronal ion channel essential for airway inflammation and hyperreactivity in asthma. *Proceedings of the National Academy of Sciences of the United States of America* **106**, 9099-9104 (2009).
18. Wei, H., Hämäläinen, M.M., Saarnilehto, M., Koivisto, A. & Pertovaara, A. Attenuation of Mechanical Hypersensitivity by an Antagonist of the TRPA1 Ion Channel in Diabetic Animals. *Anesthesiology* **111**, 147-154 (2009).
19. Kremeyer, B. et al. A Gain-of-Function Mutation in TRPA1 Causes Familial Episodic Pain Syndrome. *Neuron* **66**, 671-680 (2010).

20. Kim, Y.S. et al. Expression of Transient Receptor Potential Ankyrin 1 (TRPA1) in the Rat Trigeminal Sensory Afferents and Spinal Dorsal Horn. *Journal of Comparative Neurology* **518**, 687-698 (2010).
21. Lapointe, T.K. & Altier, C. The role of TRPA1 in visceral inflammation and pain. *Channels* **5**, 525-529 (2011).
22. Engel, M.A. et al. TRPA1 and Substance P Mediate Colitis in Mice. *Gastroenterology* **141**, 1346-1358 (2011).
23. Malin, S. et al. TRPV1 and TRPA1 Function and Modulation Are Target Tissue Dependent. *Journal of Neuroscience* **31**, 10516-10528 (2011).
24. Kunkler, P.E., Ballard, C.J., Oxford, G.S. & Hurley, J.H. TRPA1 receptors mediate environmental irritant-induced meningeal vasodilatation. *Pain* **152**, 38-44 (2011).
25. Koivisto, A. et al. Inhibiting TRPA1 ion channel reduces loss of cutaneous nerve fiber function in diabetic animals: sustained activation of the TRPA1 channel contributes to the pathogenesis of peripheral diabetic neuropathy. *Pharmacol Res* **65**, 149-58 (2012).
26. Sisignano, M. et al. 5,6-EET Is Released upon Neuronal Activity and Induces Mechanical Pain Hypersensitivity via TRPA1 on Central Afferent Terminals. *Journal of Neuroscience* **32**, 6364-6372 (2012).
27. Lennertz, R.C., Kossyryeva, E.A., Smith, A.K. & Stucky, C.L. TRPA1 Mediates Mechanical Sensitization in Nociceptors during Inflammation. *Plos One* **7**(2012).
28. Ohkawara, S., Tanaka-Kagawa, T., Furukawa, Y. & Jinno, H. Methylglyoxal activates the human transient receptor potential ankyrin 1 channel. *Journal of Toxicological Sciences* **37**, 831-835 (2012).
29. Bautista, D.M., Pellegrino, M. & Tsunozaki, M. TRPA1: A Gatekeeper for Inflammation. *Annual Review of Physiology, Vol 75* **75**, 181-200 (2013).
30. Andersson, D.A. et al. Methylglyoxal Evokes Pain by Stimulating TRPA1. *Plos One* **8**(2013).
31. Julius, D. TRP channels and pain. *Annu Rev Cell Dev Biol* **29**, 355-84 (2013).
32. Wilson, S.R. et al. The Ion Channel TRPA1 Is Required for Chronic Itch. *Journal of Neuroscience* **33**, 9283-9294 (2013).
33. Liu, B.Y. et al. TRPA1 controls inflammation and pruritogen responses in allergic contact dermatitis. *Faseb Journal* **27**, 3549-3563 (2013).
34. Grace, M.S., Baxter, M., Dubuis, E., Birrell, M.A. & Belvisi, M.G. Transient receptor potential (TRP) channels in the airway: role in airway disease. *Br J Pharmacol* **171**, 2593-607 (2014).
35. Meseguer, V. et al. TRPA1 channels mediate acute neurogenic inflammation and pain produced by bacterial endotoxins. *Nature Communications* **5**(2014).
36. Nassini, R., Materazzi, S., Benemei, S. & Geppetti, P. The TRPA1 Channel in Inflammatory and Neuropathic Pain and Migraine. *Reviews of Physiology, Biochemistry and Pharmacology, Vol 167* **167**, 1-43 (2014).
37. Liu, B. & Jordt, S.E. TRPA1 Controls Inflammation and Pruritogen Responses in Allergic Contact Dermatitis. *Journal of General Physiology* **144**, 10a-10a (2014).
38. Asgar, J. et al. The Role of Trpa1 in Muscle Pain and Mechanical Hypersensitivity under Inflammatory Conditions in Rats. *Neuroscience* **310**, 206-215 (2015).
39. Chen, J. & Hackos, D.H. TRPA1 as a drug target-promise and challenges. *Naunyn-Schmiedeberg's Archives of Pharmacology* **388**, 451-463 (2015).
40. Huang, Q., Chen, Y., Gong, N.A. & Wang, Y.X. Methylglyoxal mediates streptozotocin-induced diabetic neuropathic pain via activation of the peripheral TRPA1 and Nav1.8 channels. *Metabolism-Clinical and Experimental* **65**, 463-474 (2016).
41. Gallo, V. et al. gene polymorphisms and childhood asthma. *Pediatric Allergy and Immunology* **28**, 191-198 (2017).

42. Gouin, O. et al. TRPV1 and TRPA1 in cutaneous neurogenic and chronic inflammation: pro-inflammatory response induced by their activation and their sensitization. *Protein Cell* **8**, 644-661 (2017).
43. Cseko, K., Beckers, B., Keszthelyi, D. & Helyes, Z. Role of TRPV1 and TRPA1 Ion Channels in Inflammatory Bowel Diseases: Potential Therapeutic Targets? *Pharmaceuticals* **12**(2019).
44. Wang, Z. et al. The TRPA1 Channel in the Cardiovascular System: Promising Features and Challenges. *Frontiers in Pharmacology* **10**(2019).
45. Talavera, K. et al. Mammalian Transient Receptor Potential Trpa1 Channels: From Structure to Disease. *Physiological Reviews* **100**, 725-803 (2020).
46. Maglie, R. et al. The Role of TRPA1 in Skin Physiology and Pathology. *International Journal of Molecular Sciences* **22**(2021).
47. Balestrini, A. et al. A TRPA1 inhibitor suppresses neurogenic inflammation and airway contraction for asthma treatment. *Journal of Experimental Medicine* **218**(2021).
48. Landini, L. et al. TRPA1 Role in Inflammatory Disorders: What Is Known So Far? *International Journal of Molecular Sciences* **23**(2022).
49. Liu, Y. et al. Exploring the TRP channel superfamily: research hotspots and development trends from function to disease. *Eur Rev Med Pharmacol Sci* **27**, 9478-9498 (2023).
50. Marchi, M. et al. TRPA1 rare variants in chronic neuropathic and nociplastic pain patients. *Pain* **164**, 2048-2059 (2023).
51. Bali, A. et al. Molecular mechanism of hyperactivation conferred by a truncation of TRPA1. *Nature Communications* **14**(2023).
52. Jordt, S.E. et al. Mustard oils and cannabinoids excite sensory nerve fibres through the TRP channel ANKTM1. *Nature* **427**, 260-265 (2004).
53. Zurborg, S., Yurgionas, B., Jira, J.A., Caspani, O. & Heppenstall, P.A. Direct activation of the ion channel TRPA1 by Ca. *Nature Neuroscience* **10**, 277-279 (2007).
54. Nagata, K., Duggan, A., Kumar, G. & García-Añoveros, J. Nociceptor and hair cell transducer properties of TRPA1, a channel for pain and hearing. *Journal of Neuroscience* **25**, 4052-4061 (2005).
55. Doerner, J.F., Gisselmann, G., Hatt, H. & Wetzel, C.H. Transient receptor potential channel a1 is directly gated by calcium ions. *Journal of Biological Chemistry* **282**, 13180-13189 (2007).
56. Cavanaugh, E.J., Simkin, D. & Kim, D. Activation of transient receptor potential A1 channels by mustard oil, tetrahydrocannabinol and Ca reveals different functional channel states. *Neuroscience* **154**, 1467-1476 (2008).
57. Wang, Y.Y., Chang, R.B., Waters, H.N., Mckemy, D.D. & Liman, E.R. The Nociceptor Ion Channel TRPA1 Is Potentiated and Inactivated by Permeating Calcium Ions. *Journal of Biological Chemistry* **283**, 32691-32703 (2008).
58. Patil, M.J., Jeske, N.A. & Akopian, A.N. Transient receptor potential V1 regulates activation and modulation of transient receptor potential A1 by Ca<sup>2+</sup>. *Neuroscience* **171**, 1109-19 (2010).
59. Hasan, R., Leeson-Payne, A.T.S., Jaggar, J.H. & Zhang, X.M. Calmodulin is responsible for Ca<sup>2+</sup>-dependent regulation of TRPA1 Channels. *Scientific Reports* **7**(2017).
60. Zimova, L. et al. Intracellular cavity of sensor domain controls allosteric gating of TRPA1 channel. *Science Signaling* **11**(2018).
61. Zhao, J., Lin King, J.V., Paulsen, C.E., Cheng, Y. & Julius, D. Irritant-evoked activation and calcium modulation of the TRPA1 receptor. *Nature* **585**, 141-145 (2020).
62. Sura, L. et al. C-terminal Acidic Cluster Is Involved in Ca<sup>2+</sup>-induced Regulation of Human Transient Receptor Potential Ankyrin 1 Channel. *Journal of Biological Chemistry* **287**, 18067-18077 (2012).

63. Paulsen, C.E., Armache, J.P., Gao, Y., Cheng, Y. & Julius, D. Structure of the TRPA1 ion channel suggests regulatory mechanisms. *Nature* **525**, 552 (2015).
64. Kim, D. & Cavanaugh, E.J. Requirement of a soluble intracellular factor for activation of transient receptor potential A1 by pungent chemicals: Role of inorganic polyphosphates. *Journal of Neuroscience* **27**, 6500-6509 (2007).
65. Dunker, A.K. et al. Intrinsically disordered protein. *Journal of Molecular Graphics & Modelling* **19**, 26-59 (2001).
66. Chin, D. & Means, A.R. Calmodulin: a prototypical calcium sensor. *Trends Cell Biol* **10**, 322-8 (2000).
67. Cartaud, A., Ozon, R., Walsh, M.P., Haiech, J. & Demaille, J.G. Xenopus laevis oocyte calmodulin in the process of meiotic maturation. *J Biol Chem* **255**, 9404-8 (1980).
68. Cicirelli, M.F. & Smith, L.D. Calmodulin synthesis and accumulation during oogenesis and maturation of Xenopus laevis oocytes. *Dev Biol* **113**, 174-81 (1986).
69. Cordero-Morales, J.F., Gracheva, E.O. & Julius, D. Cytoplasmic ankyrin repeats of transient receptor potential A1 (TRPA1) dictate sensitivity to thermal and chemical stimuli. *Proceedings of the National Academy of Sciences of the United States of America* **108**, E1184-E1191 (2011).
70. Gracheva, E.O. et al. Molecular basis of infrared detection by snakes. *Nature* **464**, 1006-11 (2010).